Technische Universität München
TUM School of Life Sciences

Diet Induced Obesity in an Adipose Tissue Specific Monoacylglycerol Lipase Knockout Mouse Model

Patrick Hartmut Herbert Pann

Vollständiger Abdruck der von der TUM School of Life Sciences der Technischen Universität München zur Erlangung eines

Doktors der Naturwissenschaften (Dr. rer. nat.)

genehmigten Dissertation.

Vorsitz:		Prof. Dr. Heiko Witt
Prüfer*innen der Dissertation:	1.	apl. Prof. Dr. Jerzy Adamski
	2.	Prof. Dr. Johann J. Hauner

Die Dissertation wurde am 14.04.2022 bei der Technischen Universität München eingereicht und durch die TUM School of Life Sciences am 29.11.2022 angenommen.

Table of Contents

Abstract **4**

Zusammenfassung **5**

1 Introduction **6**

1.1 The Epidemiological Burden of Obesity 6

1.2 The Pathophysiology of Obesity 7

1.3 Biochemistry and Regulation of Adipocyte Lipolysis 8

1.4 Lipolysis in Obesity and Insulin Resistance 10

1.5 The Monoacylglycerol Lipase 12

1.5.1 From Gene to Protein 12

1.5.2 Structure and Function 13

1.5.3 Regulation 16

1.5.4 Tissue Distribution and Pathways 17

1.6 The Aim of the Thesis 18

2 Methods **19**

2.1 Animals 19

2.2 Cohort Data and Diet 19

2.3 Body Weight Analysis 20

2.4 Quantitative Nuclear Magnetic Resonance Analysis 20

2.5 Tail Vein Blood Collection 21

2.6 Fasted Insulin Analysis 21

2.7 Glucose Tolerance Test 21

2.8 Insulin Tolerance Test 22

2.9 Retro-Orbital Blood Collection 23

2.10 Organ Withdrawal 23

2.11 Clinical Blood Parameter Analysis 24

2.12 Flow Cytometry Analysis 24

2.13 Cytokine Analysis 26
2.14 Targeted Metabolomics 27
2.15 Total RNA Sequencing 29
2.16 Quantitative Real-Time PCR 30
2.17 Immunohistochemistry 31
2.18 Statistics 31
3 Results 33
3.1 Knockout Verification 33
3.2 Experimental Design 34
3.3 Body Composition 35
3.4 Immune System 41
3.5 Clinical Chemistry 46
3.6 Diabetes 48
3.7 Metabolomics 50
3.8 Total RNA Sequencing 56
4 Discussion 59
4.1 Adipose Tissue MGLL Does Not Affect the Body Composition of Mice 60
4.2 Dysfunction of Adipocyte Lipolysis in MGLL KO Mice Cannot Be Confirmed 62
4.3 Interplay of HFD and MGLL KO Induces Complex Immunological Changes 63
4.4 KO of MGLL in Adipocytes Does Not Protect from Diet-Induced Insulin Resistance 65
4.5 MGLL KO Mildly Affects Adipocyte mRNA Expression and Lipid Metabolism 66
4.6 Final Thoughts 67
5 Bibliography 70
6 Appendix 77
Abbreviations 81
Danksagung 83

Abstract

With its prevalence increasing, especially in the western world, obesity has become a serious epidemic. The causes lie mainly in the expansion of a sedentary lifestyle and the popularity of a high-caloric diet. Obesity is a serious burden on health and is linked to hypertension, type 2 diabetes, cardiovascular disease, and cancer. Therefore, obesity is not only responsible for millions of premature deaths each year, but also strains healthcare systems and economies worldwide. Behavioral measures such as diet and physical activity remain the primary measures in obesity control but often fail due to lack of compliance. Anti-obesity medications can support these strategies by affecting appetite and energy expenditure, but often cause side effects. Adipocyte lipolysis is increased in obesity and is associated with diabetes, making it a potential drug target. One of the lipases primarily responsible for the breakdown of lipid storages in adipocytes is monoacylglycerol lipase (MGLL). The aim of this thesis was to shed light on the role of adipocyte MGLL in obesity.

For this purpose, an adipocyte-specific MGLL knockout mouse model with high-fat diet-induced obesity was characterized for the first time with respect to body composition, systemic inflammation, glucose- and lipid metabolism, as well as metabolomic and transcriptomic changes. Female and male knockout (KO) and wildtype (WT) mice were fed a high-fat diet (HFD) or a control diet (CD) for up to 24 weeks. Feeding a HFD significantly increased the body weight and fat mass of male and female mice. Obese mice showed impaired glucose clearance and increased fasted glucose and insulin levels suggesting a prediabetic phenotype. They exhibited increased levels of cholesterol, free fatty acids, and glycerol as well as changes in pro- and anti-inflammatory cytokine levels. The HFD also induced significant metabolomic changes in all tested tissues and plasma.

When comparing MGLL KO mice to their WT littermates, obvious phenotypic differences were missing. Small genotype dependent differences were only found in male mice fed a HFD for 24 weeks. Here, the MGLL KO amplified the HFD-induced increase of TNFα, CXCL1, and IL-10 plasma levels. Metabolomics analysis of white adipose tissue suggested an impairment of adipocyte lipolysis. However, this did not translate into any significant differences in the metabolomic profiles of blood plasma or liver tissue. Transcriptomics analysis of white adipose tissue did not reveal any compensatory changes in gene expression of male KO mice.

The results of the thesis clearly demonstrate the independence of adipocyte lipolysis from the activity of MGLL even in the presence of prolonged dietary fat excess. Adipocyte MGLL can therefore be excluded as a potential target for the treatment of obesity and diabetes. However, due to its ubiquitous expression and involvement in various pathways, MGLL remains a worthwhile target, for example, in the brain or intestine.

Zusammenfassung

Übergewicht und Fettleibigkeit (Adipositas) hat sich in den letzten Jahren zu einer ernstzunehmenden Epidemie entwickelt und steht in Zusammenhang mit Bluthochdruck, Typ-2-Diabetes, Herz-Kreislauf-Erkrankungen und Krebs. Ernährungsumstellung und körperliche Betätigung sind nach wie vor das Maß der Dinge bei der Bekämpfung von Adipositas scheitern aber häufig an mangelnder Compliance. Medikamente können unterstützend eingesetzt werden, sind aber oft mit Nebenwirkungen verbunden. Die Lipolyse im Fettgewebe ist bei Fettleibigkeit erhöht und wird mit Diabetes in Verbindung gebracht. Dies macht sie zu einem potenziellen Wirkstoffziel. Eine der Lipasen, die für den Abbau von Fettspeichern in Adipozyten verantwortlich ist, ist die Monoacylglycerol-Lipase (MGLL). Ziel dieser Arbeit war es, die Rolle von MGLL im Fettgewebe bei Adipositas zu beleuchten.

Zu diesem Zweck wurde erstmals ein fettgewebespezifisches MGLL Knockout-Mausmodell mit Diät-induzierter Adipositas umfassend charakterisiert. Weibliche und männliche Knockout- (KO) und Wildtyp-Mäuse (WT) wurden bis zu 24 Wochen mit einer Hochfettdiät (HFD) oder einer Kontrolldiät (CD) gefüttert. Die HFD führte bei männlichen und weiblichen Mäusen zu einer deutlichen Zunahme des Körpergewichts und der Fettmasse. Die fettleibigen Mäuse zeigten einen verzögerten Abfall der Blutglukosekonzentration nach Glukoseinjektion und erhöhte basale Glukose- und Insulinspiegel. Sie wiesen erhöhte Blutplasmawerte von Cholesterin, freien Fettsäuren- und Glycerin sowie Veränderungen von pro- und anti-inflammatorischen Zytokinkonzentrationen auf. Die HFD führte zu signifikanten metabolomischen Veränderungen in der Leber, im Fettgewebe und im Blut. Der Vergleich von KO- und WT-Mäusen ergab keine offensichtlichen phänotypischen Unterschiede. Geringe Genotyp-abhängige Unterschiede wurden nur bei männlichen Mäusen nach 24 Wochen Hochfettdiät gefunden. Hier verstärkte der KO von MGLL den HFD-induzierten Anstieg von TNFα, CXCL1 und IL-10 im Blut. Die Metabolomanalyse des weißen Fettgewebes deutete auf eine Beeinträchtigung der Lipolyse hin. Diese führte jedoch nicht zu signifikanten metabolomischen Unterschieden im Blut oder in der Leber. Die Transkriptomanalyse des weißen Fettgewebes ergab keine kompensatorischen Veränderungen der Genexpression bei männlichen KO-Mäusen.

Die Ergebnisse dieser Arbeit zeigen deutlich, dass MGLL nicht zwingend für die Lipolyse im Fettgewebe benötigt wird. Auch ein langfristiger Fettüberschuss in der Nahrung ändert daran nichts. MGLL im Fettgewebe kann daher als potenzielles Ziel für die Behandlung von Fettleibigkeit und Diabetes ausgeschlossen werden. Aufgrund seiner ubiquitären Expression und seiner Beteiligung an verschiedenen Stoffwechselwegen bleibt MGLL jedoch ein mögliches Wirkstoffziel, zum Beispiel im Gehirn oder im Darm.

1 Introduction

1.1 The Epidemiological Burden of Obesity

Obesity has become an epidemic and its prevalence has increased in recent decades. According to the World Health Organization the worldwide prevalence of obesity has almost tripled between 1975 and 2016. A body mass index of ≥25 kg/m² is considered overweight, while ≥30 kg/m² are defined as obese. In 2016, over 1.9 billion adults worldwide were overweight and of these more than 650 million were obese. This corresponds to 39 % and 13 % of the world's population, respectively. Overweight and obesity are especially prevalent in high income countries which are characterized by a sedentary lifestyle and a "western diet". In 2016, levels of inactivity in the adult population of high-income countries reached 36.8 %, twice as high as in low-income countries [1,2]. Automated technologies, higher volumes of workplace sitting, the availability of cars and public transportation, as well as passive entertainment such as video games, TV watching, and social media, have created an environment that encourages physical inactivity. Combined with a highly processed and calorie-dense diet that is cheap, fast, and constantly available this results in a calorie excess which paves the way for excessive weight gain. Genetic factors also play a role in the development of obesity but have limited impact on their own [3].

Overweight and obesity entail numerous health consequences. They directly cause or are linked to hypertension, type 2 diabetes (T2D), cardiovascular disease, and cancer [3]. Abdominal (central) obesity in particular is strongly associated with metabolic syndrome, which is a cluster of medical conditions including hyperglycemia, insulin resistance, dyslipidemia, and hypertension. Metabolic syndrome, in turn, is closely tied to the risk of developing T2D and cardiovascular disease [4]. Modelling by the Organisation for Economic Co-operation and Development (OECD) predicts disease treatment caused by obesity to cost an average of 8.4 % of the total health care expenditure, not including long-term care, of OECD, EU, and G20 countries in 2020-2050. Nevertheless, overweight will cause about 3 million premature deaths (age 30-70) per year. Together with its comorbidities, it will reduce life expectancy by an average of 2.7 years in OECD countries. According to the OECD, obesity also burdens the labor market by reducing the employment rate, and increasing early retirement, absenteeism, and presenteeism [5]. In summary, obesity and its comorbidities threaten the health of the society and burden healthcare systems and economies. They call not only for improved prevention strategies but also for extensive research on the underlying pathomechanisms and on new effective therapies.

1.2 The Pathophysiology of Obesity

Adipose tissue represents about 20 % and 30 % of the total body mass in healthy men and women. However, in morbidly obese individuals it can expand to more than 50 % of body fat percentage. The primary function of adipocytes which are the main component of adipose tissue is to maintain energy balance. During states of positive energy balance, for example after food consumption, excess fat and glucose are stored in the form of triacylglycerol (TAG) in adipocyte lipid droplets (**Figure 1**). During states of negative energy balance, induced by fasting or physical activity, adipocytes break down stored lipids to glycerol and free fatty acids (FFA) which are needed as energy source in peripheral tissues [6]. The primary cause for obesity is an energy imbalance where energy intake and storage exceed energy expenditure.

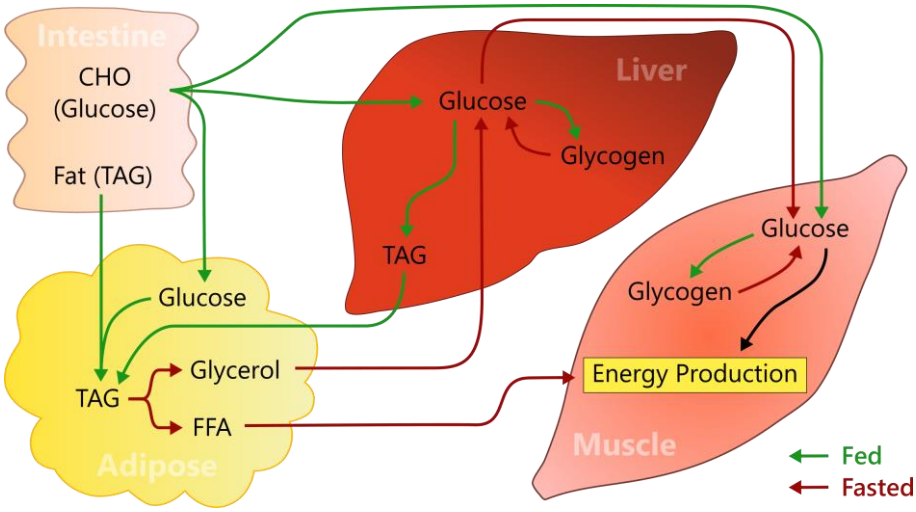

Figure 1. Metabolism during states of positive (Fed) and negative (Fasted) energy balance. During states of positive energy balance adipocytes store excess lipids originating from dietary fat absorbed from the small intestine. Glucose is used as the primary energy source and in glycogenesis in the liver and skeletal muscle. Fatty acids are synthesized in the liver and adipose tissue from excess glucose and are stored as well in adipocyte lipid droplets. During states of negative energy balance adipocytes break down lipids stored in the form of TAGs into glycerol and FFAs. FFAs and glycerol are released into the blood stream and serve as energy source in β-oxidation in peripheral tissues and in gluconeogenesis in the liver, respectively.

Excess calories can be stored in the form of subcutaneous adipose tissue (SAT) in between the skin and the outer abdominal wall or as visceral adipose tissue (VAT) in between abdominal organs and in the omentum. Premenopausal women accumulate fat mainly subcutaneously on the hips and thighs as well as in gluteal depots. In contrast, men store fat preferentially in the form of VAT in the abdominal region [7]. Excess VAT manifests in the typical android or apple body shape and is associated with hypertension, insulin resistance, T2D, dyslipidemia, and metabolic syndrome independent of SAT or total fat mass [8–10]. While the association of abdominal obesity with

metabolic complications is clear at the epidemiological level, knowledge of the pathomechanisms responsible remains incomplete and often contradictory. The 'expandability hypothesis' integrates the accumulated findings about obesity related comorbidities into a currently well-accepted but ever evolving narrative. It takes the position that not fat mass itself is the culprit of metabolic complications but the limited capacity of subcutaneous adipose tissue to expand in face of a sustained calorie surplus. Consequently, excess lipids accumulate in VAT and ectopic tissues. In VAT lipid overload leads to morbid adipose tissue remodeling, while in non-adipose tissues such as liver, skeletal muscle, heart, and pancreas it interferes with insulin signaling and general tissue function. These effects are summarized under the term lipotoxicity [11]. In that sense, obesity has a lot in common with lipodystrophy, a genetic disorder that prevents fat storage in adipocytes resulting in ectopic lipid accumulation, insulin resistance and metabolic syndrome [12].

To store excess calories adipose tissue can grow either by enlarging existing adipocytes (hypertrophy) or by recruitment and differentiation of pre-adipocytes to increase the total adipocyte number (hyperplasia). While SAT predominantly expands through hyperplasia and exhibits a high differentiation capacity, VAT shows a preference for hypertrophic expansion [13]. Adipose tissue hyperplasia is characterized by small adipocytes with higher fat storage capacity and insulin sensitivity compared to hypertrophic adipocytes in obesity. Indeed, removal of visceral fat improves insulin sensitivity and diabetes in obese humans and animals. Likewise, lipectomy of subcutaneous fat impairs metabolic profiles and insulin sensitivity and leads to increased accumulation of fat in the liver [7]. Hypertrophic VAT is characterized by hypoxia, increased lipolysis, immune cell infiltration and secretion of proinflammatory cytokines such as tumor necrosis factor alpha (TNF-α), interleukin 6 (IL-6) and C-reactive protein [14]. Increased lipolysis as well as adipose tissue dysfunction leads to fat deposition in ectopic tissues where it can interfere with tissue function. Lipid moieties such as diacylglycerol (DAG) and ceramides as well as proinflammatory cytokines such as TNF-α and IL-6 were shown to induce insulin resistance in liver and skeletal muscle consequently leading to T2D [15].

1.3 Biochemistry and Regulation of Adipocyte Lipolysis

Lipolysis is the breakdown of fat storages primarily in adipocytes to provide energy in the form of FFAs to peripheral tissues during states of energy demands, like fasting or physical exercise. It therefore plays a pivotal role in maintaining energy balance. However, obesity is characterized by sustained energy imbalance and FFA spillover in ectopic tissues which is associated with comorbidities such as insulin resistance and T2D. Understanding adipocyte lipolysis and its regulation as well as its role in the pathophysiology of obesity is a necessary step in the prevention

and treatment of obesity-related diseases. Adipocyte lipolysis takes place at the surface of lipid droplets, large organelles composing the majority of the cell volume. Lipid droplets consist of a neutral lipid core mainly comprised of TAGs and sterol esters surrounded by a phospholipid monolayer and associated proteins controlling lipid turnover. Three enzymes are primarily responsible for the consecutive hydrolysis of stored TAGs. In the first step, adipose triglyceride lipase (ATGL, aka PNPLA2) cleaves TAG into DAG and one fatty acid. Then, hormone-sensitive lipase (HSL) converts DAG into monoacylglycerol (MAG) and another fatty acid. Finally, monoacylglycerol lipase (MGLL) hydrolyses MAG setting free the last fatty acid and one glycerol in the process.

The major hormonal regulators of adipocyte lipolysis are catecholamines, natriuretic peptides, and insulin (**Figure 2**). The catecholamines adrenaline and noradrenaline are secreted by the adrenal medulla or by direct sympathetic innervation of the adipose tissue. They play a special role in the regulation of lipolysis as they can induce lipolytic activity via $\beta_{1/2}$-adrenergic receptors ($\beta_{1,2}$-AR) as well as antilipolytic activity by binding to α_2-adrenergic receptors (α_2-AR). Activation or inhibition of lipolysis therefore depends on relative adrenergic receptor surface expression and relative catecholamine affinity towards the receptors. Both, $\beta_{1,2}$-AR and α_2-AR are G-protein coupled receptors associated with the G-proteins Gαs and Gαi, respectively. Gαs promotes lipolysis via adenylyl cyclase activation, which leads to cyclic adenosine monophosphate (cAMP) production and protein kinase A (PKA) activation. Conversely, Gαi inhibits lipolysis by inactivating adenylyl cyclase. Activated PKA phosphorylates perilipin 1 (PLIN1) on the lipid droplet causing it to increase lipid droplet fragmentation which facilitates enzyme access by increasing the lipid droplet surface area. PLIN1 phosphorylation also causes its dissociation from the 1-acylglycerol-3-phosphate O-acyltransferase (ABHD5). ABHD5 then interacts with ATGL stimulating its activity. Under antilipolytic conditions ABHD5 is sequestered by PLIN1 and ATGL activity is low. PKA also phosphorylates HSL inducing its translocation from the cytosol to the lipid droplet surface.

Atrial and brain natriuretic peptides (NP) are regulating adipocyte lipolysis in a similar way. NPs are released from cardiomyocytes and induce vasodilatation in response to increased stretching and blood volume. Apart from maintaining cardiovascular homeostasis NPs also regulate energy and fat metabolism [16]. Similar to catecholamines NP binding to adipocytes can induce lipolytic as well as antilipolytic effects depending on the receptor they bind. NP binding and activation of type A natriuretic peptide receptors (NPR-A) stimulates lipolysis. NPR-A guanylyl cyclase activity increases cyclic guanosine monophosphate (cGMP) which activates protein kinase G (PKG). Finally, PKG phosphorylates the same targets as PKA. In contrast, NP binding to type C natriuretic peptide receptors (NPR-C) leads to its internalization and degradation, effectively inhibiting lipolysis. Similar to catecholamines, the direction of NP regulation depends on the relative expression of its receptors.

While a negative energy balance increases NPR-A and decreases NPR-C expression, the contrary is true during states of energy supply.

Insulin is the major inhibitor of adipocyte lipolysis and acts via activation of phosphoinositol-3-kinase (PI3K) signaling which finally leads to the activation of protein kinase B among other kinases. Protein kinase B then activates phosphodiesterase 3B (PDE3B) which converts cAMP into 5′-AMP. While this mechanism counteracts cAMP production induced by catecholamine signaling it has no effect on the lipolytic effect of NP which relies on increased cGMP levels [6].

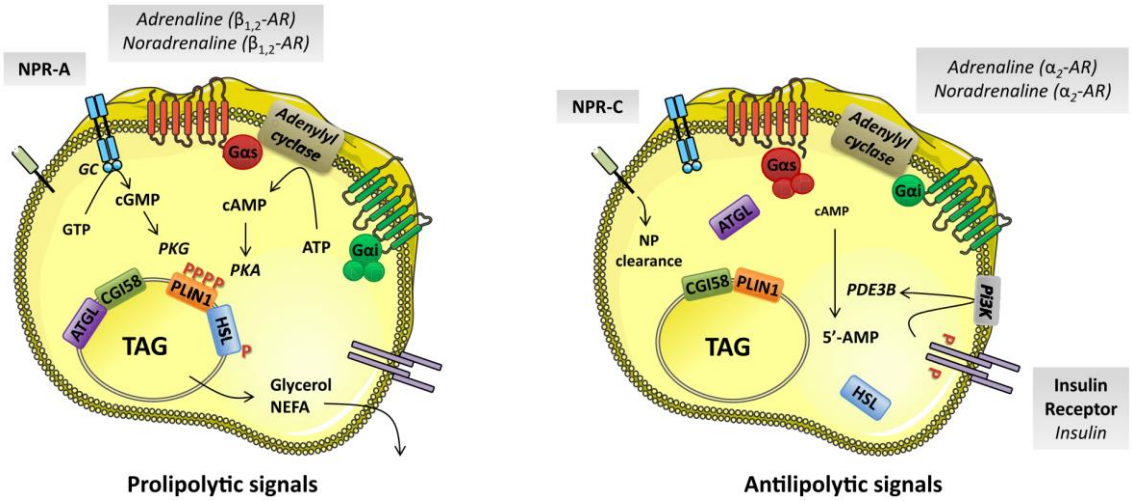

Figure 2. Major hormonal regulators of adipocyte lipolysis. (**left**) Prolipolytic signals. $\beta_{1,2}$-AR and NPR-A activate PKA and PKG, respectively. This leads to the phosphorylation of HSL and PLIN1. HSL then translocates to the lipid droplet surface. Phosphorylation of PLIN1 facilitates lipid droplet fragmentation. (**right**) Antilipolytic signals. Insulin activation of PDE3B through Pi3K and adenylyl cyclase inhibition through α2-AR dampen cAMP production and PKA activation. NPR-C expression in antilipolytic conditions leads to NP clearance and impairment of lipolysis. $\beta_{1,2}$-AR: $\beta_{1,2}$-adrenergic receptor; NPR-A: type A natriuretic peptide receptor; PKA: protein kinase A; PKG: protein kinase G; HSL: hormone sensitive lipase; PLIN1: perilipin 1; ATGL: adipose triglyceride lipase; CGI-58: comparative gene identification 58; PDE3B: phosphodiesterase 3B; PI3K: phosphatidyl inositol 3 kinase; NPR-C: type C natriuretic peptide receptor; GC: guanylyl cyclase; TAG: triacylglycerol; NEFA: non esterified fatty acid; cGMP: cyclic guanosine monophosphate; cAMP: cyclic adenosine monophosphate; P: phosphate groups. Figure adapted from Morigny *et al.* 2016 [6].

1.4 Lipolysis in Obesity and Insulin Resistance

There are several indicators that suggest dysregulation of adipocyte lipolysis in obesity and its involvement in the development of insulin resistance and diabetes. Basal or unstimulated lipolysis is increased in obesity possibly due to adipocyte hypertrophy [6,17]. Hypertrophy itself is associated with hypoxia, immune cell infiltration, proinflammatory cytokine secretion, and insulin resistance [14]. Furthermore, regain of insulin sensitivity after bariatric surgery was reported to be correlated with the regression of basal lipolysis [18]. In contrast, NP induced lipolysis was found to be decreased in obese humans and mice due to a shift in the NPR-A/NPR-C expression ratio [19]. Interestingly, NP

levels are negatively correlated with visceral fat mass and serum insulin levels [16]. Lipolytic catecholamine signaling is decreased as well in SAT of obese and insulin resistant patients but increased in VAT [20]. Visceral fat appears to be more innervated in comparison to subcutaneous fat, which might enhance dysregulation in VAT [21]. Rising levels of proinflammatory cytokines such as TNF-α and IL-6 released by infiltrating macrophages might also play a role in the dysregulation of adipocyte lipolysis. TNF-α enhances FFA-induced insulin resistance in adipocytes *in vitro* thereby attenuating lipolysis inhibition by insulin [22]. IL-6 infusion in healthy humans was shown to increase FFA plasma concentrations and body fat oxidation suggesting a prolipolytic effect [23].

Chronic elevation of adipocyte lipolysis might induce or enhance insulin resistance in the obese individuals through various pathways. First, increased lipolytic activity increases FFA output which might contribute to ectopic accumulation in tissues such as muscle and liver leading to insulin resistance [11]. DAG and ceramide are two metabolite classes that have been studied in this context. Both are suggested to interfere with insulin signaling in muscle and liver via PKC activation [17]. Additionally, it is assumed that FFAs released from adipose tissue is the primary mechanism stimulating gluconeogenesis, increasing hepatic acetyl CoA, and activating pyruvate carboxylase. Increased hepatic gluconeogenesis is a major cause of hyperglycemia in T2D [24]. Apart from its lipid storage capacity adipose tissue possesses endocrine activity thereby regulating energy homeostasis in various tissues such as brain, pancreas, and liver. Adipocyte lipolysis modulates adipokine and lipokine secretion [6]. Adipocyte fatty acid binding protein 4 (aP2, aka FABP4) is one of these adipokines and exhibits increased secretion with increasing lipolytic activity. aP2 is known to stimulate gluconeogenesis in the liver and is involved in the pathogenesis of T2D, atherosclerosis and fatty liver disease [25].

Because of the disruptive effects of increased adipocyte lipolysis in the obese, lipase inhibition is researched as a possible therapeutic strategy. ATGL is considered the rate limiting enzyme in hydrolysis of TAGs in fat storages. Surprisingly, adipocyte-specific knockout (KO) of ATGL in mice reduces adipocyte lipolysis and serum lipid levels, while not affecting fat or total body mass. Furthermore, glucose and insulin sensitivity are improved in diet-induced obesity primarily due to improved insulin signaling in the liver [26]. In contrast, mice with an adipocyte-specific deficiency of HSL, the major enzyme hydrolyzing DAG, exhibit impaired energy homeostasis. Mice are characterized by inflammatory macrophage infiltration, lipodystrophy, abnormal adipokine secretion, and systemic insulin resistance and develop a fatty liver in an age-dependent manner.

Hydrolysis of MAGs into glycerol and FFAs by MGLL marks the final step in the breakdown of lipid storages in adipocyte. Global KO models of MGLL exhibit reduced plasma lipid levels, as well as improved glucose tolerance and insulin sensitivity when challenged with a HFD [27]. Mice were

also found to be protected from hepatic steatosis and showed diminished adipose tissue inflammation [28]. The results regarding body composition are currently inconclusive, as both stable body weight and fat mass as well as a reduction in both parameters were observed [27–30]. These results identify the inhibition of MGLL as viable therapeutic strategy for the treatment of morbidities associated with obesity. However, MGLL is ubiquitously expressed and involved in different pathways besides lipolysis. An adipocyte-specific MGLL KO mouse model is needed to elucidate whether the modulation of adipocyte lipolysis is the driving mechanism behind the beneficial effects observed in the context of obesity. Currently, no such model is characterized in the literature.

1.5 The Monoacylglycerol Lipase

1.5.1 From Gene to Protein

First evidence for the existence of MGLL (aka MGL or MAGL) was found in the 1960s in rat epithelial cells in the small intestine and in rat adipose tissue [31,32]. In both cases the researchers described an enzymatic activity that specifically hydrolyzed MAGs into glycerol and free fatty acids. The first extensive purification of MGLL from rat adipose tissue was performed in 1976 by Tornqvist and Belfrage of Lund University [33]. Karlsson *et al.* again from Lund University achieved a major breakthrough in the research of MGLL by cloning and sequencing an *Mgll* cDNA and deducing a 302 amino acid long sequence in 1997 [34]. In later works, the group showed that the *Mgll* gene is mapped to the chromosome 6 in mice in a region with homology to the chromosome 3q21 in humans [35]. The coding sequence for murine *Mgll* is spread on ten exons with several different 5′ leader sequences and two translation initiation codons allowing for different transcript variants [36].

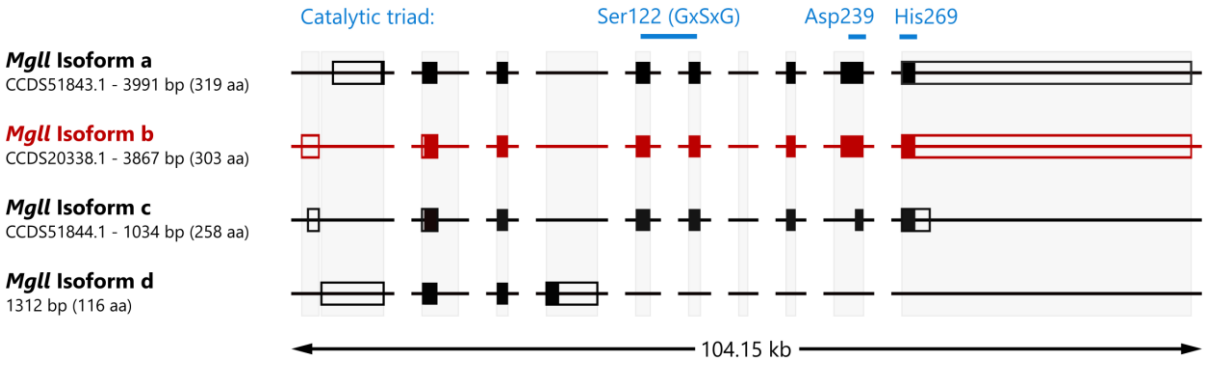

Figure 3. Map of the murine *Mgll* splice variants listed and curated by the NCBI Reference Sequence Database. CCDS identifier, transcript variant length and protein length are given below the transcript names. Clear boxes denote non-coding sequences, opaque boxes denote coding sequences. The first transcript variant deduced in 1997 by Karlsson *et al.* is labeled in red. The position of the catalytic triad is given in blue.

The transcript variant deduced 1997 uses the downstream start codon but contains all remaining coding sequences. It was the first described sequence of an enzyme with specific MAG hydrolyzing activity [34]. Today, several truncated transcription variants as well as longer isoforms that use the upstream start codon are documented [36]. A map of the four *Mgll* splice variants listed and curated by the Reference Sequence Database of the National Center for Biotechnology Information (NCBI) is given in **Figure 3** [37].

Table 1. MGLL orthologs found among eukaryotes.

Organism	Identity versus human MGLL [%]	Accession code
Human	100	NP_009214.1
Dog	92.7	XP_533717.2
Cow	85.8	XP_581556.4
Mouse	84.2	NP_035974.1
Rat	83.8	NP_612511.1
Chicken	70.4	XP_414365.2
Zebrafish	56.3	NP_956591.1
Arabidopsis thaliana	32.4	NP_568327.1
Oryza sativa	29.4	NP_001064121.1

Table from Labar *et al.* 2010 [38].

In 1997 only yeast, bacterial, and viral proteins with homologous sequences were known. A cowpox virus hypothetical protein showed more than 40 % sequence identity. Between 20 and 25 % identity were found for an esterase from *Pseudomonas putida* and one lysophospholipase each from *Escherichia. coli* and *Haemophilus. influenzae* [34]. Later, highly identical orthologs of MGLL were found in humans, dogs, cows, chickens, zebrafish, and *Arabidopsis thaliana* (**Table 1**). The human ortholog shows an amino acid sequence similarity of 84.2 % [38].

1.5.2 Structure and Function

Karlsson *et al.* were also the first to predict the secondary structure of MGLL using homology modeling techniques [34]. They located an α/β-hydrolase fold as the central core of the protein including its catalytical triad. Later, their findings were substantiated by crystal structure analysis [39–41]. The α/β-hydrolase fold is a common fold in hydrolytic enzymes of differing phylogenetic origin, substrate specificity, and catalytic activity. Still, enzymes with an α/β-hydrolase fold are assumed to be related by diverging evolution [42–44]. The fold was found in proteases, lipases, peroxidases, esterases, epoxide hydrolases and dehalogenases, which explains the sequence similarities between MGLL and bacterial enzymes discovered by Karlsson *et al.* [34,44]. The α/β-hydrolase fold is an α/β sheet, not a barrel, consisting of eight β-strands with the second strand being anti-parallel. The strands are connected and surrounded by α-helices [42]. The fold always contains a catalytic triad that facilitates substrate hydrolyzation by three interacting amino acid

residues: a base, an acid, and a nucleophile. In the case of MGLL these amino acids are His269, Asp239, and Ser122 which are brought into close proximity to each other by the secondary structure of the protein. The serine is located in the nucleophilic elbow, a sharp turn formed by the consensus sequence GXSXG [39–41]. Aspartate stabilizes the histidine which in turn polarizes the hydroxyl group of the serine. This allows serine to attack the carbonyl group of a MAG by forming a covalently bound intermediate. This intermediate is stabilized by an oxyanion hole formed by the backbone amides of Ala51 and Met123. This enables the hydrolysis of MAG in further steps (**Figure 4**).

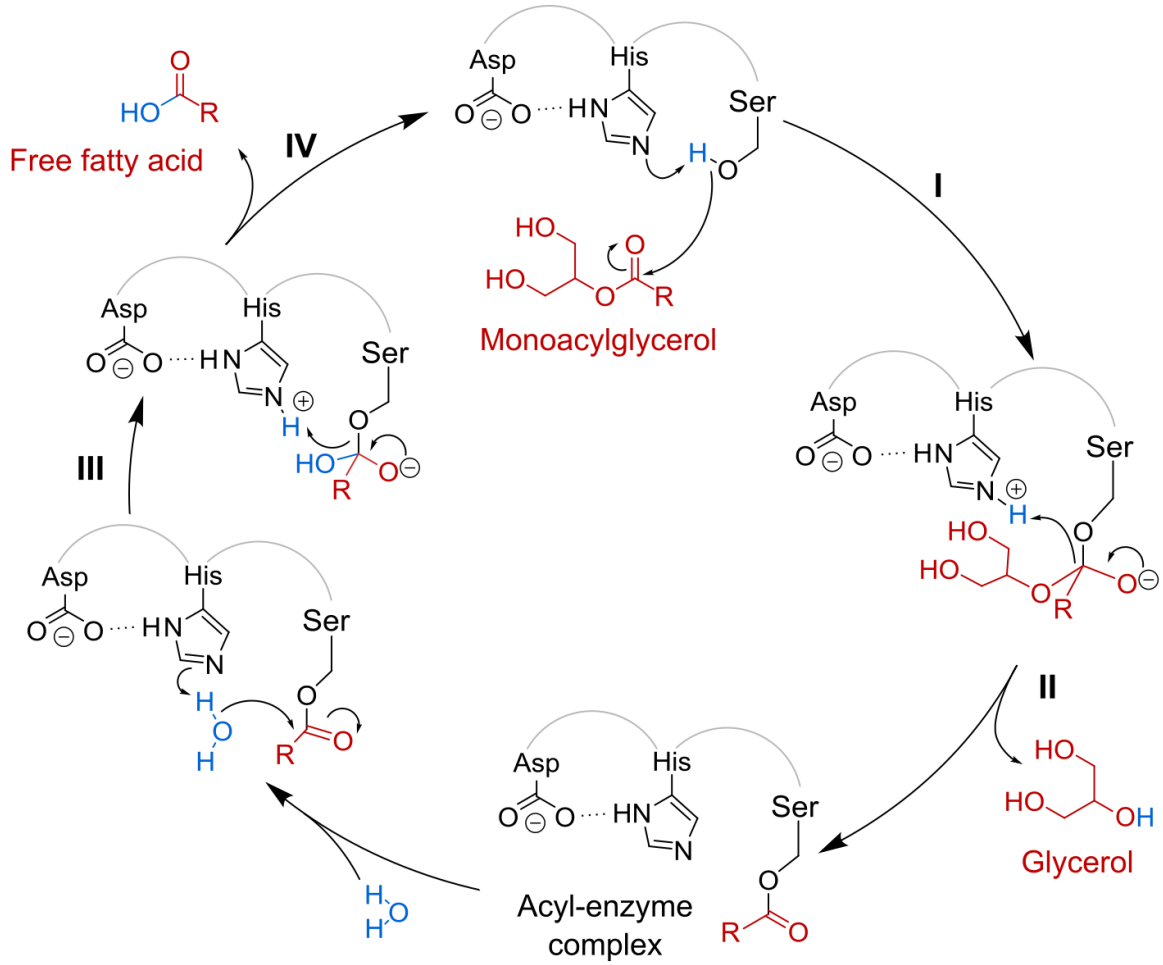

Figure 4. Catalytic mechanism of MGLL-mediated hydrolysis. (**I**) Ser122 is deprotonated by His269 and thereby activated. The activated Ser122 attacks the carbonyl carbon of the substrate (MAG) and forms a tetrahedral intermediate. (**II**) Cleavage of glycerol from the intermediate forms an acyl-enzyme complex. (**III**) Nucleophilic attack to the carbonyl group of the complex by an activated water molecule leads to deacylation and (**IV**) hydrolysis of the free fatty acid. Figure adapted from Gil-Ordóñez *et al.* 2018 [45].

Crystal structure analysis of MGLL revealed that the catalytic triad is sitting in the center of a binding pocket which is covered by a cap-domain (**Figure 5**). The cap of MGLL is vastly different from other known cap-domains such as those of human esterases and haloperoxidases or bacterial

α/β-hydrolases [39,41]. It is comprised of three α-helices two of which are MGLL-specific and one of which is part of the canonical α/β-hydrolase fold [39–41]. The formation of the cap-domain helps to dictate the substrate specificity. While it allows a wider access to the active site compared to haloperoxidases it restricts the access of bigger substrates such as di- and triglycerides [39]. The α4-helix is part of the cap-domain and also lines the access to the active site. It is highly hydrophobic with its nonpolar and lipophilic residues pointing towards the outside of the protein. Therefore, it is assumed that MGLL is an amphitropic enzyme that can anchor to or get in close contact to membranes or lipid droplets and guide its substrates towards the catalytical triad [39]. Indeed, MGLL overexpressed in HeLa and COS-7 cells both revealed association with the cell cytosol and the plasma membranes [46,47].

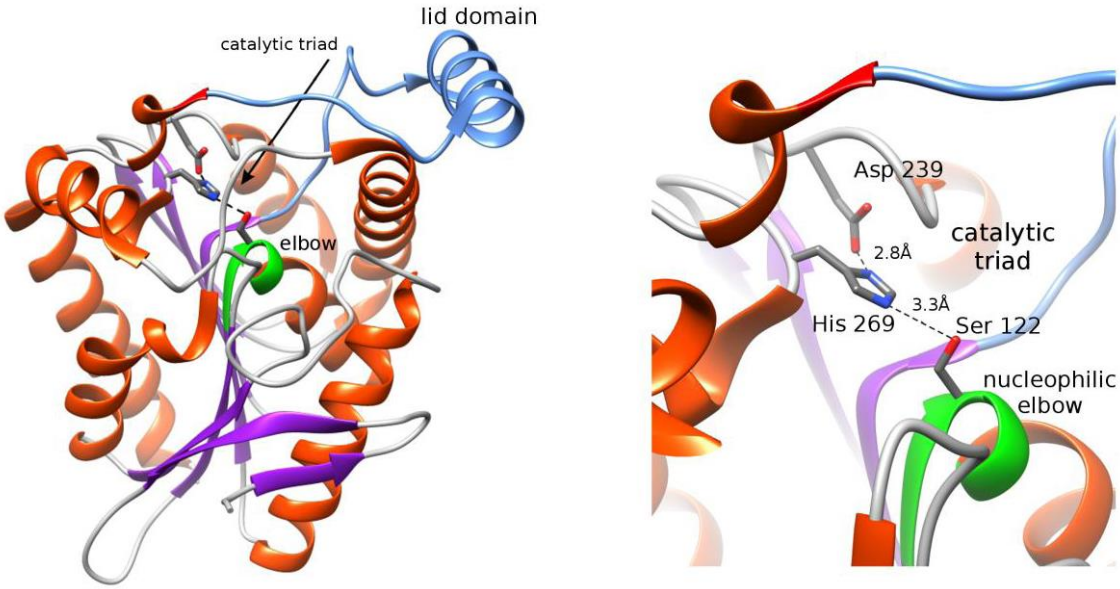

Figure 5. 3D structure of the human MGLL shown as one asymmetric subunit (PDB Code: 6BQ0). (**left**) The lid domain, the catalytic triad and the nucleophilic elbow are highlighted. (**right**) Zoom on the catalytic triad (Ser122, Asp239, and His269). Figure from Gil-Ordóñez *et al.* 2018 [45].

Furthermore, crystal structure analysis by Labar *et al.* found MGLL as a homodimer [39]. The proteins were oriented so that the active site entries with the α4-helices pointed in the same direction, allowing both proteins to interact with a membrane. As with many other lipases the cap-domain of MGLL is flexible. Crystal structures of an open conformation that allows access to the active site as well a closed conformation that completely buried a bound ligand were reported [39–41]. Schalk-Hihi and Schubert observed differences in the electrostatic potential of MGLL between the open and the closed form which in theory could affect membrane association [40]. They proposed a catalytic cycle in which MGLL naturally associates with a membrane in its open form but dissociates from it after

the uptake of a substrate and subsequent conformational change. Further studies are needed, to elucidate possible mechanisms that control enzyme activity and localization of MGLL.

1.5.3 Regulation

While not much is known about the mechanisms that regulate MGLL expression, activity, or localization there is clear evidence that these mechanisms exist. Tissue-specific changes of *Mgll* mRNA and protein expression as well as MGLL activity were observed during murine ontogeny suggesting transcriptional and post transcriptional regulation. Furthermore, MGLL expression was increased in the small intestine of mice after feeding a high-fat diet [48]. Rakhshandehroo *et al.* reported a PPAR-specific response element (PPRE) near the transcription start site of *Mgll* [49]. Peroxisome-proliferator-activated receptors (PPAR) are ligand-activated transcription factors that form heterodimers with the nuclear receptor RXR. They bind PPREs in the promoter region of target genes which leads to the recruitment of coactivators. The detected PPRE not only proved to be conserved in rat, dog, and human, it also showed an equally high putative binding strength for the PPAR types PPARα, PPARγ, and PPARβ/δ. PPARα is highly expressed in the liver and plays a role in hepatic fatty acid and glucose metabolism [49,50]. PPARγ is highly expressed in adipose tissue and is involved in adipocyte differentiation and lipid storage [51]. PPARβ/δ is ubiquitously expressed in mice and humans and has been connected to the regulation of insulin sensitivity, adipogenesis, as well as lipid and energy metabolism [52]. Rakhshandehroo *et al.* also reported the upregulation of MGLL expression by PPARα in murine, rat, and human hepatocytes [49]. Harmon *et al.* observed diminished MGLL expression in colonic epithelial cells of PPARγ KO mice and the binding of PPARγ to distal elements of the *Mgll* gene [53]. Another study found that Krüppel-like factor 4 binds to the *Mgll* promoter and accelerates MGLL expression *in vitro* [54].

Krüppel-like factor 4 is an evolutionarily conserved transcription factor and regulates processes like cell growth, proliferation, and differentiation [55]. A mode for the regulation of MGLL activity by post-translational modification was proposed by Dotsey *et al.* in neuronal cells [56]. They showed that hydrogen peroxide reduces MGLL activity in a reversible manner by sulfenylation of the cysteines C201 and C208. Molecular dynamics and metadynamics simulations as well as mass spectrometry studies confirmed these findings. They also provided evidence that the sulfenylation of the two cysteines shifts the conformation equilibrium of the cap-domain towards a closed conformation which would block active site access [57]. MGLL activity or localization could also be regulated by the tissue-specific expression of different isoforms. Western blot analysis by Karlsson *et al.* revealed heterogeneity in MGLL protein size in different mouse tissues possibly due to different sized isoforms [35]. The isoform NP_001159721.1 for example uses an alternate in-frame splice site, resulting in a large part of the cap-region being missing. It can be assumed that this alternative splice variant

significantly influences MGLL activity and localization [38]. For many lipases, a flexible cap-domain allows for a mechanism called *interfacial activation*. Contact with a lipid-water interface, such as a lipid droplet, triggers the opening of the cap, exposing the active site and increasing the enzyme activity [42–44]. Still, further studies are needed, to elucidate possible mechanisms that control MGLL expression, activity, and localization.

1.5.4 Tissue Distribution and Pathways

Research on MGLL started in rat and mouse adipose tissue in the 1960s and put the initial focus on its role in the breakdown of adipocyte lipid storages. However, soon *Mgll* mRNA transcripts were found in a variety of tissues. Especially high levels were observed in adipose tissue, testis, kidney, adrenal gland, and in the brain. This lead to the conclusion that MGLL functions as a widespread intracellular MAG hydrolyzing enzyme [34]. Indeed, MAGs are a ubiquitous intermediate during lipid breakdown. Lipids are not only broken down from TAG storages in adipocytes to mobilize energy. Dietary fat is hydrolyzed in the intestine by pancreatic lipase to free fatty acids and MAG allowing fat absorption [58]. The biggest source for MAGs are TAG-rich lipoproteins circulating the blood stream which are hydrolyzed by lipoprotein lipase to facilitate cellular uptake [59]. Internalized MAGs can then either be used for the resynthesis of TAGs by acyl-CoA:monoacylglycerol and acyl-CoA:diacylglycerol acyltransferases or get hydrolyzed by MGLL [60,61].

A major developmental push in MGLL research was triggered by the discovery of its involvement in endocannabinoid signaling in 2002 [46]. The endocannabinoid system consists of endogenous lipid neurotransmitters called endocannabinoids (EC) that bind to cannabinoid receptors (CB). EC include arachidonoyl ethanolamine and 2-arachidonoylglycerol (2-AG). The system was discovered after researching the psychoactive effects of cannabis which were caused by the cannabinoid Δ^9-tetrahydrocannabinol binding to neuronal CBs. In the central and peripheral nervous system, the endocannabinoid system acts as a retrograde signaling pathway which regulates synaptic stimulation. Briefly, postsynaptic neurons stimulated by presynaptic neurotransmitters release ECs into the synaptic cleft. The ECs then bind to presynaptic CBs which inhibits further neurotransmitter release. The fatty acid amide hydrolase and MGLL have been shown to be the primary enzymes degrading ethanolamine and 2-AG, respectively, thereby restoring presynaptic neurotransmitter release [38]. However, CBs are not only expressed in neuronal tissues. While cannabinoid receptor 1 (CB_1) is indeed highly expressed in the brain, it can also be found in lower concentrations in other tissues such as adipose tissue, liver, gastrointestinal tract, and skeletal muscle [62,63]. In contrast, cannabinoid receptor 2 (CB_2) is only found in low amounts in the brain but is also expressed in immune cells and the hematopoietic system [64,65]. Both receptors were shown to regulate a

multitude of processes in the brain and the periphery including energy metabolism, hormone release, and inflammation [65].

MGLL was also reported to be expressed and active in the mucosal and muscle layers of the small intestine [66]. However, its specific role in the intestine is currently elusive. MGLL overexpression in the small intestine of HFD-fed mice was shown to increase fat mass and food intake and to decrease energy consumption [67]. Yoshida *et al.* reported a CB_1-indipendent role of MGLL in intestinal fat absorption [68]. They also suggested involvement of MGLL in the regulation of food consumption via the gut–brain axis.

1.6 The Aim of the Thesis

Dysregulation of adipocyte lipolysis plays an important role in pathogenesis of obesity and its comorbidities such as insulin resistance and 2TD. The inhibition of the lipases involved is a promising therapeutic strategy. Global KO of MGLL in mice in the setting of diet-induced obesity reportedly improves adipose tissue inflammation, glucose tolerance, and insulin sensitivity while maintaining or improving body composition. However, because MGLL is ubiquitously expressed in the body and is involved in several metabolic pathways, it remains unclear whether reduced lipolytic activity in adipocytes is the actual cause of the observed effects. The aim of this thesis was to shed light on this issue by characterizing an adipose tissue-specific MGLL KO mouse model challenged with a high-fat diet. The mice will be analyzed in terms of body composition, glucose- and lipid metabolism, and inflammation, as well as metabolomic and transcriptomic changes. The thesis should provide insights into the role of MGLL in adipocyte lipolysis of obese individuals. It should also explore adipocyte-specific inhibition of MGLL as a therapeutic strategy in the treatment of obesity-related diseases.

2 Methods

2.1 Animals

All animal experiments were performed in accordance with the EU Directive 2010/63/EU and the German Animal Welfare Act and were approved by the District Government of Upper Bavaria (reference number: ROB-55.2-2532.Vet_02-13-145). MGL flox/AdiQ-Cre mice were used for this study and were kindly provided by Prof. Robert Zimmermann (Institute of Molecular Biosciences, University of Graz). These mice lack the expression of MGLL specifically in white and brown adipose tissue. They harbor two intronic loxP sites flanking *Mgll* exon three and four in chromosome six as well as a *cre* transgene under the control of an adiponectin promoter in chromosome nine. More details on the generation of this mouse model can be found in the publication of Taschler and Radner *et al.* in 2011 [27]. MGL flox/AdiQ-Cre mice were backcrossed to a C57BL/6J background (Charles River, Germany) for at least eight generations. C57BL/6J mice were bred in the animal facility of the German Mouse Clinic (Helmholtz Zentrum München, Germany) for up to three generations before reordering. The mice were housed in the animal facility of the German Mouse Clinic (Helmholtz Zentrum München, Germany) in type II polycarbonate cages in individually ventilated caging systems (Sealsafe plus, GM 500, Tecniplast, Buggugiate, Italy) under specific pathogen-free conditions. The cages were occupied with a maximum of five adult mice (floor area of 501 cm^2). Autoclaved wood chips and paper stripes (Lignocel select fine, Arbocel crinclets natural, J. Rettenmaier & Soehne, Rosenberg, Germany) were supplied as nesting material. The mice had *ad libitum* access to sterile-filtered tap water and an irradiated breeding diet (1314, Altromin, Lage, Germany). Room temperature and relative humidity were kept at 22 ± 2 °C and 55 ± 10 %. The lighting was set to a 12-hour light/dark cycle (on at 6 AM) with a 10 min transition period to simulate sunrise and sunset.

2.2 Cohort Data and Diet

Female and male homozygous loxP-flanked mice hemizygous for the *cre* transgene (KO) and homozygous loxP-flanked littermates not carrying the *cre* transgene (WT, Wildtype) were allocated to four groups at five to eight weeks of age (**Table 2**). They received either a high-fat diet (HFD, 60 kJ% fat, E15741-34) or a control diet (CD, 11 kJ% fat, E15000-04) both from ssniff Spezialdiäten GmbH, Soest, Germany. Detailed information on the diet composition is given in the appendix (**Table A1**). The groups 1 and 2 consisted of 40 male and 40 female mice, respectively, that were kept on the diet

for 12 weeks. The groups 3 and 4 consisted of 60 male and 60 female mice, respectively, that were kept on the diet for 24 weeks.

Table 2. Animal data.

Group	Weeks on diet	Sex	n	Genotype	Diet	Body weight [g]	Age [d]
1	12	Male	10	WT	CD	17.0±1.6	37±1
			10	WT	HFD	16.7±2.2	36±1
			10	KO	CD	17.6±1.0	37±1
			10	KO	HFD	16.6±2.0	36±1
2	12	Female	10	WT	CD	15.9±0.6	43±1
			10	WT	HFD	16.4±0.8	43±0
			10	KO	CD	15.6±1.2	43±1
			10	KO	HFD	16.8±1.0	43±0
3	24	Male	15	WT	CD	21.3±3.2	47±10
			15	WT	HFD	21.8±3.8	47±10
			15	KO	CD	21.2±3.1	46±10
			15	KO	HFD	21.2±3.4	46±10
4	24	Female	15	WT	CD	18.9±2.3	56±10
			15	WT	HFD	20.0±1.7	57±10
			15	KO	CD	17.9±2.4	52±11
			15	KO	HFD	19.2±2.8	52±11

Animal body weight at week 0 in grams (g) and age at week 0 in days (d) are given as mean ± SD. n: Number of animals.

2.3 Body Weight Analysis

The body weight of the mice was assessed on a weekly basis. In addition to the physical appearance and behavior of the mice, the body weight was also used as a measure of health. Mice that exhibited a consecutive weight loss of more than 10 % over a time period of 3 weeks were considered ill. In this case all data gathered at or after the moment the weight loss was detected were discarded. The same procedure was followed if a mouse died during the experiment.

2.4 Quantitative Nuclear Magnetic Resonance Analysis

Fat and lean mass as well as free fluid were quantified by quantitative nuclear magnetic resonance analysis (qNMR) using the Time Domain NMR analyzer minispec LF65 (Bruker BioSpin GmbH, Rheinstetten, Germany). The calibration of the instrument was validated on a daily basis using Bruker's daily check sample. The measurements were performed in accordance with the manufacturer's instructions. Briefly, the mouse was weighted shortly before the measurement and then carefully put in the restrainer. The restrainer was inserted into the probe of the instrument and

the body composition was analyzed. Finally, the mouse was put back into its cage and the restrainer was cleaned before the next measurement.

2.5 Tail Vein Blood Collection

Mice were restrained and the tail was warmed for 1 min under a heat lamp and wiped clean with 80 % ethanol. The lateral tail vein was punctured with a sterile needle (26G, 0.45 × 12 mm, Sterican, B. Braun Melsungen AG, Melsungen, Germany) and the blood was collected with EDTA-coated (K2E) capillary blood collection tubes (GK, Kabe Labortechnik GmbH, Nümbrecht-Elsenroth, Germany). The collection tubes were inverted several times immediately after sample collection to mix the blood with the anticoagulant. The tail puncture was compressed to stop the bleeding. Blood samples were kept at room temperature until they were centrifuged for 10 min at 4,500 x g and 4 °C within 45 min after sampling. The plasma supernatant was collected and stored at −80 °C.

2.6 Fasted Insulin Analysis

Before blood sampling mice were weighted and then fasted for four hours (6 AM to 10 AM). Then 50 µL of blood were sampled from the tail vein and blood plasma was isolated as described above. The quantification of insulin levels in murine plasma was performed in the Clinical Chemistry Screen of the German Mouse Clinic (Helmholtz Zentrum München, Germany) headed by Dr. Birgit Rathkolb. For the analysis, the Mouse/Rat Insulin Kit (Cat No: K152BZC, Meso Scale Diagnostics, Rockville, USA) was used. The kit is a sandwich immunoassay that utilizes an insulin detection antibody conjugated with an electrochemiluminescent label. The analysis was performed according to the manufacturer's instructions. Briefly, calibrator dilutions, block solution, detection antibody solution, and read buffer were prepared. The microwell plate provided by the kit was blocked with 150 µL/well of block solution. The plate was sealed and incubated for one hour with vigorous shaking (300–1000 rpm) at room temperature. The plate was washed three times with PBS-T. Then 40 µL/well of detection antibody solution as well as 10 µL/well of calibrator or plasma sample were added. The plate was sealed again and incubated for two hours with vigorous shaking (300–1000 rpm) at room temperature. The plate was washed 3 times with PBS-T and 150 µL/well of read buffer were added. Finally, the plate was analyzed using the MESO QuickPlex SQ 120 multiplexing imager (Meso Scale Diagnostics, Rockville, USA).

2.7 Glucose Tolerance Test

The blood sampling for insulin measurement and the glucose tolerance test (GTT) were performed consecutively. The mice were weighted and then fasted for a total of six hours (6 AM to 12 noon).

Two hours before the GTT, blood was drawn from the tail vein to perform insulin measurement. After that, the mice were put back into their cages. At 12 noon, the mice were transferred to separate cages without bedding. Blood glucose concentrations were measured using the Accu-Chek Aviva blood glucose meter and test strips (Roche Diagnostics Deutschland GmbH, Mannheim, Germany). To determine basal blood glucose levels a lateral cut was made in the last third of the tail. A small drop of blood was placed on the test strip and the glucose concentration was measured. A clean tissue was used to stop further bleeding. After that, 2 g glucose per kg body weight (sterile 20 % aqueous glucose solution, B. Braun Melsungen AG, Melsungen, Germany) were injected intraperitoneally. Depending on the body fat content of the mice needles of different length were used: 27G × 12 mm or 26G × 20 mm (Sterican, B. Braun Melsungen AG, Melsungen, Germany). Blood glucose levels were measured consecutively at 15, 30, 60, and 120 min after injection by removing the scab from the cut with a clean, moist tissue. Between measurements mice were kept separate in their bedding-free cages. At the end of the test, it was made sure that any bleeding had stopped. Finally, the mice were transferred back to their original cages and *ad libitum* access to food and water was provided. Mice whose blood glucose concentrations were outside the limits of quantification were removed from the dataset.

2.8 Insulin Tolerance Test

Before the insulin tolerance test (ITT) mice were weighted and then fasted for five hours (6:30 AM to 11:30 AM). The mice were transferred to separate cages without bedding shortly before the test. Blood glucose concentrations were measured using the Accu-Chek Aviva blood glucose meter and test strips (Roche Diagnostics Deutschland GmbH, Mannheim, Germany). To determine basal blood glucose levels a lateral cut was made in the last third of the tail. A small drop of blood was placed on the test strip and the glucose concentration was measured. A clean tissue was used to stop further bleeding. After that, 0.75 IU human insulin per kg body weight (Huminsulin® Normal 100, Lilly Deutschland GmbH, Bad Homburg, Germany; in 0.9 % sterile NaCl) were injected intraperitoneally. Depending on the body fat content of the mice needles of different length were used: 27G × 12 mm or 26G × 20 mm (Sterican, B. Braun Melsungen AG, Melsungen, Germany). Blood glucose levels were measured consecutively at 15, 30, 60, and 90 min after injection by removing the scab from the cut with a clean, moist tissue. Between measurements mice were kept separate in their bedding-free cages. At the end of the test, it was made sure that any bleeding had stopped. Finally, the mice were transferred back to their original cages and *ad libitum* access to food and water was provided.

2.9 Retro-Orbital Blood Collection

The blood collection by retro-bulbar puncture was performed between 6 and 11 AM. The food was removed from all cages at 5 AM and the mice were weighted. The procedure is described in detail in Rathkolb *et al.* 2013 [69]. Isoflurane anesthesia was induced using a Sigma Delta vaporizer, a SF2 flowmeter for compressed air and an anesthesia induction chamber for mice (UNO Roestvaststaal BV, Zenvenaar, Netherlands). The air flow was set to 1.5 L/min and the vaporizer was set to add 5 % isoflurane to the gas flow. Then the mouse was placed in the anesthesia induction chamber for two to three minutes until it showed no movement, relaxed muscles and a lowered breathing frequency indicating deep anesthesia. Then up to 1 mL blood was drawn from the retro-orbital venous sinus using non-heparinized glass capillaries about 1 mm in diameter and 20 to 30 mm in length (NeoLab Migge GmbH, Heidelberg, Germany). The blood was collected in EDTA-coated (K2E) collection tubes (GK, Kabe Labortechnik GmbH, Nümbrecht-Elsenroth, Germany). The collection tubes were inverted several times immediately after sample collection to mix the blood with the anticoagulant. Blood samples were kept at room temperature and then further processed for plasma collection or directly provided to the Immunology Screen. For plasma collection samples were centrifuged for 15 min at 5,000 x g and 8 °C within one hour after sampling. The plasma supernatant was collected and divided for different plasma analyses.

2.10 Organ Withdrawal

The mice were sacrificed directly after retro-orbital blood collection by cervical dislocation while still being under deep anesthesia. After the abdominal surface was wetted with 80 % ethanol, the abdominal skin was cut open longitudinally along the central midline and fixated at the sides. The abdominal cavity was opened, and organ samples were dissected. One liver lobe was dissected and cut into five aliquots. The left kidney was dissected and divided by a sagittal and transversal cut into four aliquots. Parametrial and epididymal white adipose tissue was completely excised and cut into two to six aliquots depending on the size of the fat depot. The lung was dissected completely and cut into four aliquots. Muscle tissue of the left thigh was excised and cut into four aliquots. The mouse was turned around, the back was wetted with 80 % ethanol, and the skin was cut open longitudinally between the scapulae. Then, the two interscapular depots of brown adipose tissue were excised. The aliquots were immediately snap-frozen by placing them on a dry ice-cooled metal plate and stored at −80 °C. However, one aliquot of white and brown adipose tissue was set aside and submerged in formalin + Zn for fixation. The carcass including the remaining organs was fixated by submersion in formalin. The dissection was executed as quickly as possible within a maximum of 15 min to minimize tissue degradation.

2.11 Clinical Blood Parameter Analysis

The analysis of clinical chemistry parameters in murine plasma was performed by the Clinical Chemistry Screen of the German Mouse Clinic (Helmholtz Zentrum München, Germany) headed by Dr. Birgit Rathkolb. The parameters cholesterol, non-esterified fatty acids (NEFA), glucose, glycerol, HDL-cholesterol, LDL-cholesterol, and triglycerides were quantified using the automated clinical chemistry analyzer AU480 (Beckman-Coulter GmbH, Krefeld, Germany). The AU480 system has capacity for up to 63 photometric tests for different parameters. The specific materials used for the analyzed parameters are given in **Table 3**. The sample preparation and analysis using the AU480 system are described in Rathkolb *et al.* 2013 [70].

Table 3. Parameters and Materials for the AU480 analyzer.

Parameter (SI units)	Test kit[a]	Calibrator	Control	Sample volume
Cholesterol (mmol/liter)	OSR6116 (BC)	OE66300	ODC0003 (Level 1), ODC0004 (Level 2)	1.6 µL
HDL-cholesterol (mmol/liter)	OSR6187 (BC)	ODC0011	ODC0005	1.6 µL
LDL-cholesterol (mmol/liter)	OSR6183 (BC)	ODC0012	ODC0005	1.6 µL
Triglycerides (mmol/liter)	OSR61118 (BC)	OE66300	ODC0003 (Level 1), ODC0004 (Level 2)	1.6 µL
NEFA (mmol/liter)	NEFA HR (Wako), REF434-91795 (HR-1), REF436-91995 (HR-2)	NEFA Standard, REF91096	REF410-00102 (Control I), REF416-00202 (Control II)	6 µL
Glycerol (mmol/liter)	GY105 (Randox)	151 GY	GY 1369	6 µL
Glucose (mmol/liter)	OSR6121 (BC)	OE66300	ODC0003 (Level 1), ODC0004 (Level 2)	1.6 µL

Information taken from Rathkolb *et al.* 2013 [70]; [a]The providers of the kits are given in brackets (BC: Beckman-Coulter GmbH, Krefeld, Germany; Wako: FUJIFILM Wako Chemicals Europe GmbH, Neuss, Germany; Randox: Randox Laboratories GmbH, Wülfrath, Germany). Calibrator and controls are from the same provider.

2.12 Flow Cytometry Analysis

Flow cytometry analysis was performed in murine whole blood. The analysis was conducted by the Immunology Screen of the German Mouse Clinic (Helmholtz Zentrum München, Germany) headed by Dr. Irina Treise. Two antibody panels were utilized. The first panel covered the frequencies of main leukocyte subsets (T cells, B cells, Neutrophils, NK cells, NK T cells, monocytes) as well as monocyte subpopulations. The second panel covered T cell and NK cell subpopulations. The

materials and solutions used for the analysis are given in **Table 4**. First, 15 µL/well of Fc-Block were added to 96-well plates. EDTA whole blood samples were resuspended carefully and 30 µL/well were added to the Fc-Block. The plates were shaken for 5 min at 600-700 rpm and 4 °C.

Table 4. Materials and solutions for flow cytometry analysis.

Material / Solution	Details	Provider
HEPES		Thermo Fisher Scientific. Waltham, USA (Life Technologies)
BSA		Sigma Aldrich, St. Louis, USA
EDTA (0.5M)		Thermo Fisher Scientific. Waltham, USA (Life Technologies)
DPBS	without Ca^{2+} and Mg^{2+}	Thermo Fisher Scientific. Waltham, USA (Life Technologies)
FC-Block	1:400 dilution in FACS Buffer	BD Biosciences, San Jose, USA
BD FACS Lysing Solution (10x)	1:10 dilution in aqua dest.	BD Biosciences, San Jose, USA
FACS Buffer	0,5 l DPBS, 0,372 g EDTA, 2,5 g BSA, 5 ml HEPES, sterile filtered	

Depending on the cell panel to be analyzed 15 µL/well of antibody mix were added (**Table 5**, **Table 6**). The plates were shaken at 600-700 x g and room temperature before they were incubated for 30-60 min at 4 °C. Then 150 µL/well of FACS Lysing Solution were added and the plates were shaken for 15 min at 600 x g and room temperature. The plates were centrifuged for 5 min at 400 x g and 10 °C. The supernatant (approx. 200 µL) was discarded and the cells were carefully resuspended in 200 µL/well of FACS-Buffer. The plates were centrifuged again for 5 min at 400 x g and 10 °C and the supernatant was discarded. Finally, the cells were resuspended in 120 µL/well of FACS-Buffer, stored at 4 °C and analyzed on the same day. The samples were analyzed with a Gallios flow cytometer (Beckman-Coulter GmbH, Krefeld, Germany) connected to a Hypercyt autosampler (Sartorius Group, Göttingen, Germany). If possible, a minimum of 10,000 cells per sample was measured.

Table 5. Antibody master mix for leukocyte and monocyte panel.

Antigen	Conjugate	Clone	Dilution factor	Provider
CD11b	Pacific Blue	M1/70.15	800	Thermo Fisher Scientific. Waltham, USA (Life Technologies)
CD11c	FITC	HL3	100	BD Biosciences, San Jose, USA
Ly-6G	Pacific Orange	RB6-8C5	1000	Thermo Fisher Scientific. Waltham, USA (Life Technologies)
NKp46	PE	29A1.4	200	Thermo Fisher Scientific. Waltham, USA (eBioscience)
NK1.1	PE	PK136	200	BD Biosciences, San Jose, USA
CD3e	PE-CF594	145-2C11	100	BD Biosciences, San Jose, USA
CD5	APC	53-7.3	2000	BD Biosciences, San Jose, USA
Ly-6C	PerCP-Cyanine5.5	HK1.4	400	Thermo Fisher Scientific. Waltham, USA (eBioscience)
CD45	Alexa Fluor 700	30-F11	1000	BioLegend, San Diego, USA
CD19	PE-Cyanine7	1D3	1000	BD Biosciences, San Jose, USA
CD45R	APC-Alexa Fluor 750	RA3-6B2	100	Thermo Fisher Scientific. Waltham, USA (Life Technologies)

Antibody conjugates were diluted with FACS-Buffer.

Table 6. Antibody master mix for T cell and NK cell panel.

Antigen	Conjugate	Clone	Dilution factor	Provider
CD5	eFluor 450	53-7.3	1000	Thermo Fisher Scientific. Waltham, USA (eBioscience)
γδ TCR	FITC	GL3	100	BD Biosciences, San Jose, USA
NK1.1	PE	PK136	200	BD Biosciences, San Jose, USA
NKp46	PE	29A1.4	200	Thermo Fisher Scientific. Waltham, USA (eBioscience)
CD44	Brilliant Violet 570	IM7	100	BioLegend, San Diego, USA
Ly-6C	PE-CF594	AL-21	200	BD Biosciences, San Jose, USA
CD25	APC	PC61	100	BD Biosciences, San Jose, USA
CD4	PerCP-Cyanine5.5	RM4-5	1000	Tonbo Biosciences, San Diego, USA
CD45	Alexa Fluor 700	30-F11	1000	BioLegend, San Diego, USA
CD62L	PE-Cyanine7	MEL-14	2000	Thermo Fisher Scientific. Waltham, USA (eBioscience)
CD8a	APC-Alexa Fluor 750	5H10	400	Thermo Fisher Scientific. Waltham, USA (Invitrogen)

Antibody conjugates were diluted with FACS-Buffer.

A life/dead staining was not performed. Instead, the amount of non-characterized cells (without T cells, B cells, NK cells, granulocytes, monocytes) was checked to be below 10 % of the total cells. The gating hierarchy for the analyzed subpopulations is described in **Table 7**.

Table 7. Gating hierarchy.

Panel	Cell type	Description
Leucocytes + Monocytes	B cells	B cells (CD19+ CD45R+)
	T cells	T cells (CD3+ CD5+ non-B cells)
	NK T cells	NKT cells (NK1.1+ NKp46+ T cells)
	Neutrophils	Neutrophils (Ly-6G+ CD11b+ non-B non-T cells)
	NK cells	NK cells (NK1.1+ NKp46+ non-B non-T non-Neutrophils)
	Monocytes	Monocytes (CD11b+ non-B non-T non-Neutrophile non-NK cells)
T cells + NK cells	T cells	CD5+ NK1.1- NKp46- cells
	NK cells	CD5- NK1.1+ NKp46+ cells
	CD4+ T cells	CD4+ CD8- T cells
	CD8+ T cells	CD8+ CD4- T cells

All cell types derived from CD45+ population.

2.13 Cytokine Analysis

The quantification of proinflammatory cytokine levels in murine plasma was performed in the Allergy Screen of the German Mouse Clinic (Helmholtz Zentrum München, Germany) headed by Dr. Juan Antonio Aguilar-Pimentel. For the analysis, the V-PLEX Proinflammatory Panel 1 Mouse Kit (Cat No: K15048D, Meso Scale Diagnostics, Rockville, USA) was used. This kit is a sandwich immunoassay that utilizes detection antibodies conjugated with electrochemiluminescent labels to quantify up to 10 proinflammatory cytokines (IFN-γ, IL-1β, IL-2, IL-4, IL-5, IL-6, CXCL1, IL-10,

IL-12p70, TNF-α). The analysis was performed according to the manufacturer's instructions. Briefly, 30 µL of plasma sample were diluted two-fold with the kit provided diluent. Calibrator dilutions, detection antibody solution, Wash Buffer, and Read Buffer were prepared. The microwell plate provided by the kit was washed three times with 150 µL/well of Wash Buffer. Then 50 µL/well of prepared samples and calibrators were added. The plate was sealed and incubated for two hours while shaking at room temperature. The plate was washed three times with 150 µL/well of Wash Buffer. Then 25 µL/well of detection antibody solution were added. The plate was sealed again and incubated for two hours while shaking at room temperature. The plate was washed three times with 150 µL/well of Wash Buffer and 150 µL/well of 2x Read Buffer were added. Finally, the plate was analyzed using the MESO QuickPlex SQ 120 multiplexing imager (Meso Scale Diagnostics, Rockville, USA). Samples with more than 60 % of cytokines below the limit of quantification were removed from the dataset.

2.14 Targeted Metabolomics

The targeted metabolomics analysis of murine plasma and tissue samples was performed with the Absolute*IDQ*™ p180 Kit (Biocrates, Innsbruck, Austria). The kit is using liquid chromatography-electrospray ionization-tandem mass spectrometry (LC-ESI-MS/MS) and flow injection analysis-electrospray ionization-tandem mass spectrometry (FIA-ESI-MS/MS) measurements to simultaneously quantify up to 188 endogenous metabolites from six compound classes (hexoses, amino acids, biogenic amines, acylcarnitines, glycerophospholipids, sphingolipids). Sample preparation and measurement were performed according to manufacturer's instructions (manual UM-P180) and have been described previously [71,72]. Tissue samples were preprocessed before being used in the kit. They were weighted and, if necessary, cut on a dry ice-cooled metal plate. The samples were transferred in dry ice-cooled homogenization tubes containing 1.4 mm ceramic beads (Precellys® Ceramic kit, PEQLAB, Erlangen, Germany). Pre-cooled ethanol/phosphate buffer (85/15 v/v) was added at a ratio of either 6 µL/mg sample for liver or 12 µL/mg sample for white and brown adipose tissue. The samples were homogenized with a Precellys® 24 homogenizer at −4 °C in three consecutive 20 sec cycles at 5,500 rpm with 30 sec breaks in between. The tissue homogenates were centrifuged for 5 min at 10,000 x g at 4 °C before they were either used in the kit or stored at −80 °C. Kit preparations began with the addition 10 µL of internal standard to the wells of an Absolute*IDQ* kit plate with the exception of the blank well. Then 10 µL of plasma samples or tissue homogenates, as well as PBS (zero sample), calibrators, quality control, and reference samples were added to the plate. Plasma and tissue samples were randomized in terms of plate number and position on the plate. The reference samples served as a second quality control and were used to

normalize measurement results of multiple kit plates. For the normalization of plasma samples pooled plasma from healthy humans (lot A9012311, Sera Laboratories International, West Sussex, United Kingdom) was used as reference sample. However, for the normalization of tissue samples pooled tissue from male and female MGL flox/AdiQ-Cre KO and WT mice was used. The samples were dried under a continuous nitrogen stream (Ultravap nitrogen evaporator, Porvair Sciences, Leatherhead, United Kingdom) for 30 min. Then 20 µL of derivatization solution was added and incubated for 20 min at room temperature. The solution consisted of 5 % v/v phenyl isothiocyanate in a 1:1:1 mixture of ethanol, water, and pyridine. The samples were dried again under nitrogen for 40 min. For the extraction 300 µL of 5 mM ammonium acetate in methanol were added and the plate was shaken at 450 rpm for 30 min at room temperature. Finally, the plate was centrifuged at 500 x g for 2 min and the flow-through was split into three fractions. The first 75 µL were diluted 1:2 with H_2O for LC-ESI-MS/MS analysis. A further 75 µL were diluted 1:5 with Biocrates running solvent for FIA-ESI-MS/MS analysis. Before measurement both dilutions were shaken at 600 rpm for 2 min. The remaining flow-through was stored as a backup at −80 °C. Except for the addition of tissue and murine plasma samples all pipetting steps were performed by a Hamilton Microlab STAR™ robot (Hamilton, Bonaduz, Switzerland).

While the LC-ESI-MS/MS analysis allows the quantification of up to 21 amino acids and 21 biogenic amines, the FIA-ESI-MS/MS analysis facilitates the quantification of up to 40 acylcarnitines, 90 glycerophospholipids (14 lysophosphatidylcholines, 76 phosphatidylcholines), 15 sphingolipids, and the sum of hexoses (90-95 % glucose). Metabolite identification and quantification are based on scheduled multiple reaction monitoring measurements (sMRM). HPLC separation and mass spectrometry measurement were performed according to manufacturer's instructions (manual UM-P180) using a PAL HTC autosampler (CTC Analytics, Zwingen, Switzerland) connected to a 1200 Series HPLC system (Agilent, Santa Clara, USA) followed by an API4000 mass spectrometer with a TurboV™ ESI source (Sciex, Darmstadt, Germany). Samples for the FIA-ESI-MS/MS analysis were directly injected into the mass spectrometer. However, samples for LC-ESI-MS/MS analysis were separated with an XDBC18 column (3 × 100 mm, 3.5 µm) and a C18 pre-column (Agilent, Santa Clara, USA) running an acetonitrile/water gradient containing 0.2 % formic acid. Autosampler, HPLC, and mass spectrometer were controlled by the Analyst software v1.6.2 (Sciex, Darmstadt, Germany). Raw data analysis for quantification and quality assessment were performed with MultiQuant™ v3.0 (Darmstadt, Germany) and MetIDQ™ software v6.4.8 (Biocrates, Innsbruck, Austria). Metabolite concentrations were calculated in µM using internal standards.

Before statistical evaluation of metabolomics data, quality control, missing value imputation, and plate normalization were applied using R software v3.5.1 in conjunction with RStudio v1.1.453 [73].

Metabolites with more than 60 % of sample concentrations below LOD on an individual plate were removed from the dataset. The LOD was calculated as the median zero sample concentration multiplied by three. Metabolites with more than 50 % of missing values on an individual plate were removed from the dataset as well. A missing value occurs if the metabolite concentration is below the detection limit of the mass spectrometer. To allow statistical analysis of the metabolomics data, the remaining missing values were imputed by replacing them with a randomly picked concentration from the median zero sample concentration ± 25 %. If the median zero sample concentration was missing as well, the minimum sample concentration ± 25 % was used instead. With every Absolute*IDQ* kit plate five replicates of either pooled human plasma or pooled murine tissue were measured as a reference for quantification accuracy and precision. The spread of these reference samples was evaluated by calculating the coefficient of variation (CV). All metabolites with a reference sample CV higher than 25 % on an individual plate were excluded from the dataset. Plate normalization allowed the joint analysis of samples located on different plates. For this purpose, sample concentrations were divided by the mean reference sample concentration of the individual plates and then multiplied with the mean value of all reference sample means.

2.15 Total RNA Sequencing

Total RNA sequencing was performed with white adipose tissue (WAT) from male mice after 24 weeks of diet. The RNA was isolated from WAT samples using the RNeasy Lipid Tissue Mini Kit (QIAGEN N.V., Venlo, The Netherlands) including the on-column DNase I digestion step, in accordance with the manufacturer's instructions. RNA concentration and purity were assessed (260/280 and 260/230 ratio) using the NanoDrop spectrophotometer (Thermo Fisher Scientific. Waltham, USA). The integrity of the RNA samples was analyzed using the 2100 Bioanalyzer system, 2100 Expert Software, and Bioanalyzer RNA 6000 Nano assay (Agilent Technologies, Inc., Santa Clara, USA). RNA integrity analysis was performed in accordance with the manufacturer's instructions. All samples exhibited RNA integrity numbers (RIN) greater than nine. Before sequencing RNA concentration was measured using the Qubit 4 Fluorometer and the Qubit RNA BR Assay Kit (Thermo Fisher Scientific. Waltham, USA) in accordance with the manufacturer's instructions. RNA samples were randomized and 1 µg (100 ng/µL) per sample was provided to the Institute of Human Genetics (Helmholtz Zentrum München, Germany) headed by Prof. Thomas Meitinger.

There, the library preparation was performed using the TruSeq Stranded Total RNA Library Prep Kit with Ribo-Zero (Illumina, San Diego, USA). Briefly, the cytoplasmatic rRNA was depleted and the RNA was fragmented and reverse transcribed. A-tailing, adaptor ligation, and library enrichment were performed as described in the High Throughput protocol of the TruSeq RNA Sample Prep

Guide (Illumina, San Diego, USA). cDNA libraries were assessed for quality and quantity with the 2100 Bioanalyzer system (Agilent Technologies, Inc., Santa Clara, USA) and the Quant-iT PicoGreen dsDNA Assay Kit (Thermo Fisher Scientific. Waltham, USA). The libraries were sequenced as 150 bp paired-end runs on an Illumina HiSeq4000 platform (San Diego, USA) with seven samples per lane and approx. 35 million reads. Split-read alignment against the human genome assembly hg19 (GRCh37) and UCSC known Gene annotation was performed using the STAR aligner v2.4.2a with modified parameter settings (--twopassMode=Basic) [74]. The python script HTseq-count v0.6.0 was used to quantify the number of reads mapping to annotated genes [75]. Fragments per kilobase of transcript per million fragments mapped values were calculated using custom scripts.

2.16 Quantitative Real-Time PCR

Quantitative real-time PCR was conducted by Anne Scheuvens as part of her bachelor thesis. The work was supervised by the author of this dissertation. Tissue samples for RNA isolation were obtained from backup mice that were not used in the animal experiments described in the paragraphs above. The mice were sacrificed by cervical dislocation and WAT, brown adipose tissue (BAT), and liver samples were collected and snap-frozen as described under section 2.9. The RNA was isolated from tissue samples using the RNeasy Lipid Tissue Mini Kit (QIAGEN N.V., Venlo, The Netherlands) including the on-column DNase I digestion step, in accordance with the manufacturer's instructions. RNA concentration and purity were assessed (260/280 and 260/230 ratio) using the NanoDrop spectrophotometer (Thermo Fisher Scientific. Waltham, USA). The integrity of the RNA samples was analyzed using the 2100 Bioanalyzer system, 2100 Expert Software, and Bioanalyzer RNA 6000 Nano assay (Agilent Technologies, Inc., Santa Clara, USA). RNA integrity analysis was performed in accordance with the manufacturer's instructions. All samples exhibited RNA integrity numbers (RIN) greater than nine. cDNA was synthesized from the isolated RNA using the RevertAid First Strand cDNA Synthesis Kit (Thermo Fisher Scientific. Waltham, USA) following the manufacturer's instructions. The quantitative PCR (qPCR) was carried out using the Power SYBR Green Mastermix and the ABI PRISM7900 HT Sequence Detection System (Thermo Fisher Scientific. Waltham, USA) in accordance with the manufacturer's instructions. The sequences of the primers used a listed in **Table 8**. Relative RNA expression was calculated using Delta-Delta-Ct method [76].

Table 8. Primer sequences for qPCR

Primer	Sequence
Mgll Fw (Exon 3)	GAG AGG ATG GTG TCG GA
Mgll Rv (Exon 4)	GAT TCC GGA TTG GCA AGG AC
Lipe Fw	GTG GCG AAA AGG CAA GAT CA
Lipe Rv	TGT TCC CGA ACA CCT GCA AA
Hprt1 Fw	GCC GAG GAT TTG GAA AAA GTG
Hprt1 Rv	TGT AAT CCA GCA GGT CAG CA

2.17 Immunohistochemistry

The immunohistochemical staining was conducted by Anne Scheuvens as part of her bachelor thesis with the support of the Pathology Screen of the German Mouse Clinic (Helmholtz Zentrum München, Germany) headed by Dr. Julia Calzada-Wack. The work was supervised by the author of this dissertation. Briefly, tissue samples were obtained from backup mice that were not used in the animal experiments described in the paragraphs above. The mice were sacrificed by cervical dislocation. WAT, BAT, and liver samples were collected as described under section 2.9 before they were fixed in formalin for 24 h and embedded in paraffin. Immunohistochemistry was performed on sections with a thickness of 2 µm in an automated immunostainer (Discovery®XT, Roche, Penzberg, Germany). Briefly, sections were incubated with a primary antibody against MGLL (ab24701, Abcam, Cambridge, United Kingdom) and a secondary biotin-conjugated goat anti-rabbit antibody with a streptavidin–peroxidase detection reagent. As a negative control, the primary antibody was omitted. While diaminobenzidine was used for the immunohistochemical staining, hematoxylin was used as counterstain. Digital images were captured with the digital slide scanner NanoZoomer® 2.0HT (Hamamatsu Photonics, Hamamatsu, Japan).

2.18 Statistics

Statistical analyses were performed using R software v3.5.1 in conjunction with RStudio v1.1.453 [73]. For comparison of two independent groups Wilcoxon rank sum test was used. P-values were corrected for multiple testing using the Benjamini & Hochberg procedure [77]. Differences between more than two independent groups were tested for significance using Kruskal-Wallis with post-hoc Dunn's tests. P-values were corrected for multiple testing using the Holm procedure [78]. Linear mixed-effects modelling was used for the longitudinal analysis of the effects of diet and genotype on body weight, body composition, and plasma metabolite levels. Models were fitted separately for each group and parameter. For body weight and body composition random and fixed effects were added consecutively. The corresponding model formulas are given in **Table 9**. Principle component analysis

was performed by singular value decomposition of the centered and scaled metabolomics and transcriptomics data. Partial least squares discriminant analysis (PLS-DA) was performed on metabolomics data using the web-based platform MetaboAnalyst v5.0 [79]. Differential expression analysis of transcriptomics data was performed using R software in conjunction with the Bioconductor package DESeq2 [80].

Table 9. Linear model formulas for the prediction of body weight, fat mass, lean mass, or free fluid.

Model	Added effects	Formula
Body weight		
1	Intercept-only	$y_i = b_0 + \varepsilon_i$
2	Random intercept	$y_i = b_0 + \mathbf{u_{0,ID}} + \varepsilon_i$
3	Diet week	$y_i = b_0 + u_{0,ID} + \mathbf{b_1 week_i} + \varepsilon_i$
4	Random slope	$y_i = b_0 + u_{0,ID} + \mathbf{u_{1,ID} week_i} + b_1 week_i + \varepsilon_i$
5	Diet	$y_i = b_0 + u_{0,ID} + u_{1,ID} week_i + b_1 week_i + \mathbf{b_2 diet_i} + \mathbf{b_3 week_i diet_i} + \varepsilon_i$
6	Genotype	$y_i = b_0 + u_{0,ID} + u_{1,ID} week_i + b_1 week_i + b_2 diet_i + b_3 week_i diet_i + \mathbf{b_4 genotype_i} + \mathbf{b_5 week_i genotype_i} + \mathbf{b_6 diet_i genotype_i} + \mathbf{b_7 week_i diet_i genotype_i} + \varepsilon_i$
Fat mass / Lean mass / Free fluid		
1	Intercept-only	$y_i = b_0 + \varepsilon_i$
2	Random intercept	$y_i = b_0 + \mathbf{u_{0,ID}} + \varepsilon_i$
3	Diet week	$y_i = b_0 + u_{0,ID} + \mathbf{b_1 week_i} + \varepsilon_i$
4	Diet	$y_i = b_0 + u_{0,ID} + b_1 week_i + \mathbf{b_2 diet_i} + \mathbf{b_3 week_i diet_i} + \varepsilon_i$
5	Genotype	$y_i = b_0 + u_{0,ID} + b_1 week_i + b_2 diet_i + b_3 week_i diet_i + \mathbf{b_4 genotype_i} + \mathbf{b_5 week_i genotype_i} + \mathbf{b_6 diet_i genotype_i} + \mathbf{b_7 week_i diet_i genotype_i} + \varepsilon_i$
Metabolomics		
1		$y_i = b_0 + u_{0,ID} + b_1 week_i + b_2 diet_i + b_3 week_i diet_i + b_4 genotype_i + b_5 week_i genotype_i + b_6 diet_i genotype_i + b_7 week_i diet_i genotype_i + \varepsilon_i$

y_i: Dependent variable (body weight, fat mass, lean mass, free fluid, or metabolite concentration); b_0: intercept; $u_{0,ID}$: random intercept for individual mouse; b_1-b_7: slopes; ε_i: residual.

3 Results

3.1 Knockout Verification

The verification of the adipose tissue-specific KO of MGLL of the mouse model used in this study was conducted by Anne Scheuvens as part of her bachelor thesis. The thesis is entitled "Validation of a Fat Tissue Specific Monoacylglycerol Lipase Knockout in Murine Tissue" and was submitted to the Technical University of Munich on July 2, 2018. The bachelor project was supervised by the author of this dissertation.

First, the KO was analyzed by relative quantification of *Mgll* mRNA in WAT and BAT (**Figure 6**). Liver tissue served as a control. The expression of *Lipe*, which encodes HSL, was also analyzed for comparative reasons. While MGLL has only MAG hydrolase activity, HSL has hydrolase activity specific for MAG as well as DAG. In comparison to WT mice, KO mice showed an approx. 0.15-fold decrease of *Mgll* in WAT and BAT, while mRNA levels in liver tissue were slightly increased. Relative expression of *Lipe* was not affected in WAT and BAT, but slightly increased in liver tissue as well.

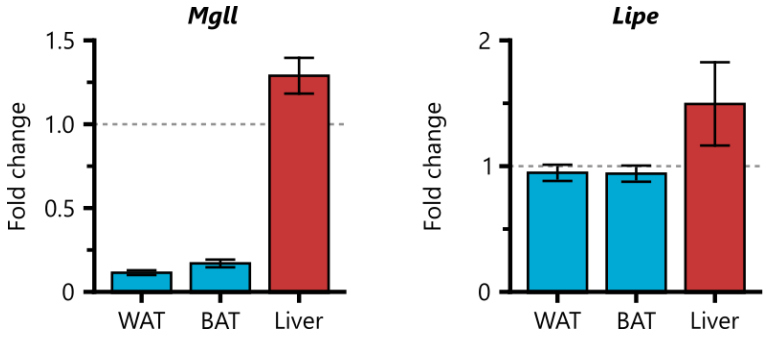

Figure 6. Relative RNA expression of *Mgll* and *Lipe* in WAT, BAT, and liver tissue of MGLL KO mice compared to WT mice. Total RNA was isolated from tissue samples. RNA integrity was verified before cDNA synthesis. Relative cDNA content was measured using qPCR. Fold change in RNA expression of *Mgll* and *Lipe* was calculated using Delta-Delta Ct method [76]. Hprt1 was used as normalizer and RNA levels of WT mice were used as calibrator.

Since the results of the qPCR analysis showed a residual, albeit very low, *Mgll* expression, an immunohistochemical analysis was performed (**Figure 7**). In contrast to WT mice, adipocytes of KO mice were negative for MGLL. However, other MGLL-positive cells and structures were found in WAT and BAT of KO mice. Liver tissue showed a faint staining for MGLL, but no differences between WT and KO mice could be observed.

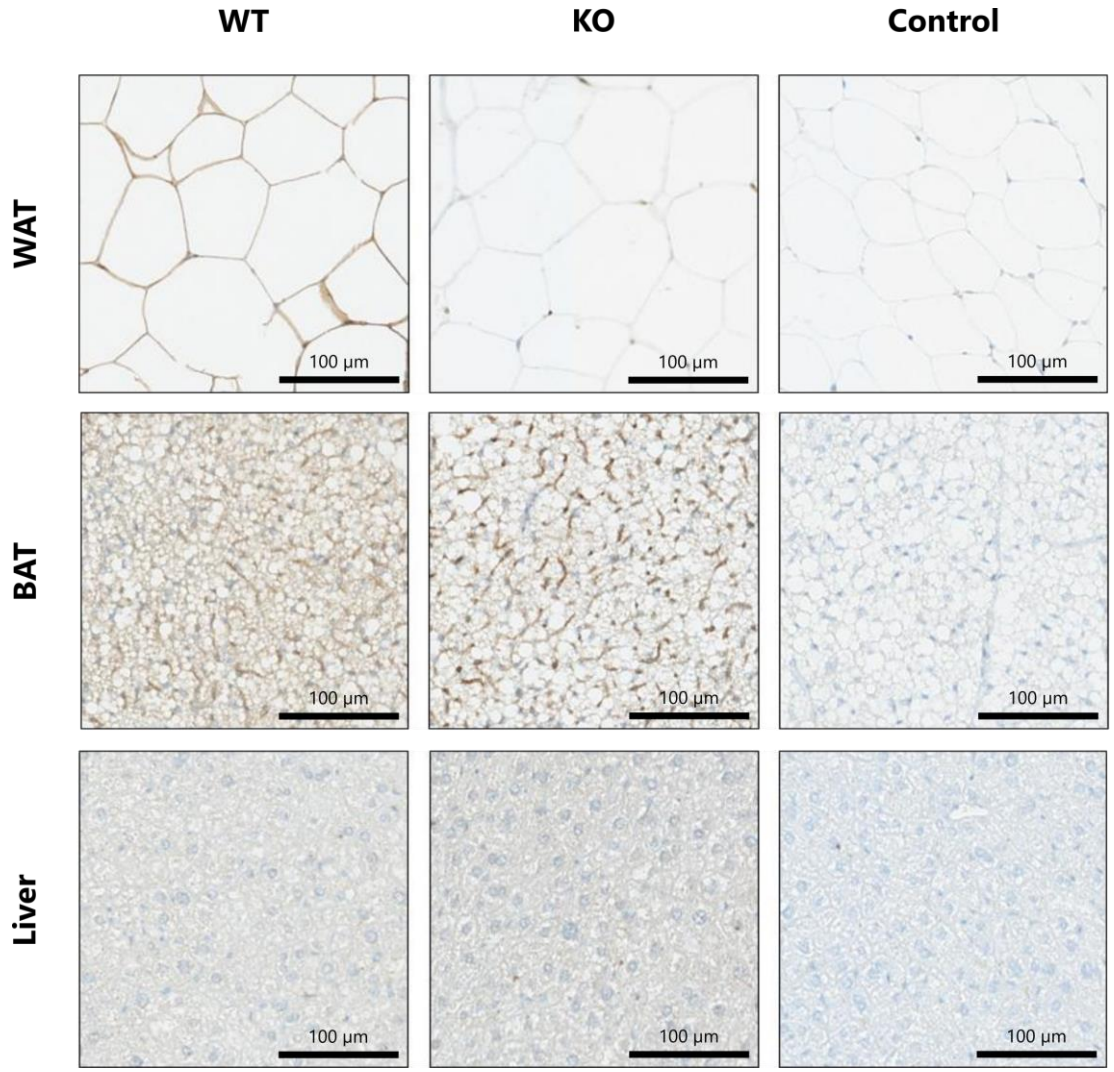

Figure 7. MGLL protein expression in WAT, BAT, and liver tissue of WT and KO mice. Immunohistochemical staining of MGLL using diaminobenzidine. Hematoxylin was used as counterstain. For the control WT tissues were stained but the primary antibody was omitted.

Key Results

1. *Mgll* mRNA levels are strongly reduced in adipose tissue of KO mice compared to WT mice
2. Adipocytes of KO mice show no MGLL protein expression, but adipose tissue contains other MGLL-positive cells or structures that are not affected by the KO.

3.2 Experimental Design

WT and KO mice were allocated to four groups at five to eight weeks of age and received either a high-fat diet (HFD) or a control diet (CD). The groups 1 and 2 consisted of male and female mice, respectively, that were kept on the diet for 12 weeks. The groups 3 and 4 consisted of male and female mice, respectively, that were kept on the diet for 24 weeks. Throughout the experiment analyses were

performed and samples were collected (**Figure 8**). The body weight was assessed on a weekly basis. Blood was collected from the tail vein at weeks 0, 6, 10, 14, and 22 and the isolated plasma was used for targeted metabolomics analysis. Body composition analysis using qNMR was carried out at weeks 0, 8, 16, and 23. Glucose metabolism was investigated by intraperitoneal ITT at week 16 as well as intraperitoneal GTT and fasted insulin test at week 18. At the end of the experiment at weeks 12 and 24 mice were sacrificed by terminal bleeding. Samples of the obtained whole blood were used to determine the frequencies of main leukocyte subsets by flow cytometry. Isolated blood plasma was used for targeted metabolomics analysis, analysis of clinical chemical parameters, and proinflammatory cytokine analysis. Organs were harvested to perform targeted metabolomics analysis.

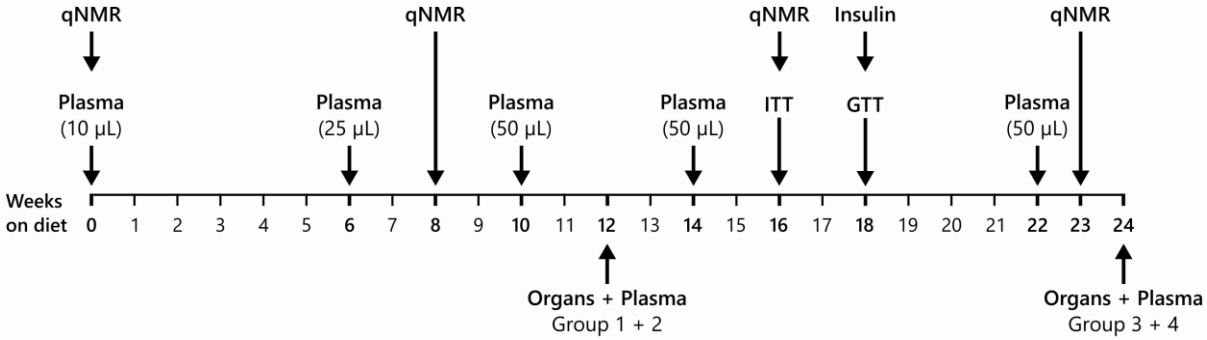

Figure 8. Experiment schedule. Animals received either CD or HFD right after the initial qNMR measurement and plasma collection at week 0. The gathered plasma volume is given in brackets. qNMR: Quantitative nuclear magnetic resonance; ITT: Intraperitoneal insulin tolerance test; GTT: Intraperitoneal glucose tolerance test; Insulin: Fasted insulin test.

3.3 Body Composition

The development of body composition during the experiment was assessed by body weight measurements as well as fat mass, lean mass, and free fluid analysis. The animal body weight was assessed on a weekly basis (**Figure 9**). During the experiment all mice showed in increase in body weight. Animals fed a HFD exhibited a higher body weight gain and a significantly higher final body weight compared to animals fed a CD. Furthermore, male mice showed a higher body weight gain and a higher final body weight compared to their female counterparts. In general, animals fed a HFD exhibited a higher variability in body weight compared to animals fed a CD. Minor and inconsistent genotype-dependent differences were observed in male mice. WT mice of group 1 fed a HFD were found to be heavier than KO mice fed the same diet, while in group 3 the opposite was the case. Furthermore, genotype-dependent differences of the final body weight were not significant.

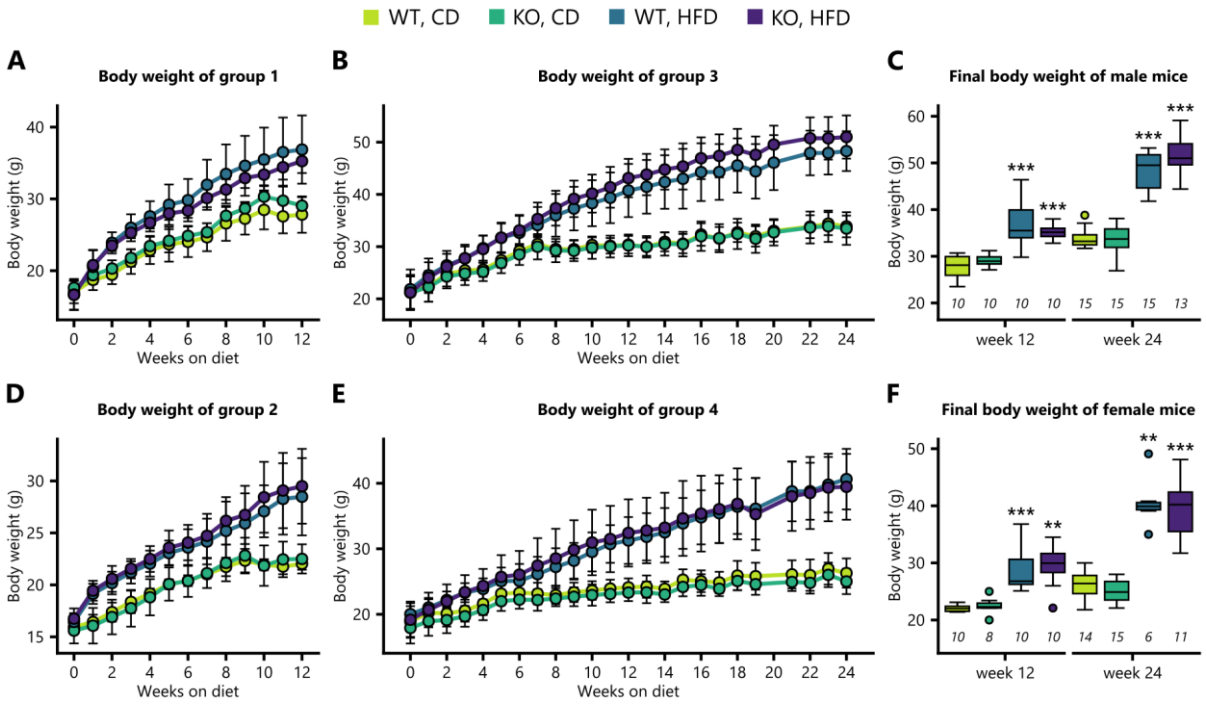

Figure 9. Body weight is affected by diet duration and diet but not by genotype. (**A**, **B**, **D**, **E**) Body weight changes during 12 or 24 weeks of diet. Dots and error bars represent the mean and the standard deviation, respectively. (**C**, **F**) Final body weight differences after 12 or 24 weeks of diet. Body weight differences were tested for significance using Wilcoxon rank sum tests. *P*-values were corrected for multiple testing using the Benjamini & Hochberg procedure [77]. No significant genotype-dependent differences were found. Significant diet-dependent differences between mice with the same sex, genotype, and duration of diet are labeled with asterisks: * p≤0.05; ** p≤0.01; *** p≤0.001. The number of animals is given below the boxes in italics.

Linear mixed-effects modelling was used for a longitudinal analysis of the effects of diet and genotype factoring in all body weight measurements performed during the experiment. The modelling approach allowed the use of random intercepts and slopes for each individual mouse which allows to factor in missing values and the correlation introduced by repeated measurements. To assess their importance for the model fit the predictors diet week, diet, and genotype were added incrementally and the model fit was compared using the chi-square test (**Table A2**). Random intercepts and slopes significantly improved the model fit for all groups capturing the differences in body weight and body weight gain of the individual animals. Diet week and diet significantly improved the model fit in all groups as well, suggesting that both are important predictors of body weight. However, the predictor genotype only improved the model fit for group 3 suggesting a more nuanced effect of the KO of MGLL on body weight. The coefficients of the final models were analyzed with WT mice fed a HFD as reference (**Table 10**). The model coefficients with WT mice fed a CD as reference can be found in the appendix (**Table A3**). The coefficient diet week exhibited a highly significant and positive slope for both references and all groups indicating a body weight increase during the experiment in WT mice fed either a HFD or a CD. The interaction term for diet week and

diet was highly significant as well, showing that the body weight gained per week differed in WT mice fed a HFD compared to WT mice fed a CD. A significant effect of the KO of MGLL was only observed in male mice for the interaction terms of diet week and genotype as well as diet week, diet, and genotype. This shows that the genotype of the mice affects their diet-induced body weight gain. However, the coefficient values describing the effect direction in the groups 1 and 3 were opposed to each other and therefore inconclusive.

Table 10. Model coefficient statistics for the prediction of body weight with WT, HFD mice as reference.

Group	Coefficient	Value	SE	DF	*t*-value	*p*-value
1	Diet week	1.58	0.07	476	21.78	<0.001
	Diet (CD)	-1.80	0.57	36	-3.13	0.003
	Genotype (KO)	-0.10	0.57	36	-0.17	0.865
	Diet week : Diet (CD)	-0.64	0.10	476	-6.22	<0.001
	Diet week : Genotype (KO)	-0.19	0.10	476	-1.83	0.067
	Diet (CD) : Genotype (KO)	0.47	0.81	36	0.58	0.566
	Diet week : Diet (CD) : Genotype (KO)	0.29	0.15	476	2.02	0.044
2	Diet week	0.92	0.07	470	13.57	<0.001
	Diet (CD)	-1.33	0.46	36	-2.88	0.007
	Genotype (KO)	0.21	0.46	36	0.46	0.652
	Diet week : Diet CD)	-0.37	0.10	470	-3.88	<0.001
	Diet week : Genotype (KO)	0.07	0.10	470	0.75	0.454
	Diet (CD) : Genotype (KO)	-0.89	0.65	36	-1.37	0.179
	Diet week : Diet (CD) : Genotype (KO)	0.06	0.14	470	0.44	0.658
3	Diet week	1.06	0.04	1354	26.22	<0.001
	Diet (CD)	-1.37	0.89	56	-1.53	0.132
	Genotype (KO)	-0.62	0.89	56	-0.69	0.491
	Diet week : Diet (CD)	-0.62	0.06	1354	-10.73	<0.001
	Diet week : Genotype (KO)	0.23	0.06	1354	3.93	<0.001
	Diet (CD) : Genotype (KO)	0.25	1.26	56	0.19	0.846
	Diet week : Diet (CD) : Genotype (KO)	-0.22	0.08	1354	-2.74	0.006
4	Diet week	0.80	0.04	1217	21.16	<0.001
	Diet (CD)	-0.27	0.75	56	-0.36	0.717
	Genotype (KO)	0.53	0.75	56	0.71	0.481
	Diet week : Diet (CD)	-0.52	0.05	1217	-10.47	<0.001
	Diet week : Genotype (KO)	0.00	0.05	1217	0.03	0.973
	Diet (CD) : Genotype (KO)	-1.44	1.06	56	-1.36	0.179
	Diet week : Diet (CD) : Genotype (KO)	0.00	0.07	1217	-0.06	0.950

SE: Standard error; DF: Degrees of freedom.

Fat mass, lean mass and free fluids were quantified using quantitative nuclear magnetic resonance analysis. Measurements were performed at week 0 and 8 with the groups 1 and 2 and at week 0, 8, 16, and 23 with the groups 3 and 4. Fat mass, lean mass, and free fluids are affected by changes in total body weight. Therefore, percentages of the quantified parameters relative to the body weight were calculated (**Figure 10**). Despite clear differences in body weight between male and female mice, similar changes in body composition were observed in both sexes.

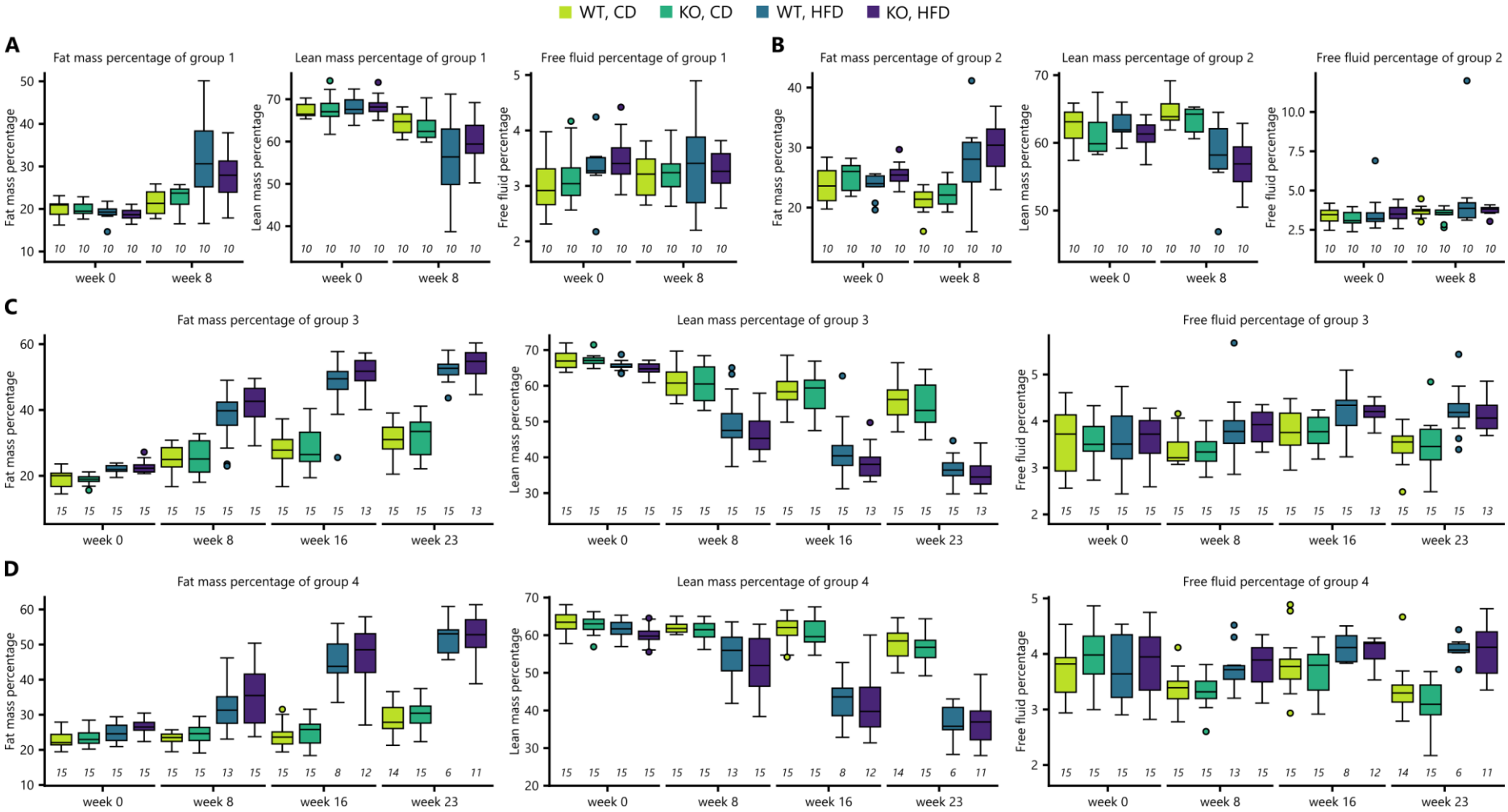

Figure 10. Body composition is affected by time and diet but not by genotype. Fat mass, lean mass, and free fluid were quantified by qNMR at different time points. Percentages were calculated by division by body weight. The groups 1 (**A**) and 2 (**B**) were analyzed at the beginning of the experiment and after 8 weeks of diet. The groups 3 (**C**) and 4 (**D**) were additionally analyzed after 16 and 23 weeks of diet. The number of animals is given below the boxes in italics.

Male and female mice started with body fat percentages of 20 % and 25 %, respectively. Animals fed a CD reached approx. 30 % body fat at week 23, while mice fed a HFD reached approx. 55 %. While no clear genotype-dependent differences were detected, a tendency for higher body fat percentages in KO mice was observed. Lean mass behaved inversely proportional to fat mass. Male and female mice started with lean mass percentages of 68 % and 63 %, respectively. Animals fed a CD reached approx. 55 % lean mass at week 23, while mice fed a HFD reached approx. 35 %. Again, no clear genotype-dependent differences were detected, but a tendency for lower lean mass percentages in KO mice was observed. The free fluid percentage ranged between 3 % and 4.5 % throughout the experiment with a high variability at week 0. In the following measurements the variability decreased and diet-dependent differences became visible. At week 23 CD-fed mice exhibited free fluid percentages of approx. 3 % while HFD-fed mice showed percentages of approx. 4 %. Genotype-dependent differences were not observed.

Linear mixed-effects modelling was used to further analyze the effects of diet and genotype on the body composition while considering all qNMR measurements performed during the experiment. The modelling approach allowed the use of random intercepts for each individual mouse which allows to factor in missing values and the correlation introduced by repeated measurements. Here, absolute values of fat mass, lean mass, and free fluid were used as outcome variable since percentages can lead to invalid results. To assess their importance for the model fit the predictor diet week, diet, and genotype were added incrementally and the model fit was compared using the chi-square test (**Table A4**). Diet week and diet significantly improved the model fit for fat mass, lean mass, and free fluid in all groups suggesting that diet week and diet are important predictors of body composition. However, the predictor genotype only improved the model fit for fat mass in group 3. The coefficients of the final models were analyzed with WT mice fed a HFD as reference (**Table 11**). The model coefficients with WT mice fed a CD as reference can be found in the appendix (**Table A5**). The coefficient diet week exhibited a highly significant and positive slope for both references and all outcomes of all groups confirming the observed increase in absolute fat mass, lean mass, and free fluid during the experiment in WT mice fed a HFD or CD. One exception was observed for the fat mass of the CD-fed WT mice of group 2 which was still positive but not significant. The interaction term of diet week and diet was highly significant for fat mass but not lean mass or free fluid in all groups. This substantiated the observed higher fat gain per week in WT mice fed a HFD compared to mice fed a CD. The interaction terms of diet week and genotype were largely not significant for both references and all outcomes. This shows that the gains in fat mass, lean mass, and free fluid observed during the experiment in WT mice fed a HFD or a CD are indiscernible from the gains of KO mice fed the same diet.

Table 11. Model coefficient statistics for the prediction of fat mass, lean mass, or free fluid with WT, HFD mice as reference.

		Fat mass					Lean mass					Free fluid				
Group	**Coefficient**	**Value**	**SE**	**DF**	***t***	***p***	**Value**	**SE**	**DF**	***t***	***p***	**Value**	**SE**	**DF**	***t***	***p***
1	Diet week	0.96	0.10	36	9.60	<0.001	0.89	0.07	36	13.00	<0.001	0.08	0.01	36	7.66	<0.001
	Diet (CD)	0.21	0.88	36	0.24	0.813	0.15	0.56	36	0.27	0.792	-0.03	0.08	36	-0.36	0.719
	Genotype (KO)	-0.15	0.88	36	-0.17	0.866	0.07	0.56	36	0.12	0.902	0.03	0.08	36	0.36	0.719
	Diet week : Diet (CD)	-0.68	0.14	36	-4.76	<0.001	-0.19	0.10	36	-1.95	0.059	-0.03	0.01	36	-2.44	0.020
	Diet week : Genotype (KO)	-0.27	0.14	36	-1.92	0.063	0.04	0.10	36	0.37	0.712	-0.02	0.01	36	-1.35	0.184
	Diet (CD) : Genotype (KO)	0.21	1.24	36	0.17	0.867	0.38	0.80	36	0.48	0.637	0.01	0.12	36	0.09	0.932
	Diet week : Diet (CD) : Genotype (KO)	0.32	0.20	36	1.59	0.121	-0.04	0.14	36	-0.26	0.794	0.02	0.02	36	0.96	0.345
2	Diet week	0.40	0.06	36	6.23	<0.001	0.53	0.03	36	19.84	<0.001	0.07	0.01	36	6.55	<0.001
	Diet (CD)	-0.12	0.53	36	-0.23	0.823	-0.33	0.31	36	-1.07	0.294	-0.06	0.12	36	-0.50	0.621
	Genotype (KO)	0.37	0.53	36	0.70	0.491	-0.04	0.31	36	-0.13	0.898	0.00	0.12	36	0.00	1.000
	Diet week : Diet (CD)	-0.30	0.09	36	-3.29	0.002	-0.03	0.04	36	-0.72	0.474	-0.04	0.01	36	-2.44	0.020
	Diet week : Genotype (KO)	0.06	0.09	36	0.66	0.513	0.03	0.04	36	0.89	0.381	-0.02	0.01	36	-1.43	0.161
	Diet (CD) : Genotype (KO)	-0.20	0.75	36	-0.27	0.792	-0.40	0.44	36	-0.91	0.367	-0.05	0.17	36	-0.29	0.771
	Diet week : Diet (CD) : Genotype (KO)	-0.04	0.13	36	-0.30	0.764	0.02	0.05	36	0.33	0.747	0.02	0.02	36	1.13	0.266
3	Diet week	0.89	0.03	172	29.47	<0.001	0.13	0.02	172	5.30	<0.001	0.06	0.00	172	20.46	<0.001
	Diet (CD)	-1.26	0.99	56	-1.27	0.210	-0.09	0.65	56	-0.14	0.893	-0.06	0.08	56	-0.77	0.442
	Genotype (KO)	0.45	0.99	56	0.45	0.655	-0.65	0.65	56	-0.99	0.326	0.00	0.08	56	-0.03	0.973
	Diet week : Diet (CD)	-0.61	0.04	172	-14.23	<0.001	0.07	0.03	172	1.92	0.057	-0.03	0.00	172	-9.10	<0.001
	Diet week : Genotype (KO)	0.12	0.04	172	2.82	0.005	0.04	0.04	172	1.13	0.261	0.00	0.00	172	1.26	0.209
	Diet (CD) : Genotype (KO)	-0.43	1.40	56	-0.31	0.759	0.52	0.93	56	0.56	0.577	-0.01	0.12	56	-0.05	0.957
	Diet week : Diet (CD) : Genotype (KO)	-0.12	0.06	172	-1.93	0.055	-0.06	0.05	172	-1.24	0.216	0.00	0.01	172	-0.89	0.373
4	Diet week	0.66	0.03	150	19.66	<0.001	0.11	0.02	150	5.27	<0.001	0.04	0.00	150	13.10	<0.001
	Diet (CD)	-0.39	0.88	56	-0.45	0.656	-0.36	0.41	56	-0.88	0.382	-0.03	0.06	56	-0.57	0.572
	Genotype (KO)	0.59	0.88	56	0.68	0.502	-0.50	0.41	56	-1.21	0.230	0.03	0.06	56	0.44	0.665
	Diet week : Diet (CD)	-0.52	0.04	150	-12.44	<0.001	0.04	0.03	150	1.39	0.167	-0.03	0.00	150	-7.54	<0.001
	Diet week : Genotype (KO)	0.01	0.04	150	0.17	0.866	-0.01	0.03	150	-0.25	0.805	0.00	0.00	150	-0.32	0.751
	Diet (CD) : Genotype (KO)	-0.67	1.23	56	-0.54	0.591	-0.18	0.57	56	-0.31	0.755	-0.02	0.09	56	-0.21	0.833
	Diet week : Diet (CD) : Genotype (KO)	0.00	0.06	150	0.05	0.964	0.00	0.04	150	0.09	0.931	0.00	0.00	150	-0.62	0.533

SE: Standard Error; DF: Degrees of freedom; *t*: *t*-value; *p*: *p*-value.

One exception were the HFD-fed mice of group 3 with a significant interaction of diet week and genotype suggesting genotype-dependent differences. However, as with the body weight the slope of this interaction in group 3 is positive while the slope for the male mice of group 1 is negative. The observed genotype effect is therefore inconsistent. Likewise, the interaction term of diet week, diet, and genotype was not significant for all outcomes of all groups which shows that the genotype does not affect the diet-induced gains in fat mass, lean mass, and free fluid.

Key Results

1. The body composition of mice changes with age. Within 12 or 24 weeks all mice exhibited:
   - ❖ An increase in body weight.
   - ❖ A shift towards higher fat mass and lower lean mass percentage per body weight.
2. The body composition of mice is affected by diet. Feeding an HFD:
   - ❖ Significantly increased body weight and fat mass.
   - ❖ Amplified the shift to higher fat mass percentages per body weight.
   - ❖ Increased the free fluid mass per body weight.
3. The effect of the MGLL KO on body composition of mice is weak and inconclusive.
   - ❖ Only male mice fed a HFD exhibited weak effects on body weight and body fat percentages.
   - ❖ The observed effects were in contradiction depending on the duration of the diet.

3.4 Immune System

The effects of the HFD and the adipose tissue-specific KO of MGLL on the murine immune system were investigated by analysis of proinflammatory cytokine levels and leucocyte subset frequencies at the end of the experiment after either 12 or 24 weeks of diet. Plasma levels of the proinflammatory cytokines TNF-α, interferon γ (IFN-γ), the C-X-C motif chemokine ligand 1 (CXCL1) as well as the interleukins (IL) IL-1β, IL-2. IL-4, IL-5, IL-6, and IL-10 were measured using an electrochemiluminescence-based immunoassay (**Figure 11**). Across the measured cytokines no consistent effect of diet duration, diet, or genotype was observed. Cytokine variability was high which can hide possible effects. Differences in cytokine levels were mostly observed in males. Female mice showed no differences in plasma concentrations of IL-2, IL-4, IL-10, and TNF-α. While male and female cytokine levels were within similar concentration ranges, concentrations of IL-1β and IL-6 were generally higher in male mice. Furthermore, cytokine concentrations of IL-2, IL-4, IL-10, and IFN-γ were overall lower at week 24 compared to week 12. The opposite was the case for CXCL1 with higher concentrations being observed at 24 weeks compared to 12 weeks of diet in males and females.

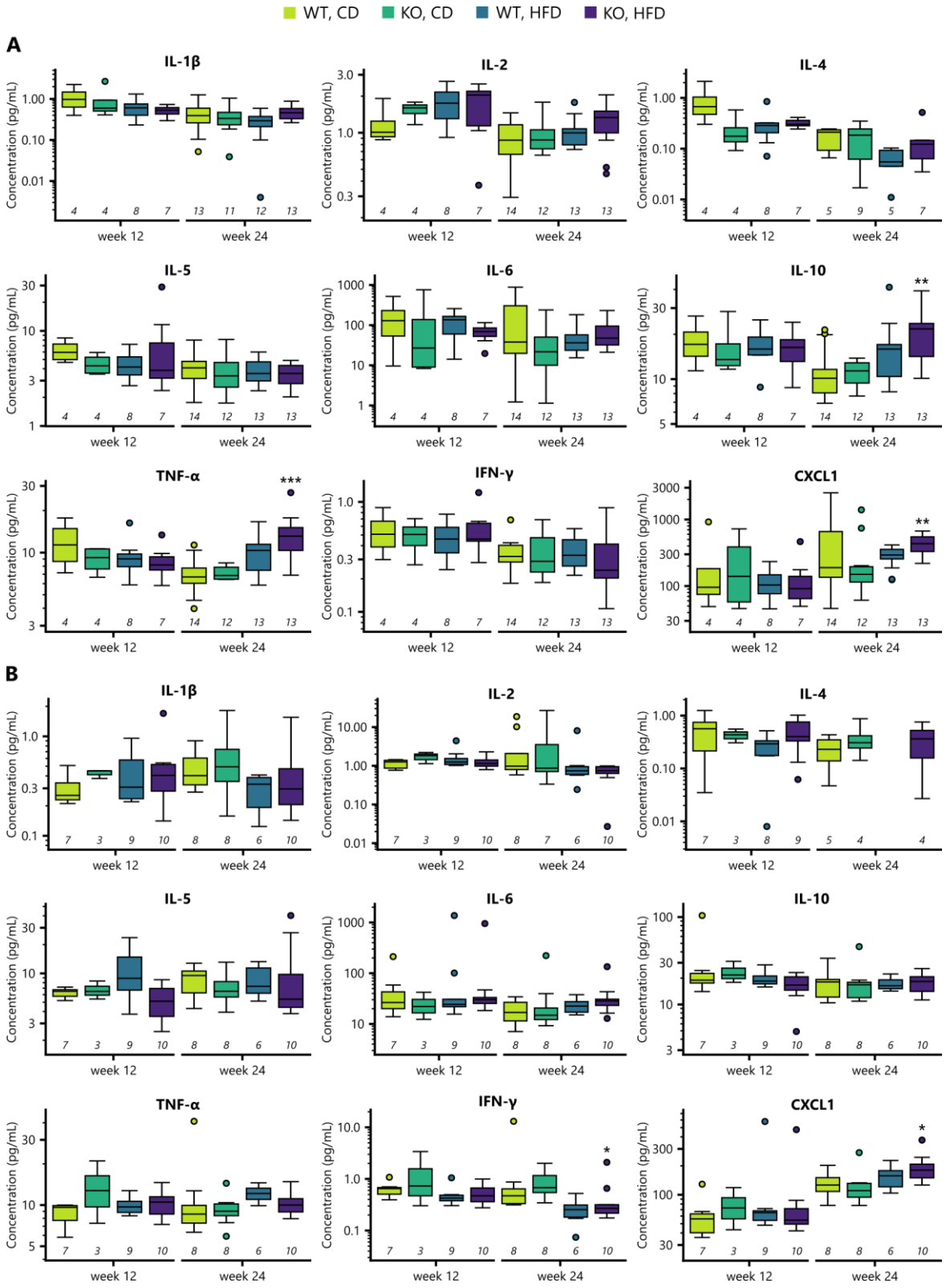

Figure 11. Plasma levels of proinflammatory cytokines are partially affected by diet but not by genotype. Cytokine levels of male (**A**) and female (**B**) mice after 12 and 24 weeks. Differences in concentration were tested for significance using Kruskal-Wallis with post-hoc Dunn's tests. *P*-values were corrected for multiple testing using the Holm procedure [78]. No significant genotype-dependent differences between mice fed the same diet were found. Significant diet-dependent differences between mice with the same genotype, and duration of diet are labeled with asterisks: * p≤0.05; ** p≤0.01; *** p≤0.001. The number of animals is given below the boxes in italics.

Diet and genotype-dependent differences were mainly detected in male mice after 24 weeks of diet (group 3). Here, the HFD and the KO of MGLL increased the plasma levels of IL-10, TNF-α, and CXCL1. However, statistical significance of these increases could only be calculated for the diet-dependent differences in KO mice. Significant differences were also detected in IFN-γ levels of females after 24 weeks of diet (group 4) with HFD-fed mice exhibiting lower concentrations than CD-fed mice. The frequencies of main leucocyte subsets and subpopulations were analyzed using flow cytometry. Main leucocyte populations depicted differences between 12 and 24 weeks of diet as well as few diet-dependent differences (**Figure 12**).

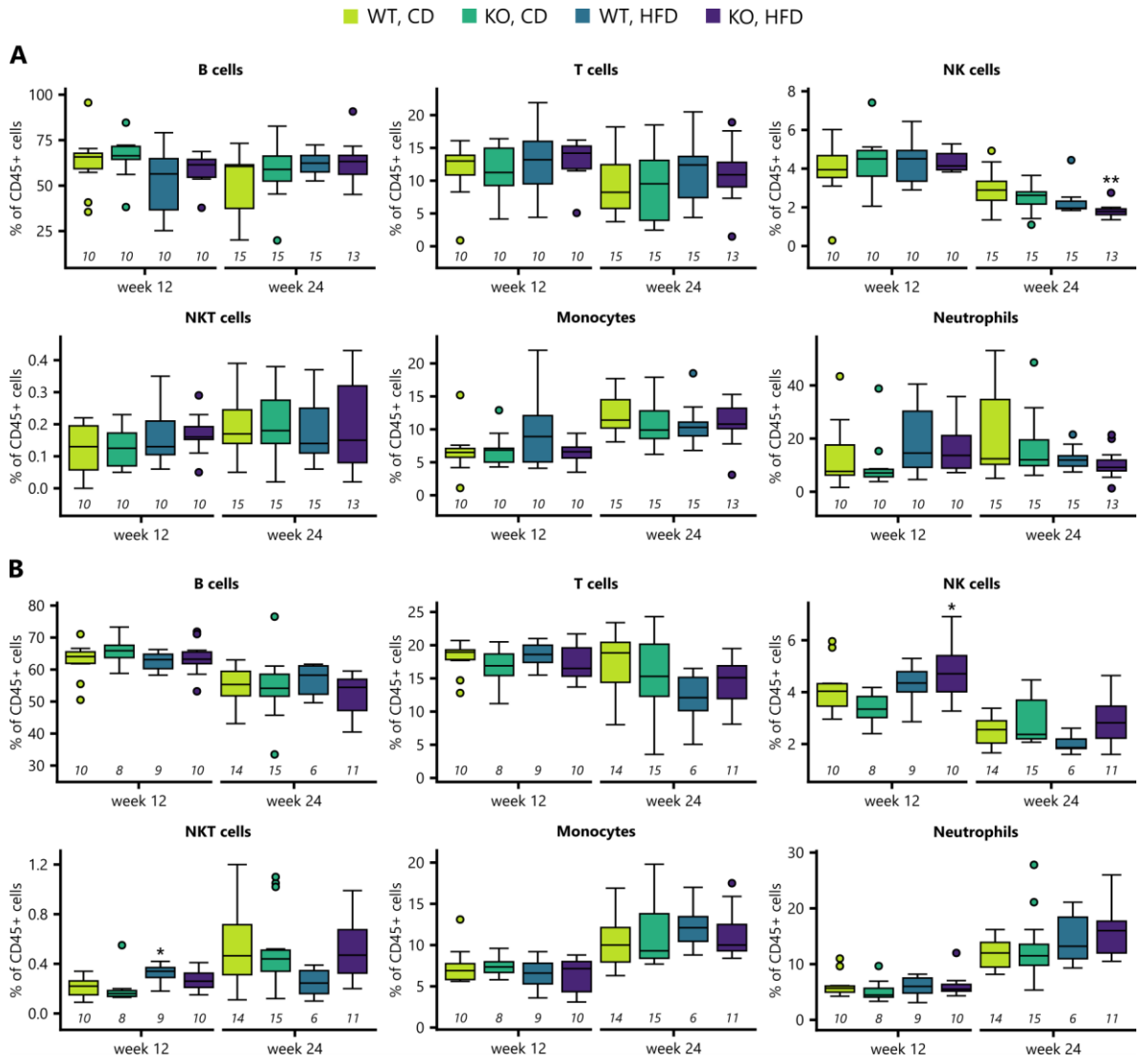

Figure 12. Main leukocyte populations are mostly not affected by diet or genotype. Leucocyte frequencies in whole blood of male (**A**) and female (**B**) mice after 12 and 24 weeks of diet. Differences in concentration were tested for significance using Kruskal-Wallis with post-hoc Dunn's tests. *P*-values were corrected for multiple testing using the Holm procedure [78]. No significant genotype-dependent differences between mice fed the same diet were found. Significant diet-dependent differences between mice with the same genotype, and duration of diet are labeled with asterisks: * p≤0.05; ** p≤0.01; *** p≤0.001. The number of animals is given below the boxes in italics.

Male and female mice exhibited lower NK cell levels and higher monocyte levels after 24 weeks of diet. Furthermore, male mice showed lower T cell frequencies and females exhibited increased neutrophil frequencies at week 24. Diet-dependent differences in male mice were only observed for NK cells which showed lower frequencies in HFD-fed mice. Females exhibited lower T cell frequencies in HFD-fed animals after 24 weeks of diet and increased NK cell frequencies in mice fed a HFD for 12 weeks. Frequencies of inflammatory (Ly-6C intermediate) and steady-state (Ly-6C low) monocytes were affected by diet but not by genotype (**Figure 13**). Mice fed a HFD showed lower frequencies of steady-state monocytes. Additionally, male mice exhibited higher frequencies of steady-state monocytes when fed a HFD for 24 weeks. Both male and female mice showed a tendency for lower inflammatory monocyte frequencies after 24 weeks compared to 12 weeks of diet. Likewise, female mice exhibited higher frequencies of steady-state monocytes after 24 weeks of diet. No differences in the frequency of monocytes recently emigrated from bone marrow (Ly-6C high) were observed. Furthermore, no genotype-dependent differences in monocyte subpopulations were detected.

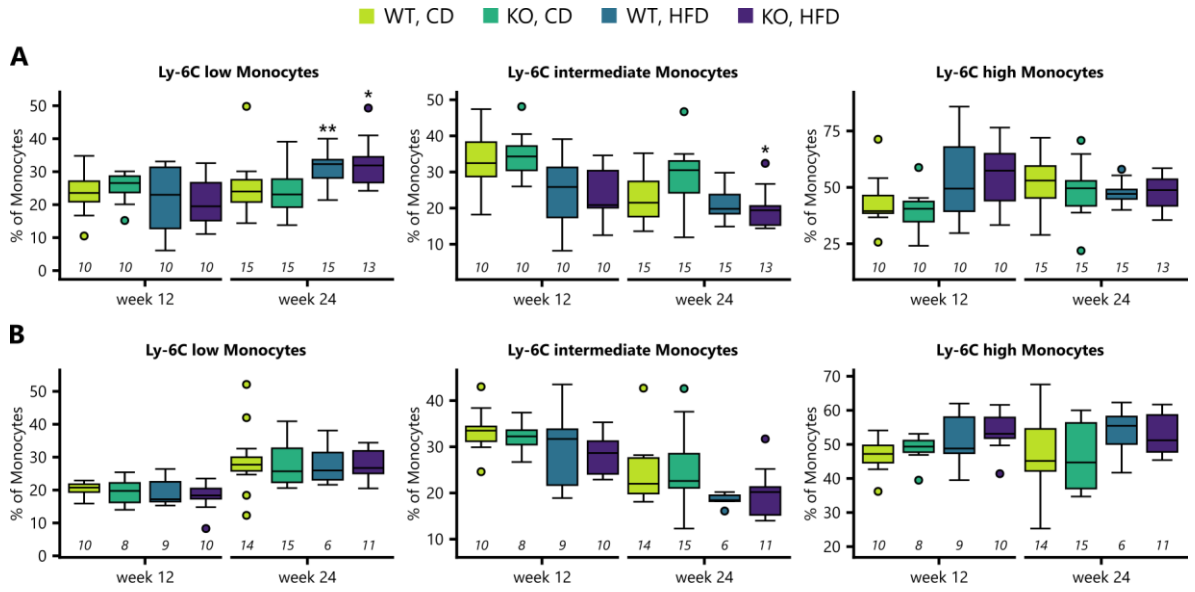

Figure 13. Inflammatory and steady-state monocyte subpopulations are affected by diet but not by genotype. Monocyte subpopulation frequencies in whole blood of male (**A**) and female (**B**) mice after 12 and 24 weeks of diet. Differences in concentration were tested for significance using Kruskal-Wallis with post-hoc Dunn's tests. *P*-values were corrected for multiple testing using the Holm procedure [78]. No significant genotype-dependent differences between mice fed the same diet were found. Significant diet-dependent differences between mice with the same genotype, and duration of diet are labeled with asterisks: * p≤0.05; ** p≤0.01; *** p≤0.001. The number of animals is given below the boxes in italics.

Looking at effector T and NK cell subpopulations only few differences were observed (**Figure 14**). Generally, mice exhibited higher frequencies of Ly-6C+ effector NK cells after 24 weeks compared to

12 weeks of diet. Likewise, females showed higher frequencies of CD44 high CD4+ effector T cells after 24 weeks of diet. Female mice also exhibited a slight tendency for higher CD44 high CD4+ effector T cell frequencies when fed an HFD. No differences in CD44 high CD8+ effector T cells were observed. Furthermore, no genotype-dependent differences in effector T and NK cell subpopulations were detected.

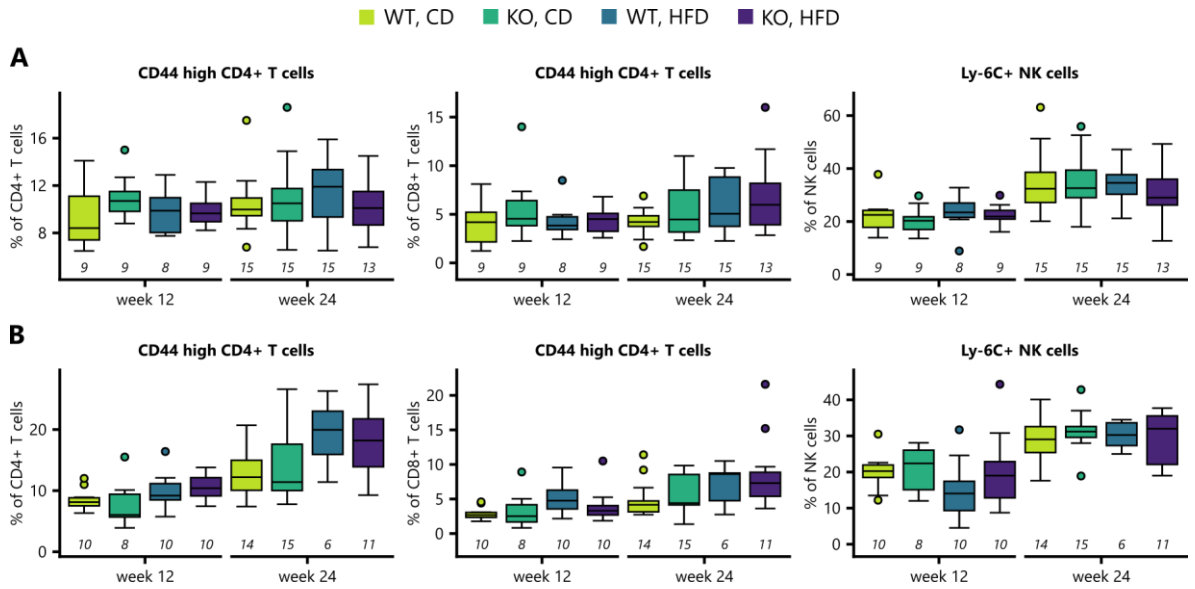

Figure 14. Effector T and NK cell populations are not affected by diet or genotype. T and NK cell subpopulation frequencies in whole blood of male (**A**) and female (**B**) mice after 12 and 24 weeks of diet. Differences in concentration were tested for significance using Kruskal-Wallis with post-hoc Dunn's tests. *P*-values were corrected for multiple testing using the Holm procedure [78]. No significant diet- or genotype-dependent differences were found. The number of animals is given below the boxes in italics.

Key Results

1. Feeding a HFD and the KO of MGLL affected plasma cytokine levels in mice after 24 weeks of diet.
   - ❖ IL-10 and TNF-α levels were increased in males.
   - ❖ CXCL1 levels were increased in males and females.
   - ❖ Only the diet-dependent differences were statistically significant.
2. Leucocyte frequencies were affected by mouse age. After 24 weeks the mice showed:
   - ❖ Lower frequencies of T cells, NK cells, and inflammatory monocytes.
   - ❖ Higher frequencies of monocytes, neutrophils, steady-state monocytes, and effector NK cells.
3. Feeding a HFD also affected leucocyte frequencies.
   - ❖ Male and female mice exhibited lower frequencies of inflammatory monocytes.
   - ❖ Male mice showed lower NK cell and higher steady-state monocyte frequencies after 24 weeks.
   - ❖ Female mice showed higher NK cells after 12 weeks and higher effector CD4+ T cells after 24 weeks.

3.5 Clinical Chemistry

Clinical blood parameters in plasma were measured at the end of the experiment after 12 and 24 weeks of diet (**Figure 15**). Cholesterol concentrations were generally higher in male mice than in female mice. A large part of the total cholesterol consists of HDL cholesterol. In terms of time- and diet-dependent effects total cholesterol as well as HDL and LDL cholesterol levels behaved similarly. In mice fed a CD, concentrations remained stable between 12 and 24 weeks of diet. In males the HFD lead to significantly increased levels after 12 weeks which increased even further after 24 weeks of diet. In female mice cholesterol concentrations were significantly increased as well after 12 weeks but remained at that level after 24 weeks of diet.

Non-HDL to HDL cholesterol ratios were significantly increased in male mice after 24 weeks of HFD (**Figure 15B**). While females did not exhibit significant differences here, a trend for a time- and diet-dependent increase was observed (**Figure 15D**). The plasma concentrations of triglycerides, glycerol, and non-esterified fatty acids (NEFA) in male mice were generally not affected by time, diet, or genotype. The only exception was a diet effect observed in NEFA of WT animals at week 12. In female mice results for triglycerides, glycerol, and NEFA were more differentiated. Triglyceride levels remained unchanged with the exception of WT mice fed a HFD for 12 weeks. Glycerol concentrations appeared to be increased by diet duration and HFD. However, only the diet effect at week 12 was significant. NEFA levels were significantly increased in females fed a HFD for 12 weeks. While NEFA concentrations were also increased after 24 weeks compared to 12 weeks of diet, no diet-dependent effect was observed here. Male mice exhibited a trend for higher plasma glucose concentrations when fed a HFD, but generally showed lower levels after 24 weeks compared to 12 weeks of diet. Glucose concentrations in female mice were increased when fed a HFD for 12 weeks. However, no such effect was observed after 24 weeks of diet.

Key Results

1. Mouse age and HFD affect plasma cholesterol levels in mice.
   - ❖ In the observed time frame cholesterol levels increased in male and female mice.
   - ❖ Feeding a HFD further enhanced the increase in cholesterol levels.
   - ❖ Male mice fed a HFD for 24 weeks exhibited a significant increase in the non-HDL to HDL ratio.
2. In female mice triglyceride, glycerol, and NEFA levels were partially increased by mouse age or HFD.
3. In general, no genotype-dependent differences in clinical blood plasma parameters were observed.

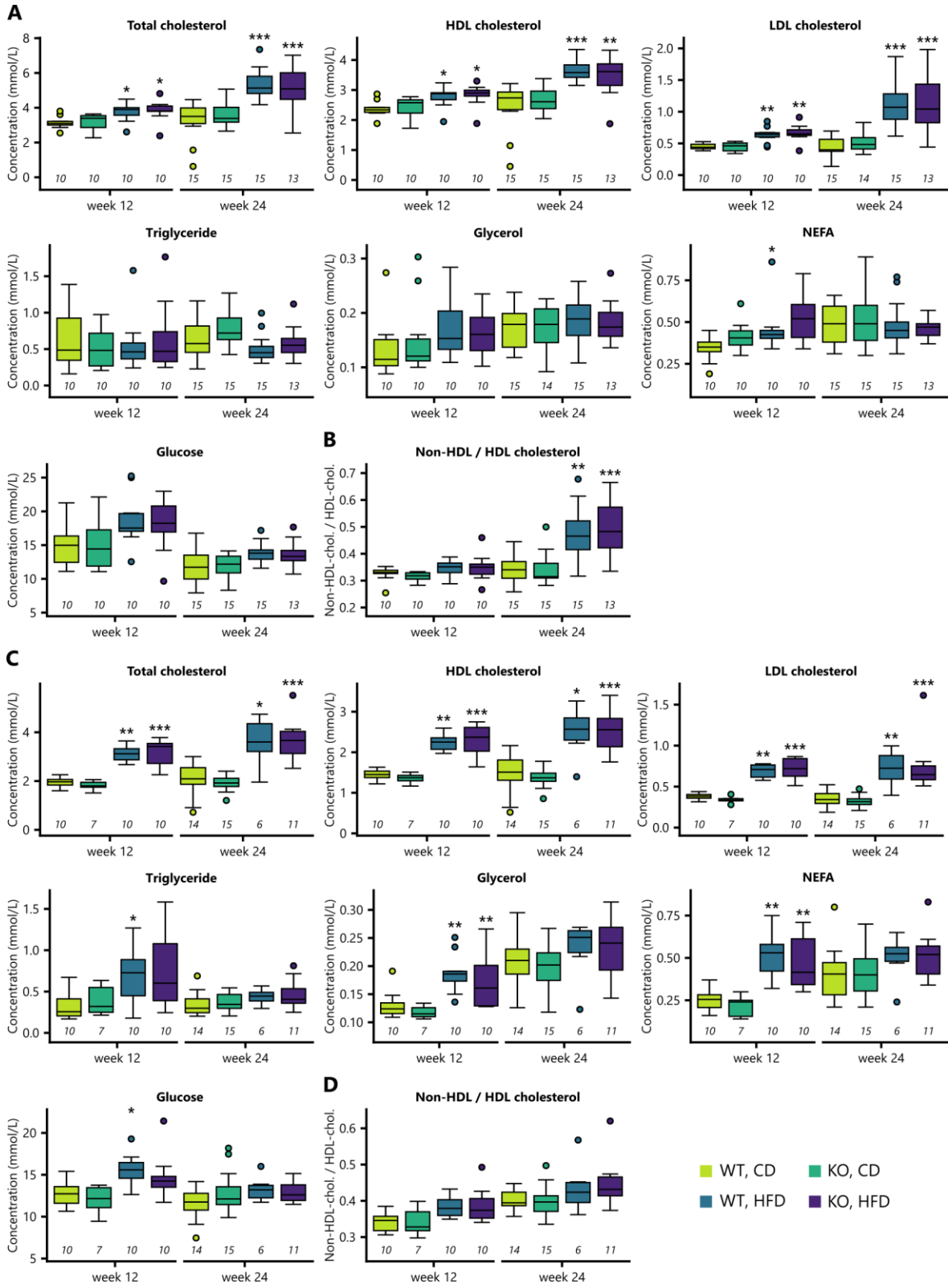

Figure 15. Clinical chemistry parameters in plasma are affected by diet but not by genotype. Clinical chemistry parameters and non-HDL-cholesterol to HDL-cholesterol ratio of male (**A**, **B**) and female (**C**, **D**) mice after 12 and 24 weeks. Differences in concentration were tested for significance using Kruskal-Wallis with post-hoc Dunn's tests. *P*-values were corrected for multiple testing using the Holm procedure [78]. No significant genotype-dependent differences between mice fed the same diet were found. Significant diet-dependent differences between mice with the same genotype, and duration of diet are labeled with asterisks: * p≤0.05; ** p≤0.01; *** p≤0.001. The number of animals is given below the boxes in italics.

3.6 Diabetes

The influence of the KO of MGLL in adipose tissue on the development of HFD-induced diabetes was investigated by analysis of insulin sensitivity and glucose tolerance as well as of fasted glucose and insulin levels. ITT was performed after 16 weeks of diet in five hours fasted mice (**Figure 16**). While mice fed a HFD exhibited higher blood glucose levels before insulin injection compared to CD-fed mice, they showed a similar progression in glucose concentration. Glucose levels dropped for the first 30 min after insulin injection, remained stable for the next 30 min and then started to increase again. The similarity is also reflected in the areas over the curve (AOC) of the first 30 min and the last 60 min. Here, no significant diet- or genotype-dependent differences were observed.

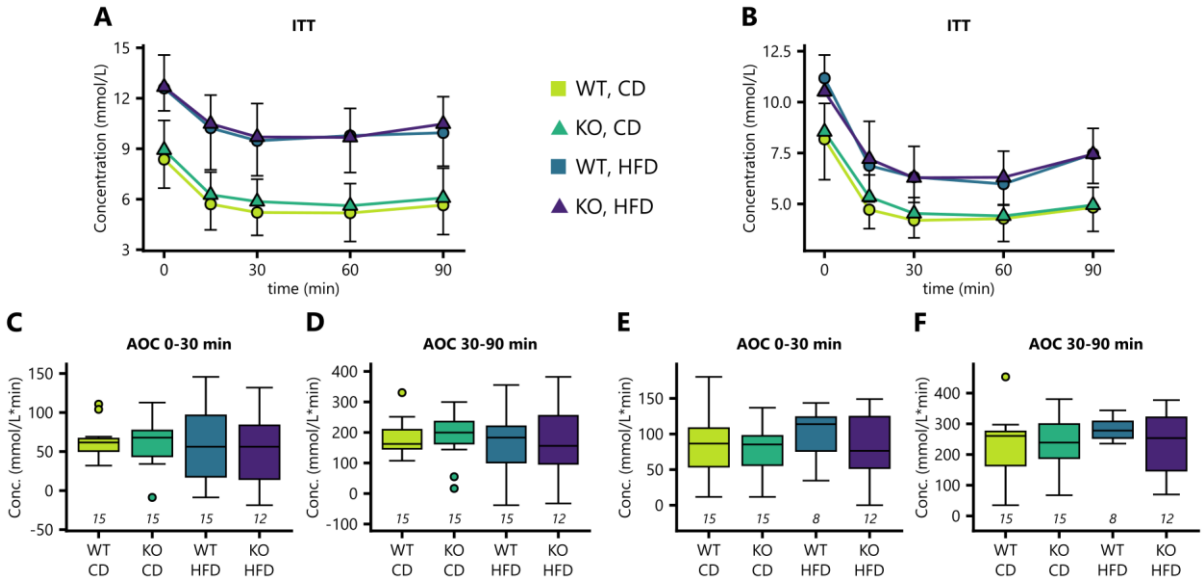

Figure 16. Insulin sensitivity is impaired in mice fed an HFD. ITT was performed with male (**left**) and female (**right**) mice after 16 weeks of diet. (**A**, **B)** Blood glucose levels after intraperitoneal insulin injection. Dots and error bars represent the mean and the standard deviation, respectively. (**C**-**F**) Area over the curve (AOC) of blood glucose levels at the first 30 min and the last 60 min of the ITT. The number of animals is given below the boxes in italics.

GTT as well as blood insulin quantification was performed after 18 weeks of diet in six hours fasted mice. Male and female mice fed a HFD exhibited significantly increased blood glucose and insulin levels right before intraperitoneal glucose injection (**Figure 17G-J**). While fasted glucose levels were comparable between male and female mice, the HFD induced increase in fasted insulin levels was distinctly higher in males. After glucose injection male and female mice exhibited higher maximum glucose levels as well as a delayed glucose clearance (**Figure 17A-B**). Glucose concentrations in CD-fed mice dropped 30 min after injection. In contrast, HFD-fed mice still showed rising glucose level 30 min after injection and dropping levels after 60 min. After the individual

maximum glucose concentration was reached the rate of glucose clearance was similar independent of the diet. The observed differences between mice fed a CD and those fed a HFD were more pronounced in males than in female mice. This is also reflected in the areas under the curve (AUC) of the first 30 min and the last 90 min after glucose injection (**Figure 17C-F**). While both male and female mice fed a HFD show significantly higher AUC's for the period between 30-120 min, only male mice show the same differences in AUC's for the first 30 min after injection. In addition to the impaired glucose clearance male and female mice fed a HFD also showed significantly increased insulin levels after six hours of fasting.

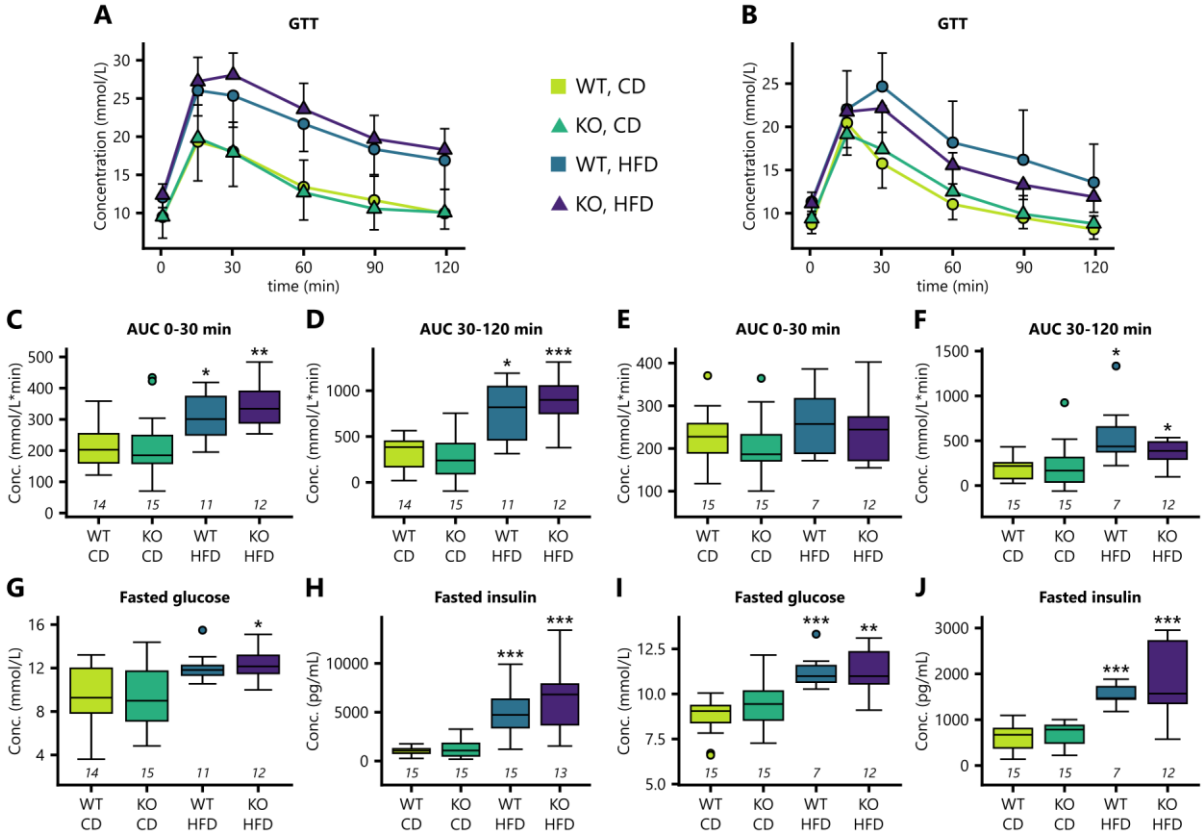

Figure 17. Glucose clearance is impaired and fasted insulin levels are increased in HFD-fed mice. GTT and insulin measurements were performed with male (**left**) and female (**right**) mice after 18 weeks of diet. (**A**, **B)** Blood glucose levels after intraperitoneal glucose injection. Dots and error bars represent the mean and the standard deviation, respectively. (**C**-**F**) Area under the curve (AUC) of blood glucose levels at the first 30 min and the last 90 min of the GTT. (**G**, **I**) Blood glucose after six hours fasting and right before glucose injection. (**H**, **J**) Blood insulin levels after six hours of fasting right before the GTT. Differences in concentration were tested for significance using Kruskal-Wallis with post-hoc Dunn's tests. *P*-values were corrected for multiple testing using the Holm procedure [78]. No significant genotype-dependent differences between mice fed the same diet were found. Significant diet-dependent differences between mice with the same genotype are labeled with asterisks: * $p \leq 0.05$; ** $p \leq 0.01$; *** $p \leq 0.001$. The number of animals is given below the boxes in italics.

Key Results

1. No diet- or genotype-dependent differences in insulin sensitivity were observed.
2. However, glucose clearance was impaired in mice fed an HFD, especially in males.
3. Male and female mice fed a HFD exhibited increased fasted glucose and fasted insulin levels.

3.7 Metabolomics

Longitudinal Plasma Metabolomics

Targeted metabolomics analysis was performed with plasma samples collected from the lateral tail at the beginning of the experiment at week 0 and after 6, 10, 14, and 22 weeks of diet. Principle component analysis (PCA) of the metabolite profiles revealed diet- and time-dependent changes in all four groups (**Figure 18**). At the beginning of the experiment the mice exhibited a high similarity in their metabolite profiles. After 6 weeks of diet distinct diet-dependent clusters were observed in all groups. While the male mice in groups 1 and 3 exhibited completely separated clusters for mice fed a CD or HFD, female mice, especially in group 4, showed a higher degree of overlap. After 10 to 20 weeks of diet the diet-dependent separation remained similar in the groups 1, 2, and 4. However, the male mice of group 3 showed an increasing overlap with each sampling time. Genotype-dependent differences were not observed at any given time point.

To identify effects of the KO of MGLL in interaction with time and diet on individual metabolites linear mixed-effects models were fitted. Metabolites with significant genotype-dependent coefficients were further analyzed (**Table 12**, **Figure 19**). Significant metabolites were only found in mice fed a diet for 22 weeks. Of the selected metabolites, most showed genotype-dependent differences that were restricted to one diet week and diet. Phenylalanine was temporally increased at week 0 in male mice fed an HFD. Acylcarnitine C5 was increased at week 0 and 6 in female mice fed a CD but exhibited similar concentrations between WT and KO mice later in the experiment. The differences between WT and KO mice observed exclusively at week 0 are by definition independent of diet and diet duration. However, the differences occurred in only one diet group at a time, making the results ambiguous. The phosphatidylcholines (PC) PC aa C28:1, PC ae C30:0, PC ae C32:1, and PC ae C32:2 were only increased at week 22 in female mice fed an HFD. In contrast, HFD-fed male KO mice exhibited sphingomyelin (SM) SM C24:1 levels that incrementally increased with time in comparison to WT mice.

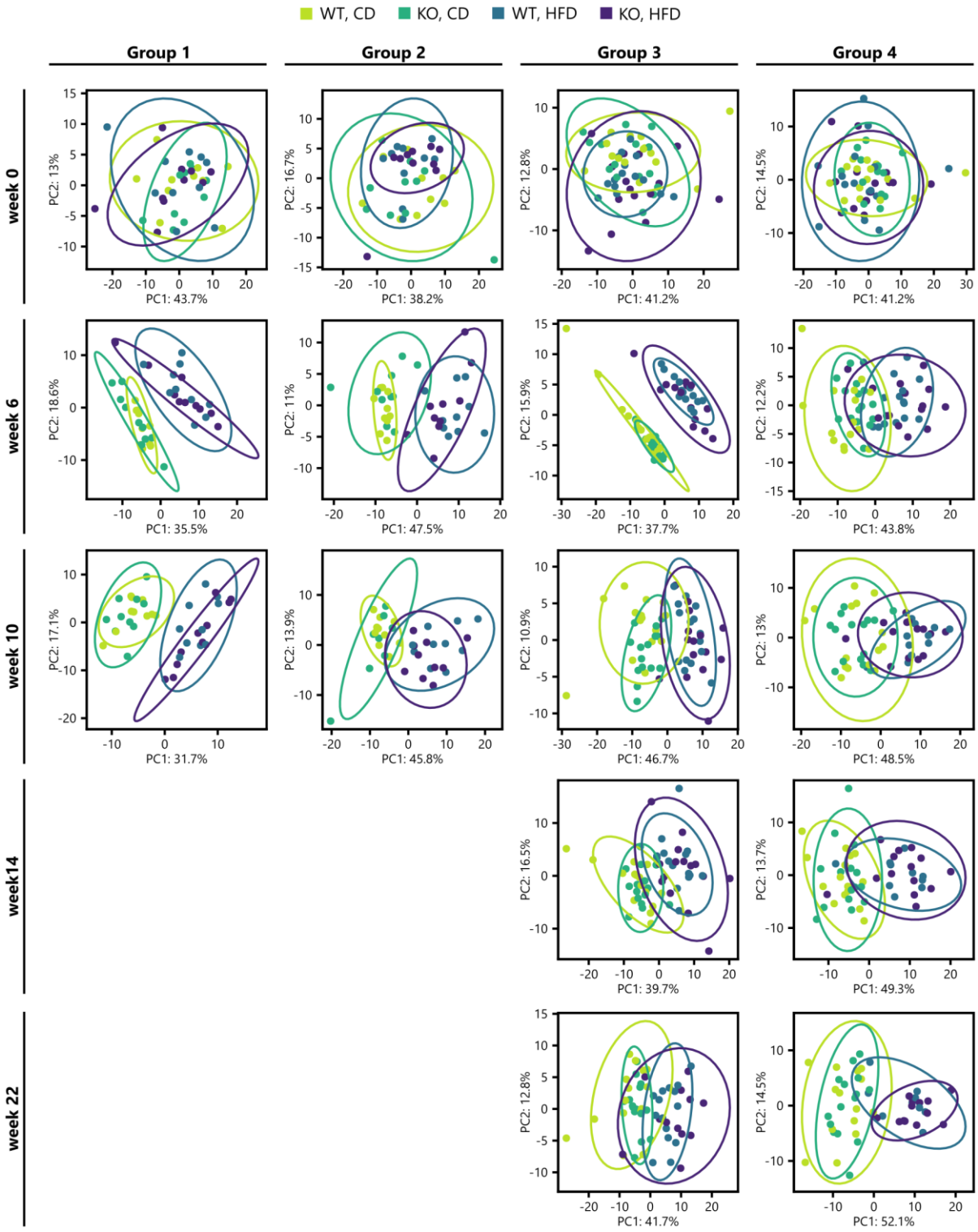

Figure 18. Plasma metabolomics profiles are affected by diet and time. PCA of targeted metabolomics data. Analysis was performed on plasma samples collected from the tail vein. Samples were collected after 0, 6, and 10 weeks of diet for the groups 1 and 2. The groups 3 and 4 were additionally sampled after 14 and 22 weeks of diet. Each dot represents the metabolite profile of one mouse. 95 % confidence regions are shown as ellipses. The percentages given in the axis labels describe the variance explained by the principal components PC1 and PC2.

Table 12. Significant model coefficients for genotype-dependent effects on the plasma metabolome.

Group	Metabolite	Coefficient	Reference	Value	SE	DF	*t*-value	*p*-value
3	Phe	Genotype (KO)	WT, HFD	12.70	4.72	56	2.69	0.009
	SM C24:1	Diet week : Genotype (KO)	WT, HFD	0.20	0.06	234	3.44	0.001
	SM C24:1	Diet week : Diet (HFD) : Genotype (KO)	WT, CD	0.27	0.08	234	3.34	0.001
4	C5	Genotype (KO)	WT, CD	0.03	0.01	56	3.77	<0.001
	C5	Diet week : Genotype (KO)	WT, CD	0.00	0.00	216	-2.89	0.004
	Putrescine	Genotype (KO)	WT, CD	0.38	0.13	56	2.93	0.005
	PC aa C28:1	Diet week : Genotype (KO)	WT, HFD	0.01	0.00	216	3.08	0.002
	PC aa C28:1	Diet week : Diet (HFD) : Genotype (KO)	WT, CD	0.02	0.00	216	3.15	0.002
	PC ae C30:0	Diet week : Genotype (KO)	WT, HFD	0.00	0.00	216	2.77	0.006
	PC ae C30:0	Diet week : Diet (HFD) : Genotype (KO)	WT, CD	0.00	0.00	216	3.01	0.003
	PC ae C32:1	Diet week : Diet (HFD) : Genotype (KO)	WT, CD	0.01	0.00	216	2.60	0.010
	PC ae C32:2	Diet week : Genotype (KO)	WT, HFD	0.00	0.00	216	2.69	0.008
	PC ae C32:2	Diet week : Diet (HFD) : Genotype (KO)	WT, CD	0.01	0.00	216	2.77	0.006

Linear mixed-effects models were fitted for each group and metabolite. Significant (p<0.01) model coefficients for genotype and its interaction with diet and diet week were selected. SE: Standard error; DF: Degrees of freedom.

Final Plasma and Tissue Metabolomics

Targeted metabolomics analysis was performed on plasma samples as well as liver, WAT, and BAT at the end of the experiment after 12 or 24 weeks of diet. Plasma samples were collected from the retro-orbital venous sinus under isoflurane anesthesia. Tissue samples were collected subsequently after cervical dislocation. PCA of the metabolite profiles revealed diet-dependent differences (**Figure 20**). Plasma, liver, and WAT samples exhibited distinct diet-dependent clusters in all four groups. WAT, in particular, stood out with a significant distance between CD and HFD clusters. BAT responded differently to the diet depending on sex. The male mice in group 1 and 3 exhibited strongly overlapping clusters and no discernable diet-dependent separation. In contrast, the female mice of group 2 and 4 showed a clear separation of CD and HFD clusters. No obvious genotype-dependent differences were observed either in the plasma or the tissue samples.

Since no obvious metabolomic differences between WT and KO mice were detected with the PCA, which is an unsupervised technique, partial least squares discriminant analysis (PLS-DA) was performed. As a supervised method PLS-DA allowed to specifically search for metabolites that differ between mice of different genotypes fed different diets. PLS-DA revealed metabolites affected by the KO of MGLL in WAT of male and female mice after 24 weeks of diet. While the components 1 and 2 displayed the diet-dependent differences already observed with the PCA, component 3 uncovered slight genotype-dependent differences (**Figure 21A, B**). The VIP Scores of the 15 most important metabolites of component 3 were examined (**Figure 21C, D**). For males, the heatmaps on the right side of the plots revealed that most of the metabolites follow a specific concentration pattern, where feeding a HFD increases metabolite concentrations and the KO of MGLL decreases concentrations.

For females, the heatmap revealed a more diverse array of concentration patterns. However, the metabolites with the highest levels showed the same pattern as the male mice.

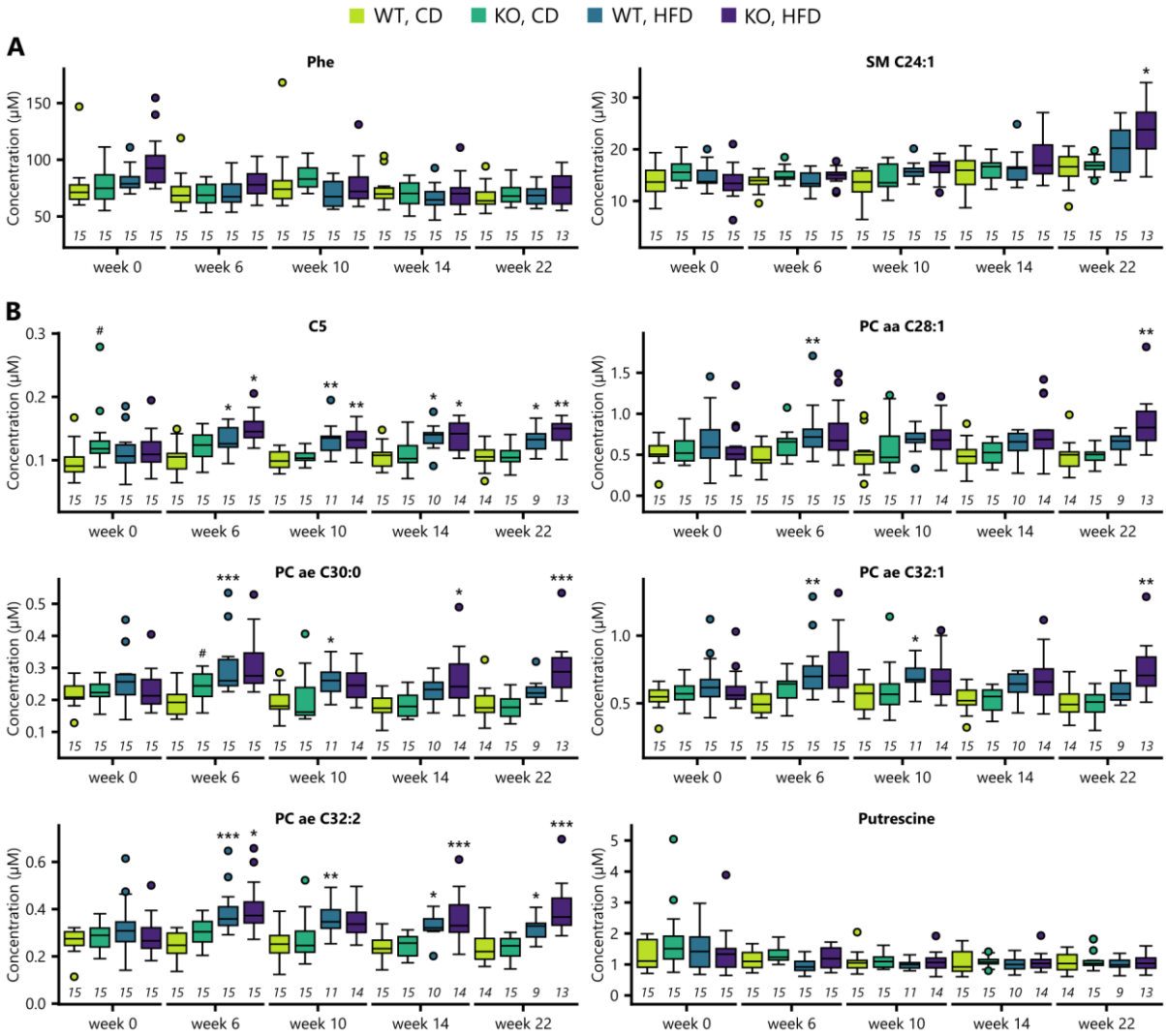

Figure 19. Genotype-dependent metabolites in longitudinal plasma samples. Targeted metabolomics analysis was performed on plasma samples collected from the lateral tail vein. Samples were collected between 0 and 22 weeks of diet. Linear mixed-effects models were fitted for each group and metabolite and metabolites with significant genotype-dependent coefficients were selected. Only male (**A**) and female (**B**) mice fed a HFD for up to 22 weeks exhibited metabolites with significant ($p<0.01$) model coefficients for the genotype and its interactions with diet and diet week. Differences in concentrations were tested for significance using Wilcoxon rank sum tests. *P*-values were corrected for multiple testing using the Benjamini & Hochberg procedure [77]. Significant diet- and genotype-dependent differences between mice are labeled with asterisks and number signs, respectively. */# $p\leq0.05$; **/## $p\leq0.01$; ***/### $p\leq0.001$. The number of animals is given below the boxes in italics.

Metabolites with particularly high VIP scores were selected for further analysis (**Figure 22**). From the seven metabolites, each selected individually from male and female mice, five metabolites were found in both sexes. Statistical analysis confirmed the findings from the heatmap. Feeding a HFD lead to a highly significant increase in metabolite concentrations. In contrast, the KO of MGLL decreased

metabolite concentration but to a much smaller degree. While the genotype-dependent decrease in metabolite concentrations was often significant in mice fed a HFD diet, it was often only subtle in mice fed a CD. Exceptions were male PC aa C32:2 and SM C18:0 which exhibited significantly decreased concentrations in KO mice fed a CD or HFD.

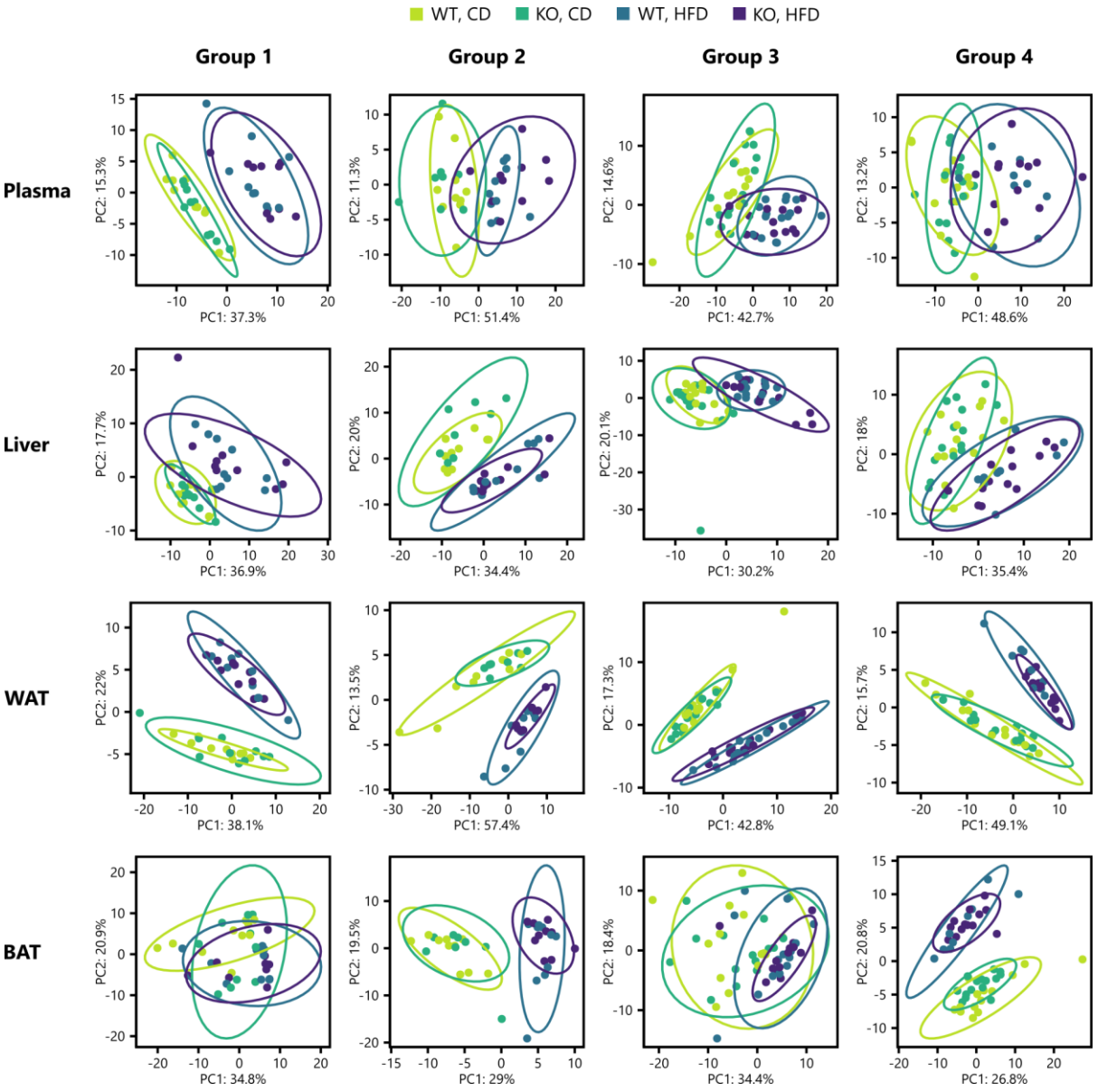

Figure 20. Final metabolomics profiles of plasma and tissue samples are affected by diet but not by genotype. PCA of targeted metabolomics data after 12 and 24 weeks of diet. Analysis was performed on plasma samples collected from the retro-orbital venous sinus under isoflurane anesthesia as well as on liver, WAT, and BAT collected after cervical dislocation. Each dot represents the metabolite profile of one mouse. 95 % confidence regions are shown as ellipses. The percentages given in the axis labels describe the variance explained by the principal components PC1 and PC2.

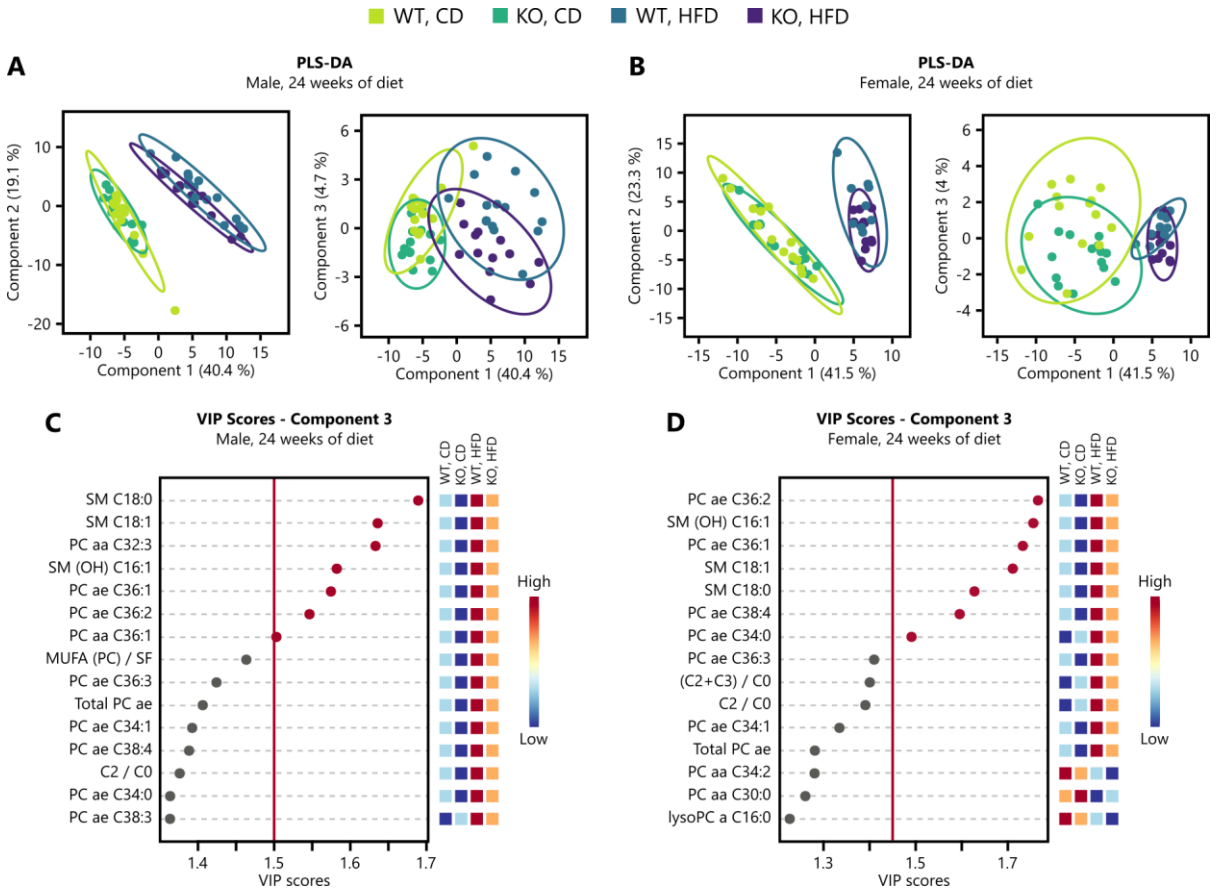

Figure 21. PLS-DA reveals genotype-dependent metabolomic differences in white adipose tissue. Targeted metabolomics data of WAT of male (**left**) and female (**right**) mice after 24 weeks of diet. Tissue was collected under isoflurane anesthesia after cervical dislocation. Partial least squares discriminant analysis (PLS-DA) was performed. Score plots of male (**A**) and female (**B**) mice. Each dot represents the metabolite profile of one mouse. 95 % confidence regions are shown as ellipses. The percentages given in the axis labels describe the variance explained by the components. VIP scores of component 3 for male (**C**) and female (**D**) mice. Metabolites above the cutoff (red line) were selected for further analysis.

Key Results

1. Feeding a HFD affected the metabolome in murine plasma, liver, WAT, and BAT.
   - ❖ Diet-dependent changes were found in plasma after six weeks of diet and beyond.
   - ❖ Diet-dependent differences were found in BAT but only in female mice.
2. The KO of MGLL lead to few but specific metabolomic changes in WAT after 24 weeks of diet.
   - ❖ The effects of the MGLL KO were opposite to those induced by the HFD.
   - ❖ The observed effects were highly similar in male and female mice.

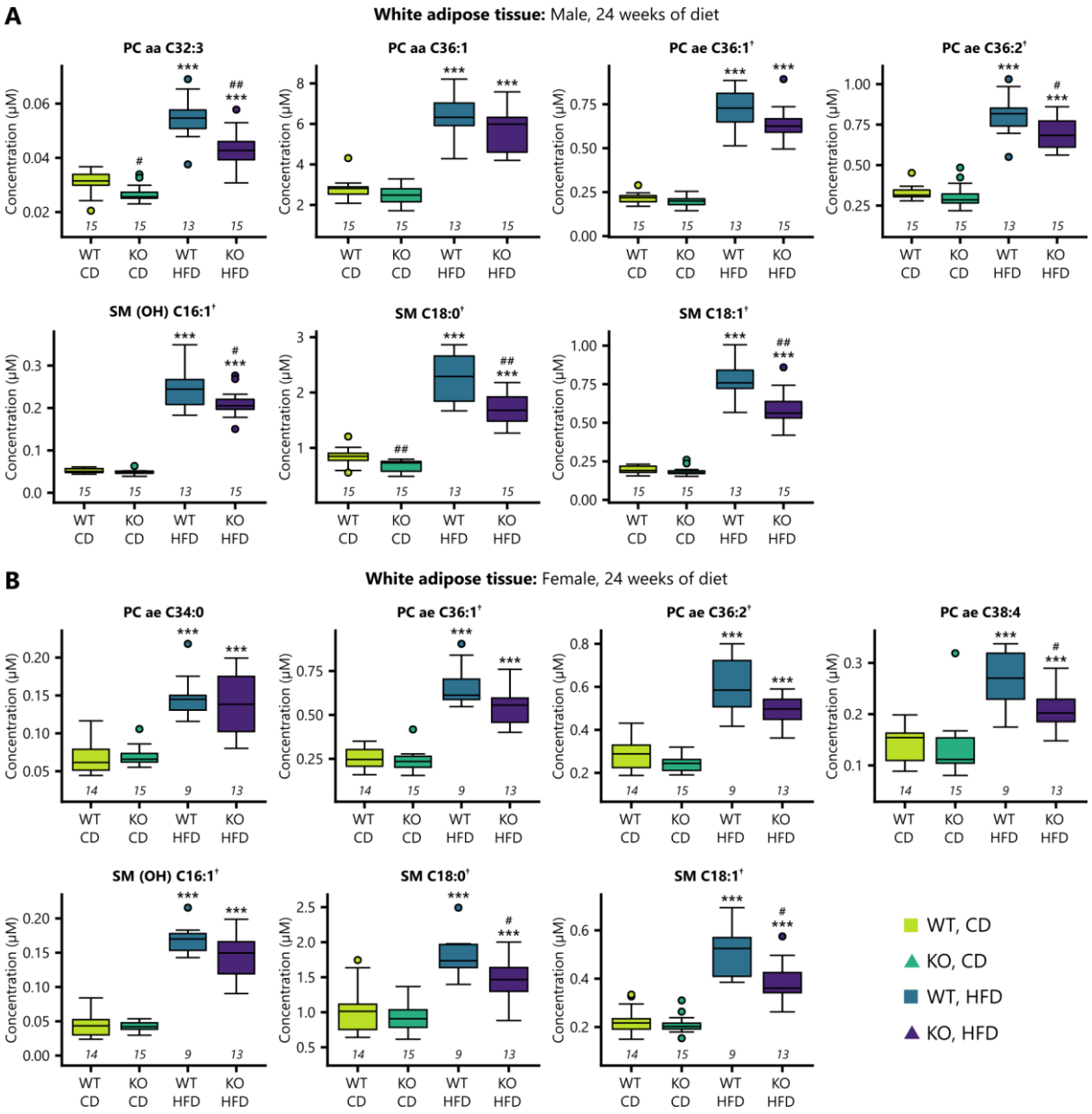

Figure 22. Genotype-dependent metabolomic differences are similar in male and female white adipose tissue. Targeted metabolomics data of WAT of male and female mice after 24 weeks of diet. Tissues were collected under isoflurane anesthesia after cervical dislocation. Partial least squares discriminant analysis (PLS-DA) was performed and metabolites with particularly high VIP scores were selected individually for male (**A**) and female (**B**) mice. Metabolites found in both sexes are labeled with a dagger (†) in the title. Differences in concentrations were tested for significance using Wilcoxon rank sum tests. *P*-values were corrected for multiple testing using the Benjamini & Hochberg procedure [77]. Significant diet- and genotype-dependent differences between mice are labeled with asterisks and number signs, respectively. */# p≤0.05; **/## p≤0.01; ***/### p≤0.001. The number of animals is given below the boxes in italics.

3.8 Total RNA Sequencing

Total RNA sequencing was performed to investigate genotype-dependent differences in gene expression. Differences in RNA expression were investigated in WAT of male mice after 24 weeks of diet. PCA showed no separation of clusters for WT and KO mice fed either a CD or a

HFD (**Figure 23A**). This indicates that the variation in gene expression within the WT and KO clusters is bigger than the variation between the clusters. KO mice fed a CD or a HFD exhibited 11.000-12.000 upregulated and downregulated genes (**Figure 23B**).

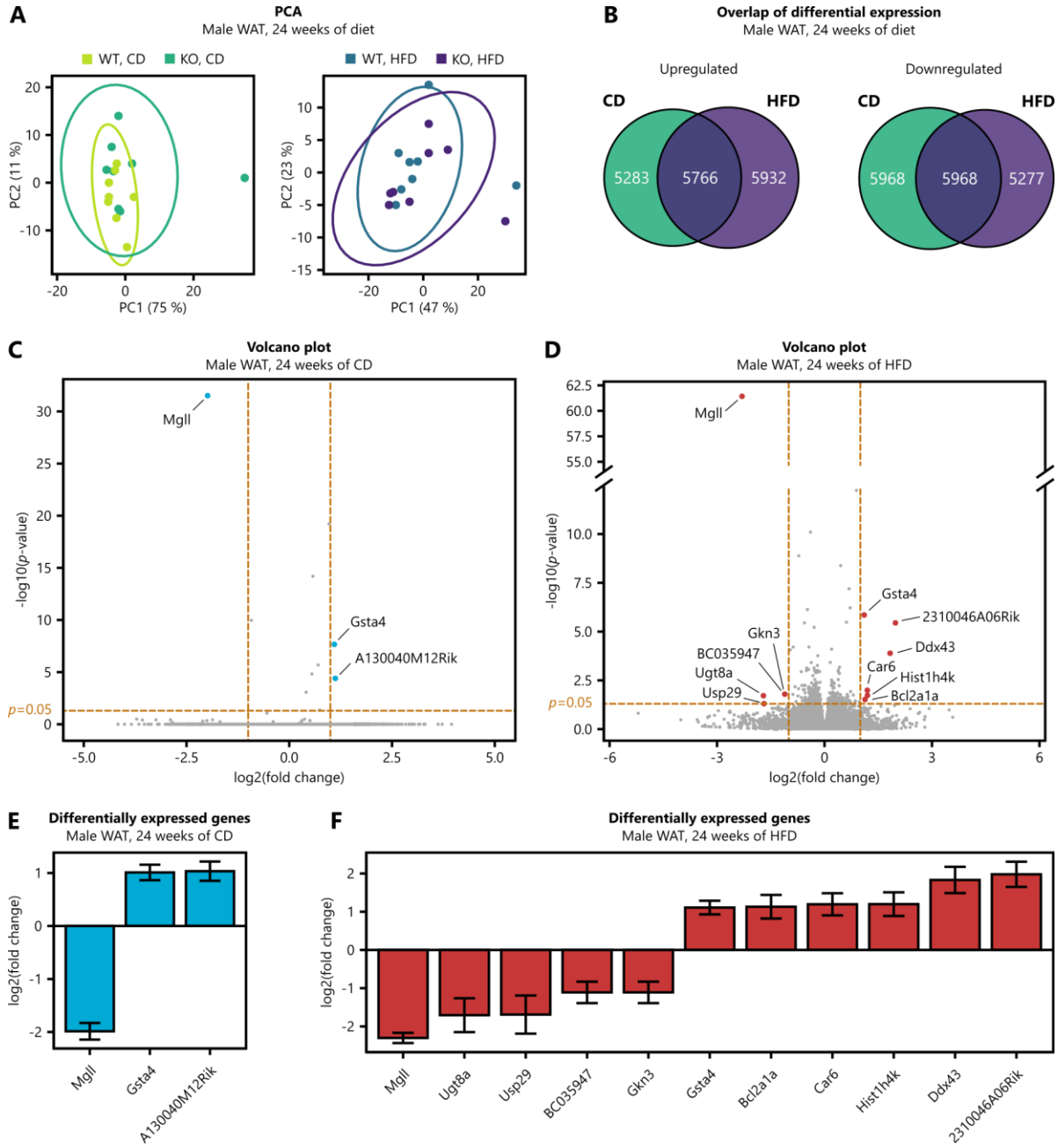

Figure 23. MGLL KO results in minimal changes in WAT mRNA expression. WAT was collected under isoflurane anesthesia after cervical dislocation. Total RNA sequencing was performed with tissues of male mice after 24 weeks of diet. (**A**) PCA was performed on log2 normalized counts. Each dot represents the metabolite profile of one mouse. 95 % confidence regions are shown as ellipses. The percentages given in the axis labels describe the variance explained by the principal components PC1 and PC2. (**B**) Overlap of upregulated and downregulated genes in CD-fed and HFD-fed KO mice. (**C**, **D**) Separate volcano plots of differentially expressed genes of CD-fed and HFD-fed mice. Genes with a log2 fold change greater 1 and a *p*-value below 0.05 are highlighted in color and are labeled. Bar plots of log2 fold changes for these genes are plotted in **E** and **F**. Number of animals: 6 per diet and genotype.

Approximately 50 % of the genes up- and downregulated were identified in both CD-fed and HFD-fed mice. However, only few genes exhibited significant differences between WT and KO mice while also showing distinct fold changes in gene expression (**Figure 23C**). For CD-fed mice three genes fulfilled these requirements, while for HFD-fed mice 11 genes were identified (**Figure 23E-F)**. Within this selection, *Mgll* stood out for its highly significant downregulation. For both diets KO mice showed a 4-fold decrease in *Mgll* expression. Another notable gene was Gsta4 which encodes the glutathione S-transferase A4 (GSTA4). Gsta4 was upregulated 2-fold in KO mice fed either a CD or an HFD. A particular interest was the expression of genes encoding lipases. Upregulation of lipase genes could potentially compensate for the KO of MGLL and would explain the mild phenotypic changes between WT and KO mice. However, RNA sequencing revealed no notable upregulation of lipase-encoding genes in KO mice fed a CD or a HFD (**Figure 24**).

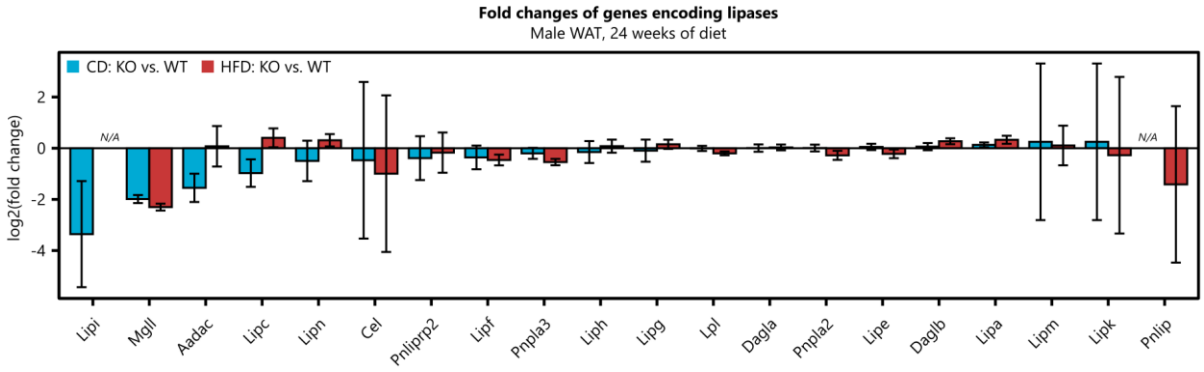

Figure 24. Lipase gene expression in WAT is not affected by the KO of MGLL. WAT was collected under isoflurane anesthesia after cervical dislocation. Total RNA sequencing was performed with tissue of male mice after 24 weeks of diet. Bar plots show log2 fold changes in mRNA expression between WT and KO mice. N/A no data available.

Key Results

1. The KO of MGLL has little effect on the murine transcriptome.
2. RNA sequencing verified the KO of MGLL on the transcriptome level.
3. Loss of MGLL had no significant effect on the RNA expression of other lipase-encoding genes.
4. GSTA4 was the only gene significantly upregulated 2-fold in KO mice fed a CD or an HFD.

4 Discussion

Obesity is a growing epidemic that threatens the health of society and burdens healthcare systems and economies [1,2,5]. It can cause hypertension, T2D, cardiovascular disease, and cancer and is associated with metabolic syndrome [3,4]. Despite major advances in obesity research, measures to curb this epidemic fall short of expectations. Lifestyle interventions such as caloric restriction, dietary changes and exercise remain the foundation for combating obesity. However, these measures must be maintained throughout life to be effective, which requires breaking fundamental lifestyle habits. Time restrictive diets like intermittent fasting as well as diets based on the exclusion of certain foods such as paleolithic diet and low carb are difficult to integrate into everyday life and therefore have a high dropout rate [81]. In addition, weight loss is often followed by body weight regain due to preservative mechanisms of the body such as an increase of ghrelin (appetite induction) and decrease of energy expenditure [82]. Bariatric surgery has proven to be an effective treatment of obesity and its comorbidities but is reserved for severe cases with a BMI ≥35 with comorbidities or for patients with a BMI ≥ 40 due to operative risks and costs [81,82].

Anti-obesity drugs can help patients to adhere to behavioral changes mostly by targeting appetite regulation and energy expenditure. Drugs that fall into this category and are approved in the US and EU for long term use are liraglutide (GLP-1 receptor agonist), naltrexone/bupropion, and phentermine/topiramate (only approved in US). However, side effects such as blood pressure elevation (phentermine), increased risk of seizures and likelihood of suicidal thoughts (naltrexone/bupropion), as well as pancreatitis (liraglutide) demand a careful patient assessment. A completely different type of drug which is also approved in the US and the EU is orlistat. It is a gastric and pancreatic lipase inhibitor that prevents the absorption of fatty acids in the intestine [81]. Although orlistat also has side effects such as steatorrhea and malabsorption of fat-soluble vitamins, it demonstrates how altering lipase activity can be used to treat obesity and its comorbidities.

Adipocyte lipolysis is increased during obesity and closely related to the development of insulin resistance and T2D [6]. Inhibition of the lipases primarily responsible for the breakdown of lipid storages in adipocytes – ATGL, HSL, and MGLL – is therefore considered a potential strategy for the treatment of obesity-induced morbidities [6]. While adipocyte-specific KO models are already described for ATGL and HSL in the context of diet-induced obesity, this is not the case for MGLL. Here, an adipocyte-specific MGLL KO mouse model was characterized for the first time in terms of body composition, systemic inflammation, glucose- and lipid metabolism, as well as metabolomic and transcriptomic changes. Male and female WT and KO mice fed a control diet (11 kJ% fat) or high-fat diet (60 kJ% fat) were analyzed for a period of up to 24 weeks. The mice were kindly provided by

Prof. Zimmermann (University of Graz) and were generated using the same technique as the global MGLL KO mouse model first characterized by his group in 2011 [27]. His global KO model has since been used in numerous publications [28,30,83,84]. Similar to the global KO model, the adipocyte-specific MGLL KO mouse model characterized here was observed to be healthy and fertile under normal conditions without any obvious phenotype [27]. In addition to the mouse model developed by Prof. Zimmermann, other researchers have developed their own global MGLL KO mice. [29,85]. For the sake of comprehensibility and clarity in the following discussion, the adipocyte-specific KO of MGLL in mice characterized here is abbreviated as AMKO while the various global MGLL KO mouse models are referred to as GMKO.

4.1 Adipose Tissue MGLL Does Not Affect the Body Composition of Mice

The effect of adipocyte-specific depletion of MGLL during prolonged calorie excess was investigated in terms of body weight development and changes in body composition using qNMR. Feeding a HFD significantly increased fat mass and total body weight gain as well as final body weight after 12 or 24 weeks compared to mice fed a CD. MGLL KO showed a positive but very weak association with body weight and fat mass gain, but only for male mice fed a HFD for 24 weeks. In line with these results, Taschler *et al.* found no differences in body composition of GMKO mice fed a HFD for 12 weeks [27]. However, most studies reported reduced body weight and fat mass in GMKO mice, although details are heterogeneous. Douglass *et al.* reported lower body weight and fat mass in mice fed a normal chow as early as eight weeks of age [29]. Gain in body weight and fat mass were reduced as well over the course of 10 weeks. Interestingly, male KO mice fed a HFD for 10 weeks showed no differences in fat mass. Similarly, Chanda *et al.* reported lower body weight in newly born as well as in three month old KO mice fed a standard chow [85]. In contrast, other groups reported no differences in body composition in mice fed a normal chow at 6-8 weeks of age and a protective effect of MGLL deletion from obesity induced by up to 22 weeks of HFD [28,30]. Such differences usually indicate differences in experimental design that are not controlled for and that the underlying mechanisms of the variables observed are more complex than expected. A complete KO is credibly demonstrated for all model cited here using procedures such as western blot, qPCR, and MGLL activity assays. The adipocyte-specific KO of MGLL in the mouse model used in this study was verified using qPCR and immunohistochemistry. However, differences in diet composition, animal age, and specifics of animal husbandry add further layers of complexity that might be responsible for the observed discrepancies. Genetic differences might be another factor. All groups cited above use the same mouse model, provided by Prof. Zimmermann with the exception of Douglass *et al.* as well as Chanda *et al.* who generated their own KO model [29,85]. In addition, prolonged breeding in

different animal facilities can lead to genetic differences in previously identical strains [86]. Chanda *et al.* used C57Bl/6NTac mice as a background strain [85]. The others used C57Bl/6 mice with the specific substrain utilized remaining unknown. Taschler *et al.* used mice with a mixed background that were backcrossed to a C57Bl/6 background only four to five times [27].

Accepting that global deletion of MGLL leads to reduced body weight and fat mass and that an adipocyte-specific MGLL KO does not, raises the question which tissues or pathways are responsible for this effect. It is indeed not unusual that tissue-specific and global deletions of lipases result in completely different phenotypes. Global KO of ATGL leads to increased body weight and fat mass, ectopic lipid accumulation especially in the heart and premature death due to cardiac dysfunction [87]. In contrast, mice with an adipose tissue-specific KO of ATGL exhibit normal body weight and were protected from diet-induced insulin resistance and hepatic steatosis [26]. This illustrates that lipases also play an important role outside of adipocyte lipolysis. In terms of GMKO, brain endocannabinoid signaling is an obvious candidate, because it is known to regulate food intake and energy metabolism and because MGLL is the primary enzyme hydrolyzing the EC 2-AG [68,88]. Indeed, GMKO leads to a 10-58-fold increase in brain 2-AG [27,85,89]. However, GMKO mice are reported to show no differences in food consumption, locomotor activity, and energy expenditure [27–30]. A proposed reason for this observation is the desensitization of brain cannabinoid receptors due to chronically increased 2-AG levels [27,85]. This is underlined by the fact that mice with an astrocyte-specific deletion of MGLL exhibit no differences in body weight or fat mass [90].

Promising results, however, were reported for the intestine of GMKO mice. MGLL expression was increased in the small intestine of mice fed a high-fat diet [68]. MGLL deletion reduced plasma TAG levels following an oral fat challenge. This suggests diminished intestinal lipid processing and secretion and might be the reason for the reduction in body weight and fat mass. The effect was found to be CB_1-independent as MGLL KO and CB_1/MGLL double knockout mice showed identical results. A different study reported that MGLL inhibition slows down whole gut transit in a CB_1 receptor-dependent manner. But CB_1 desensitization counteracts this effect [84]. Nevertheless, MGLL KO mice exhibit delayed intestinal lipid clearance resulting in a total lipid uptake comparable to WT mice [29,68]. Still, deceleration of intestinal lipid uptake might reduce postprandial hyperlipidemia a condition associated with obesity and diabetes [91]. In this context, Dione *et al.* reported differences in the gut microbiome of MGLL KO mice fed a normal chow or a HFD possibly due to differences in intestinal fat absorption [30]. They found that MGLL deletion protected mice from HFD-induced changes of microbiota populations associated with obesity and coronary artery disease. These results currently establish the intestine as the main tissue responsible for changes in body composition in GMKO mice.

4.2 Dysfunction of Adipocyte Lipolysis in MGLL KO Mice Cannot Be Confirmed

The question remains why the deletion of MGLL in adipose tissue, one of the major enzymes hydrolyzing fat storages, does not lead to lipid accumulation in the setting of diet-induced obesity. Schoiswohl *et al.* made the same observation in HFD-fed mice with an adipocyte-specific KO of ATGL [26]. They found that the reduced expression of genes involved in lipid uptake and synthesis as well as in adipogenesis was in part responsible for the unaffected body weight and fat mass. However, AMKO mice, did not exhibit transcriptomic changes in any of these genes. Even though it was not tested here, adipocytes of GMKO mice reportedly exhibit significantly increased levels of MAG species and reduced secretion of glycerol and FFAs due to diminished MAG hydrolase activity. This effect is further enhanced by feeding a high-fat diet [27,29]. Surprisingly, Taschler *et al.* found that MGLL KO mice still exhibited approx. 25 % of MAG hydrolase activity compared to WT mice [27]. They showed that HSL accounted for most of the remaining activity while HSL expression remained unchanged in MGLL KO mice. Similarly, in this study no transcriptional changes of lipase genes in AMKO mice were detected. As early as 1964, Vaughan *et al.* reported that the activity of MGLL was multiple times higher than that of HSL in an *in vitro* assay [32]. This finding led them to conclude that MGLL is unlikely to be the rate-limiting step in the degradation of lipid stores. If this is true *in vivo*, it could be hypothesized that the deletion of MGLL in adipocytes is at least partially compensated by MAG hydrolase activity of HSL, thereby mitigating any systemic effects.

Indeed, analysis of blood parameters revealed no genotype-dependent changes in FFA, glycerol, TAG, and glucose levels in AMKO mice. In contrast, Taschler *et al.* reported stable FFA levels in fed and fasted GMKO mice but a significant decrease in glycerol levels especially in 16-hour fasted KO mice [27]. Their results are compelling, as FFA release from the hydrolysis of TAGs and DAGs is assumed to be unaffected by the deletion of MGLL. But glycerol can only be released from MAG hydrolysis by MGLL. However, Douglass *et al.* reported a significant reduction of plasma FFA levels in GMKO mice fed a HFD for 12 weeks [29]. Tardelli *et al.* showed diminished FFA and glycerol levels in fasted GMKO mice fed a western diet [28]. As adipose tissue is the primary source of endogenous FFAs and glycerol especially in a fasted state, these reports clearly show the impairment of adipocyte lipolysis after MGLL deletion. Reduced plasma FFA availability is also suggested to limit VLDL production in the liver and could explain reduced plasma TAG levels reported in fasted MGLL KO mice [27,28].

Why none of these effects are present in AMKO mice is unclear. First of all, blood parameter variability was high within groups and probably masked genotype-dependent differences. Second, the absence of any diet-induced changes in FFA, glycerol, and TAG levels in male mice is rather unusual and stands in contrast to other studies which report increasing levels of these blood

parameters [27,29]. Plasma cholesterol levels were the exception and were significantly increased after 12 weeks of HFD in this study. However, the cholesterol levels reported in other studies after 10-12 weeks of HFD were only reached after a prolonged diet of 24 weeks [27–29]. Since the mice characterized here exhibited a comparable body weight gain, it can only be assumed that factors such as diet composition or genetics are responsible for these differences. The weak response of the animals to the HFD together with the high variance of the measured blood parameters may be the reason why no changes in adipocyte lipolysis were observed.

4.3 Interplay of HFD and MGLL KO Induces Complex Immunological Changes

Obese adipose tissue is characterized by low-grade inflammation due to increased infiltration of macrophages and elevated levels of proinflammatory cytokines such as TNF-α and IL-6 [92,93]. For this reason, immune cell populations and proinflammatory cytokine levels of AMKO mice were analyzed after 12 and 24 weeks of HFD. As already observed with the blood parameters, diet-dependent differences in cytokine levels were only observed after 24 weeks but not after 12 weeks of diet. In males fed a HFD concentrations of TNF-α, IL-10, and CXCL1 were increased, but only in KO mice this increase was significant. This suggests a positive interaction of HFD-induced obesity and the KO of MGLL. Female mice exhibited the same, albeit weaker, effect for CXCL1 as well as an HFD-induced reduction of IFN-γ levels. Male and female mice showed no differences in IL-6. Indeed, Douglass *et al.* showed that plasma levels of TNF-α are unaffected in WT mice after 12 weeks of HFD but increased, albeit not significantly, in GMKO mice fed the same diet [29]. However, they also observed an increase in plasma IL-6 levels in HFD-fed mice and the abrogation of this effect in GMKO mice. Other studies reported increased adipose tissue mRNA expression of *Tnfa* and *Il6* after 12 weeks of HFD as well as reduced expression in GMKO mice. Furthermore, HFD-fed GMKO showed a reduction in macrophage infiltration as well as reduced mRNA expression of Ccl2, a chemokine attracting monocytes which can differentiate into macrophages [28,68]. Macrophages account for the majority of TNF-α and IL-6 secretion in adipose tissue [92]. Suganami *et al.* suggested a paracrine loop between adipocytes and macrophages [92]. Coculture of adipocyte-like 3T3-L1 cells and the macrophage cell line RAW264 resulted in upregulation of proinflammatory cytokines such as TNF-α and IL-6. While TNF-α was found to increase FFA release in 3T3-L1 cells, incubation of macrophages with the fatty acid palmitate increased *Tnfa* mRNA expression in a dose-dependent manner. The proposed vicious cycle might bridge the gap between increased adipocyte lipolysis and adipose tissue inflammation observed in obesity. It would also provide the link between the reduction of proinflammatory cytokines and the diminished adipocyte lipolysis observed in GMKO mice.

The cytokine profiles of WT and AMKO mice characterized here were inconclusive and contradictory. The absence of diet-induced changes in WT mice after 12 and even 24 weeks of HFD matches the weak response of blood parameters to the HFD. The increase of plasma TNF-α in male AMKO mice fed a HFD suggests an amplification of diet-induced inflammation due to the deletion of MGLL in adipocytes and contradicts most findings reported in GMKO. Levels of CXL1, a neutrophil-attracting chemokine associated with inflammation, showed the same positive interaction of AMKO and HFD in male and female mice and therefore fit this picture. Hepatic and serum levels of CXCL1 were reported to be upregulated in mice fed a HFD for three days plus a single binge of ethanol. The researchers suggested an important role of CXCL1 in recruiting neutrophils to the liver and inducing liver injury. They also observed upregulation of *Cxcl1* mRNA in primary hepatocytes treated with FFAs such as palmitic acid, oleic acid, or linoleic acid [94]. It could be hypothesized that the reduced adipocyte lipolysis and reduced FFA release observed in GMKO leads to a decreased expression of CXCL1 and diminished liver inflammation. In contrast to the proinflammatory phenotype suggested by the increase of TNF-α and CXCL1, male AMKO mice fed a HFD exhibited elevated levels of the anti-inflammatory cytokine IL-10. Serum levels of IL-10 are known to be diminished in mice fed a HFD as well in humans with impaired glucose tolerance and obesity [93,95,96].

Main leucocyte populations were mostly unaffected by the HFD or the AMKO. Male mice showed reduced NK cell counts induced by the interaction of HFD and the KO of MGLL similar to the changes observed in cytokine levels. NK cells are discussed as a crucial element in adipose tissue inflammation of the obese. Wensveen *et al.* found that obesity stimulated adipocyte surface expression of ligands of the NK cell–activating receptor [97]. This induced NK cell proliferation and IFN-γ secretion which led to the activation of macrophages. Ablation of NK cells, the NK cell–activating receptor, or IFN-γ counteracted adipose tissue inflammation. While plasma NK cell counts were reduced in male AMKO mice fed a HFD no changes were observed in plasma IFN-γ levels. Surprisingly, feeding a HFD reduced IFN-γ levels in female mice regardless of genotype, whereas it did not affect plasma NK cell populations. In male mice feeding a HFD led to a shift from proinflammatory Ly-6C-intermediate monocytes to steady-state Ly-6C-low monocytes without affecting the overall monocyte count. Ly-6C-low monocytes circulate and inspect the vasculature and are early responders to inflammation and tissue repair [98]. Liu *et al.* observed an acute and transient increase in Ly-6-low monocytes together with an overall reduction of circulating monocytes after one week of HFD [99]. Nevertheless, there is currently not much known about the role of Ly-6-low monocytes in obesity and adipose tissue inflammation.

These result paint a complex picture of the immunomodulatory effect induced by the adipocyte-specific deletion of MGLL in mice fed a CD or an HFD. On the one hand, there are trends indicating

increased inflammation in KO mice such as elevated levels of TNF-α and CXCL1. On the other hand, there are indicators that the opposite is true such as increased levels of IL-10, and reduction of NK cell counts. The positive interaction of HFD- and KO-induced effects, whether they were inflammatory or anti-inflammatory, raises further questions. Especially the diet-induced effects deviate from the literature which calls the significance of the AMKO effects into question. Additionally, a sexual dimorphism can be observed where female mice are less affected by the HFD and the KO of MGLL. In comparison, studies on GMKO mice with diet-induced obesity are more conclusive. There, the KO of MGLL clearly protects from diet-induced adipocyte lipolysis, elevation of FFA levels and adipose tissue inflammation. However, these results primarily report on cytokine levels within adipose tissue and are to a certain extend less affected by changes in other tissues. Contrastingly, the plasma levels presented here represent a mixture of all diet- and KO-induced changes in the murine organism which might explain the complex and seemingly contradictory results.

4.4 KO of MGLL in Adipocytes Does Not Protect from Diet-Induced Insulin Resistance

GMKO mice are reported to be protected from diet-induced insulin resistance [27,29]. For this reason, GTT and ITT were carried out and fasting glucose and insulin levels were quantified in AMKO mice. After 18 weeks of HFD male and female mice exhibited impaired glucose tolerance as well as increased fasting insulin and glucose levels suggesting insulin resistance. An ITT at week 16 confirmed this finding. Nevertheless, the adipocyte-specific KO of MGLL did not induce any changes in terms of glucose clearance or insulin resistance.

Although the generation of diet-induced insulin resistance was a goal of this study, it is still surprising given the available data. While HFD-fed mice exhibited a significant gain in weight and fat mass, they showed no signs of increased lipolysis which is suggested to promote lipotoxicity and eventually insulin resistance [11]. Instead, plasma levels of FFA and glycerol remained stable even after an extended period of 24 weeks. In contrast, similar studies report elevated FFA and glycerol levels as early as 12 weeks after initiating HFD feeding [28,29]. Similarly, HFD-fed mice showed no signs of systemic inflammation after 12 weeks and only a mild increase in proinflammatory cytokines and NK cells after 24 weeks. Some of these changes were even less pronounced in female mice, and yet both sexes appear to be insulin resistant. Again, comparable studies report increased adipose tissue mRNA expression of proinflammatory cytokines such as *Il6* and *Tnfa* as well as an increased macrophage infiltration all of which are associated with insulin resistance [28,68]. Granted, mRNA is only a limited indicator of actual cytokine concentration and tissue levels are usually diluted in plasma. This limits the comparability of the findings presented here and the ones observed in other studies.

The lack of a genotype-dependent effect on insulin resistance of AMKO mice was not surprising after all. Studies on GMKO mice report the KO to counteract diet-induced effects associated with insulin resistance as well as an improvement of insulin resistance in KO mice [27–30,68]. In contrast, AMKO mice showed no differences in body weight, body composition, or clinical blood parameters compared to WT mice fed the same diet. Instead, the adipocyte-specific KO of MGLL was found to enhance diet-induced effects on plasma cytokine levels and immune cell populations.

4.5 MGLL KO Mildly Affects Adipocyte mRNA Expression and Lipid Metabolism

The absence of significant systemic changes induced by adipocyte-specific deletion of MGLL may be due to several reasons. One possibility is the compensation of the KO by the adipocytes themselves. Transcriptomics and metabolomics analysis were used to elucidate this question in male mice fed a HFD for 24 weeks. Total RNA sequencing revealed only few genes to be significantly up- or downregulated in AMKO mice. Most of the transcripts identified were not obviously related to MGLL, obesity, inflammation, or insulin resistance. Lipase gene expression was unaffected by the KO of MGLL. Similarly, Zimmermann *et al.* reported no compensation by other serine hydrolases in the brain of GMKO mice [100].

Interestingly, mRNA expression of the glutathione S-transferase A4 (*Gsta4*) was found to be upregulated in CD-fed as well as in HFD-fed AMKO mice. GSTA4 inactivates lipid-peroxidation products which are formed during oxidative stress [101]. Oxidative stress describes an overabundance of reactive oxygen species damaging different organs and is involved in the pathological effects of obesity and diabetes [102]. Reactive oxygen species are able to initiate peroxidation of polyunsaturated acyl chains of phospholipids in the membrane leading to the formation of lipid-derived reactive aldehydes [103]. 4 Hydroxynonenal (4-HNE) is the product of peroxidative degradation of arachidonic acid. It was shown to activate and inactivate proteins and accumulating evidence suggests that 4-HNE may play a role in metabolic syndrome causing insulin resistance [103,104]. GSTA4 displays especially high efficiency against 4-HNE inactivating it by conjugation of glutathione [101]. It could be presumed that AMKO mice accumulate 2-AG due to the diminished degradation by MGLL like it is reported for brain and liver tissue in GMKO mice [27,29]. This would in turn reduce the release of arachidonic acid, the FFA constituent of 2-AG, and impair the formation of 4-HNE. Assuming that all this is true, it is counterintuitive to observe increased GSTA4 expression in AMKO mice. There is certainly a need for additional research to elucidate the link between MGLL, GSTA4, 4-HNE, and its possible role in the pathogenesis of diet-induced insulin resistance.

Metabolomics analysis of the adipose tissue of AMKO mice, matched the results of transcriptomics analysis in that no extensive genotype-dependent changes were observed. Only few PCs and SMs affected by the KO of MGLL were identified, most of them in both male and female mice. For these metabolites deletion of MGLL counteracted the HFD-induced increase in metabolite concentrations. Additionally, few metabolites were also decreased in CD-fed KO mice. PC and SM are plasma membrane constituents and PC are the most abundant phospholipids forming the membrane of lipid droplets [105]. The fatty acid composition of the lipid metabolites reflected the HFD composition, incorporating the most available fatty acids C16:0, C16:1, C18:0, and C18:1. Arisawa *et al.* also reported these fatty acids to be highly abundant in phospholipids of 3T3L1 adipocyte lipid droplets [105]. The HFD-induced elevation in the identified metabolites is therefore most likely due to the expansion or generation of adipocyte lipid droplets. The reason for the reduction of PC and SM levels in AMKO mice is puzzling as MGLL it is not directly involved in the synthesis of these metabolites. The primary pathway of PC synthesis requires DAGs which are provided by the hydrolyzation of TAG storages by ATGL. SM are synthesized from ceramide and PC which might explain the similar changes in concentration compared to PC. SM can also be de novo synthesized from palmitic acid (C16:0) which might be less available due to the diminished breakdown of MAGs in MGLL KO mice. Hamada *et al.* reported ceramide accumulation and secretion of IL-6 and monocyte chemoattractant protein-1 in 3T3L1 cells treated with palmitic acid [106]. This opens up another pathway in which the KO of MGLL could potentially improve obesity-induced inflammation. However, no such effects were observed in AMKO mice, at least not in plasma cytokine levels.

4.6 Final Thoughts

The characterization of AMKO mice with HFD-induced obesity yielded new insights but also new questions regarding the role of adipocyte MGLL in healthy energy homeostasis as well as in obesity. On the one hand, MGLL KO mice exhibit a very mild phenotype on the systemic and fat tissue-specific level. This shows that the protective effect against diet-induced insulin resistance in GMKO is not attributable to adipocytes. It also calls into question the importance of MGLL in adipocyte lipolysis. On the other hand, effects that were observed contradict findings in global KO mice and can hardly be explained with the information currently available about MGLL. This leads to two connected questions. First, why are the observed effects so small, even though MGLL is considered one of main lipases responsible for adipocyte lipolysis? And second, which tissue or group of interacting tissues is actually responsible for the improvement of glucose tolerance and insulin sensitivity in GMKO mice?

In order to answer the first question, a consideration of the shortcomings of this study must be made. When considering the dietary effect, a high data variability was observed in HFD-fed animals possibly hiding genotype-dependent effects. This variability might have been induced by a peculiar behavior where mice ground the HFD into small flakes without eating it. The fatty flakes caused a greasy fur, skin irritations, and even ulcerations accompanied by weight loss. This behavior was found in all mice receiving a HFD irrespective of sex or genotype. No documentation of a similar behavior was found in the literature. Ultimately, severe cases had to be removed from the experiment. Still, differences in the health status of the mice due to latent inflammation of the skin might have caused increased data variability especially of immunological parameters. Smaller food portions and more frequent bedding replacement alleviated this problem to a certain degree. This practice should be implemented from the start in follow-up experiments. Another source of increased data variability might be the age differences of mice that stayed in the experiment for 24 weeks. While the standard deviation of animal age in the 12-week groups was at maximum 1 day, it was up to 11 days in the 24-week groups. This was necessary because the breeding yielded fewer offspring than expected and free places had to be filled up with slightly older mice. Age-dependent differences in adolescent and young adult mice, like the mice used for this study, are reported for behavior, food consumption, energy expenditure, and the plasma metabolome [107–109]. Breeding more animals could prevent this problem in future studies but has to be applied with care. Breeding excess offspring violates the 3R principle of reduction, which requires that the number of animals in experiments be kept to the absolute minimum.

Apart from these technical shortcomings, it has to be considered that MGLL activity is probably not mandatory for proper adipocyte lipolysis even during states of lipid overload. As mentioned before, Vaughan *et al.* showed that the *in vitro* activity of MGLL is multiple times higher than that of HSL which suggests that HSL or ATGL are the bottlenecks of adipocyte lipolysis [32]. Likewise, Taschler *et al.* showed that HSL is responsible for approx. 25 % of MAG hydrolase activity in adipocytes, which might be enough to maintain energy homeostasis in MGLL KO mice [27]. This is supported by adipose tissue transcriptomics and metabolomics data which revealed hardly any differences in MGLL KO mice and suggests unaffected adipocyte functionality. Investigation of the enzyme kinetics of adipocyte lipolysis is paramount for answering this question. Modification of the activity assays performed by Taschler *et al.* could be effective here, measuring glycerol concentrations in adipose tissue infranatants incubated with different amounts of TAG, DAG, or MAG substrates while specifically inhibiting ATGL, HSL, or MGLL [27].

Since the KO of adipocyte MGLL did not protect from insulin resistance in HFD-induced obesity, identification of the tissues and pathways responsible for these effects remains a worthwhile goal. As

discussed in section 2.1, the brain and the intestine are promising targets for further investigation, but current findings are mostly based on GMKO mice. Characterizations of tissue-specific KO models of the brain and the intestine in the setting of diet-induced obesity are needed to elucidate the link between MGLL, obesity, and insulin resistance.

5 Bibliography

1. *World health statistics 2021: monitoring health for the SDGs, sustainable development goals.*; Geneva, 2021;
2. Guthold, R. Global Health Observatory [online database] Available online: https://www.who.int/data/gho/data/themes/topics/topic-details/GHO/ncd-risk-factors (accessed on Apr 2, 2022).
3. Meldrum, D.R.; Morris, M.A.; Gambone, J.C. Obesity pandemic: causes, consequences, and solutions—but do we have the will? *Fertil. Steril.* **2017**, *107*, 833–839, doi:10.1016/j.fertnstert.2017.02.104.
4. Saklayen, M.G. The Global Epidemic of the Metabolic Syndrome. *Curr. Hypertens. Rep.* **2018**, *20*, 12, doi:10.1007/s11906-018-0812-z.
5. OECD *The Heavy Burden of Obesity: The Economics of Prevention*; OECD Health Policy Studies; OECD Publishing: Paris, 2019; ISBN 978-92-64-48458-0.
6. Morigny, P.; Houssier, M.; Mouisel, E.; Langin, D. Adipocyte lipolysis and insulin resistance. *Biochimie* **2016**, *125*, 259–266, doi:10.1016/j.biochi.2015.10.024.
7. Palmer, B.F.; Clegg, D.J. The sexual dimorphism of obesity. *Mol. Cell. Endocrinol.* **2015**, *402*, 113–119, doi:10.1016/j.mce.2014.11.029.
8. Chandra, A.; Neeland, I.J.; Berry, J.D.; Ayers, C.R.; Rohatgi, A.; Das, S.R.; Khera, A.; McGuire, D.K.; De Lemos, J.A.; Turer, A.T. The relationship of body mass and fat distribution with incident hypertension: Observations from the dallas heart study. *J. Am. Coll. Cardiol.* **2014**, *64*, 997–1002, doi:10.1016/j.jacc.2014.05.057.
9. Fox, C.S.; Massaro, J.M.; Hoffmann, U.; Pou, K.M.; Maurovich-Horvat, P.; Liu, C.Y.; Vasan, R.S.; Murabito, J.M.; Meigs, J.B.; Cupples, L.A.; et al. Abdominal visceral and subcutaneous adipose tissue compartments: Association with metabolic risk factors in the framingham heart study. *Circulation* **2007**, *116*, 39–48, doi:10.1161/CIRCULATIONAHA.106.675355.
10. Neeland, I.J.; Turer, A.T.; Ayers, C.R.; Powell-Wiley, T.M.; Vega, G.L.; Farzaneh-Far, R.; Grundy, S.M.; Khera, A.; McGuire, D.K.; De Lemos, J.A. Dysfunctional adiposity and the risk of prediabetes and type 2 diabetes in obese adults. *JAMA - J. Am. Med. Assoc.* **2012**, *308*, 1150–1159, doi:10.1001/2012.jama.11132.
11. Carobbio, S.; Pellegrinelli, V.; Vidal-Puig, A. Adipose Tissue Function and Expandability as Determinants of Lipotoxicity and the Metabolic Syndrome. In *Obesity and Lipotoxicity. Advances in Experimental Medicine and Biology*; Springer New York LLC, 2017; Vol. 960, pp. 161–196 ISBN 978-3-319-48382-5.
12. Robbins, A.L.; Savage, D.B. The genetics of lipid storage and human lipodystrophies. *Trends Mol. Med.* **2015**, *21*, 433–438, doi:10.1016/j.molmed.2015.04.004.
13. Engin, A. Fat Cell and Fatty Acid Turnover in Obesity. In *Obesity and Lipotoxicity. Advances in Experimental Medicine and Biology*; Springer New York LLC, 2017; Vol. 960, pp. 135–160 ISBN 978-3-319-48382-5.
14. Vishvanath, L.; Gupta, R.K. Contribution of adipogenesis to healthy adipose tissue expansion in obesity. *J. Clin. Invest.* **2019**, *129*, 4022–4031, doi:10.1172/JCI129191.
15. Yazıcı, D.; Sezer, H. Insulin Resistance, Obesity and Lipotoxicity. In *Obesity and Lipotoxicity. Advances in Experimental Medicine and Biology*; Springer New York LLC, 2017; Vol. 960, pp. 277–304 ISBN 978-3-319-48382-5.
16. Hamasaki, H. The Effects of Exercise on Natriuretic Peptides in Individuals without Heart Failure. *Sports* **2016**, *4*, 32, doi:10.3390/sports4020032.
17. Yang, A.; Mottillo, E.P. Adipocyte lipolysis: From molecular mechanisms of regulation to disease and therapeutics. *Biochem. J.* **2020**, *477*, 985–1008, doi:10.1042/BCJ20190468.

18. Girousse, A.; Tavernier, G.; Valle, C.; Moro, C.; Mejhert, N.; Dinel, A.L.; Houssier, M.; Roussel, B.; Besse-Patin, A.; Combes, M.; et al. Partial Inhibition of Adipose Tissue Lipolysis Improves Glucose Metabolism and Insulin Sensitivity Without Alteration of Fat Mass. *PLoS Biol.* **2013**, *11*, 1001485, doi:10.1371/journal.pbio.1001485.
19. Moro, C.; Lafontan, M. Natriuretic peptides and cGMP signaling control of energy homeostasis. *Am. J. Physiol. - Hear. Circ. Physiol.* **2013**, *304*, 358–368, doi:10.1152/ajpheart.00704.2012.
20. Arner, P.; Langin, D. Lipolysis in lipid turnover, cancer cachexia, and obesity-induced insulin resistance. *Trends Endocrinol. Metab.* **2014**, *25*, 255–262, doi:10.1016/j.tem.2014.03.002.
21. Robidoux, J.; Martin, T.L.; Collins, S. β-Adrenergic Receptors and Regulation of Energy Expenditure: A Family Affair. *Annu. Rev. Pharmacol. Toxicol.* **2004**, *44*, 297–323, doi:10.1146/annurev.pharmtox.44.101802.121659.
22. Nguyen, M.T.A.; Satoh, H.; Favelyukis, S.; Babendure, J.L.; Imamura, T.; Sbodio, J.I.; Zalevsky, J.; Dahiyat, B.I.; Chi, N.W.; Olefsky, J.M. JNK and tumor necrosis factor-α mediate free fatty acid-induced insulin resistance in 3T3-L1 adipocytes. *J. Biol. Chem.* **2005**, *280*, 35361–35371, doi:10.1074/jbc.M504611200.
23. Van Hall, G.; Steensberg, A.; Sacchetti, M.; Fischer, C.; Keller, C.; Schjerling, P.; Hiscock, N.; Møller, K.; Saltin, B.; Febbraio, M.A.; et al. Interleukin-6 stimulates lipolysis and fat oxidation in humans. *J. Clin. Endocrinol. Metab.* **2003**, *88*, 3005–3010, doi:10.1210/jc.2002-021687.
24. Perry, R.J.; Camporez, J.P.G.; Kursawe, R.; Titchenell, P.M.; Zhang, D.; Perry, C.J.; Jurczak, M.J.; Abudukadier, A.; Han, M.S.; Zhang, X.M.; et al. Hepatic acetyl CoA links adipose tissue inflammation to hepatic insulin resistance and type 2 diabetes. *Cell* **2015**, *160*, 745–758, doi:10.1016/j.cell.2015.01.012.
25. Ertunc, M.E.; Sikkeland, J.; Fenaroli, F.; Griffiths, G.; Daniels, M.P.; Cao, H.; Saatcioglu, F.; Hotamisligil, G.S. Secretion of fatty acid binding protein aP2 from adipocytes through a nonclassical pathway in response to adipocyte lipase activity. *J. Lipid Res.* **2015**, *56*, 423–434, doi:10.1194/jlr.M055798.
26. Schoiswohl, G.; Stefanovic-Racic, M.; Menke, M.N.; Wills, R.C.; Surlow, B.A.; Basantani, M.K.; Sitnick, M.T.; Cai, L.; Yazbeck, C.F.; Stolz, D.B.; et al. Impact of reduced ATGL-mediated adipocyte lipolysis on obesity-associated insulin resistance and inflammation in male mice. *Endocrinology* **2015**, *156*, 3610–3624, doi:10.1210/en.2015-1322.
27. Taschler, U.; Radner, F.P.W.; Heier, C.; Schreiber, R.; Schweiger, M.; Schoiswohl, G.; Preiss-Landl, K.; Jaeger, D.; Reiter, B.; Koefeler, H.C.; et al. Monoglyceride lipase deficiency in mice impairs lipolysis and attenuates diet-induced insulin resistance. *J. Biol. Chem.* **2011**, *286*, 17467–17477, doi:10.1074/jbc.M110.215434.
28. Tardelli, M.; Bruschi, F. V.; Claudel, T.; Fuchs, C.D.; Auer, N.; Kunczer, V.; Stojakovic, T.; Scharnagl, H.; Habib, A.; Grabner, G.F.; et al. Lack of monoacylglycerol lipase prevents hepatic steatosis by favoring lipid storage in adipose tissue and intestinal malabsorption. *J. Lipid Res.* **2019**, *60*, 1284–1292, doi:10.1194/jlr.M093369.
29. Douglass, J.D.; Zhou, Y.X.; Wu, A.; Zadrogra, J.A.; Gajda, A.M.; Lackey, A.I.; Lang, W.; Chevalier, K.M.; Sutton, S.W.; Zhang, S.P.; et al. Global deletion of MGL in mice delays lipid absorption and alters energy homeostasis and diet-induced obesity. *J. Lipid Res.* **2015**, *56*, 1153–1171, doi:10.1194/jlr.M058586.
30. Dione, N.; Lacroix, S.; Taschler, U.; Deschênes, T.; Abolghasemi, A.; Leblanc, N.; Di Marzo, V.; Silvestri, C. Mgll Knockout Mouse Resistance to Diet-Induced Dysmetabolism Is Associated with Altered Gut Microbiota. *Cells* **2020**, *9*, doi:10.3390/cells9122705.
31. Senior, J.R.; Isselbacher, K.J. Demonstration of an intestinal monoglyceride lipase: an enzyme with a possible role in the intracellular completion of fat digestion. *J. Clin. Invest.* **1963**, *42*, 187–195, doi:10.1172/JCI104705.
32. Vaughan, M.; Berger, J.E.; Steinberg, D. Hormone-sensitive Lipase and Monoglyceride Lipase Activities in Adipose Tissue. *J. Biol. Chem.* **1964**, *239*, 401–409.

33. Tornqvist, H.; Belfrage, P. Purification and some properties of a monoacylglycerol-hydrolyzing enzyme of rat adipose tissue. *J. Biol. Chem.* **1976**, *251*, 813–819.
34. Karlsson, M.; Contreras, J.A.; Hellman, U.; Tornqvist, H.; Holm, C. cDNA cloning, tissue distribution, and identification of the catalytic triad of monoglyceride lipase. Evolutionary relationship to esterases, lysophospholipases, and haloperoxidases. *J. Biol. Chem.* **1997**, *272*, 27218–27223, doi:10.1074/jbc.272.43.27218.
35. Karlsson, M.; Reue, K.; Xia, Y.R.; Lusis, A.J.; Langin, D.; Tornqvist, H.; Holm, C. Exon-intron organization and chromosomal localization of the mouse monoglyceride lipase gene. *Gene* **2001**, *272*, 11–18, doi:10.1016/S0378-1119(01)00559-5.
36. Howe, K.L.; Achuthan, P.; Allen, J.; Allen, J.; Alvarez-Jarreta, J.; Ridwan Amode, M.; Armean, I.M.; Azov, A.G.; Bennett, R.; Bhai, J.; et al. Ensembl 2021. *Nucleic Acids Res.* **2021**, *49*, D884–D891, doi:10.1093/NAR/GKAA942.
37. Sayers, E.W.; Beck, J.; Bolton, E.E.; Bourexis, D.; Brister, J.R.; Canese, K.; Comeau, D.C.; Funk, K.; Kim, S.; Klimke, W.; et al. Database resources of the National Center for Biotechnology Information. *Nucleic Acids Res.* **2021**, *49*, D10–D17, doi:10.1093/NAR/GKAA892.
38. Labar, G.; Wouters, J.; Lambert, D.M. A Review on the Monoacylglycerol Lipase: At the Interface Between Fat and Endocannabinoid Signalling. *Curr. Med. Chem.* **2010**, *17*, 2588–607, doi:10.2174/092986710791859414.
39. Labar, G.; Bauvois, C.; Borel, F.; Ferrer, J.L.; Wouters, J.; Lambert, D.M. Crystal structure of the human monoacylglycerol lipase, a key actor in endocannabinoid signaling. *ChemBioChem* **2010**, *11*, 218–227, doi:10.1002/cbic.200900621.
40. Schalk-Hihi, C.; Schubert, C.; Alexander, R.; Bayoumy, S.; Clemente, J.C.; Deckman, I.; DesJarlais, R.L.; Dzordzorme, K.C.; Flores, C.M.; Grasberger, B.; et al. Crystal structure of a soluble form of human monoglyceride lipase in complex with an inhibitor at 1.35 A ° resolution. *Protein Sci.* **2011**, *20*, 670–683, doi:10.1002/pro.596.
41. Bertrand, T.; Augé, F.; Houtmann, J.; Rak, A.; Vallée, F.; Mikol, V.; Berne, P.F.; Michot, N.; Cheuret, D.; Hoornaert, C.; et al. Structural Basis for Human Monoglyceride Lipase Inhibition. *J. Mol. Biol.* **2010**, *396*, 663–673, doi:10.1016/j.jmb.2009.11.060.
42. Ollis, D.L.; Cheah, E.; Cygler, M.; Dijkstra, B.; Frolow, F.; Franken, S.M.; Harel, M.; Remington, S.J.; Silman, I.; Schrag, J. The alpha/beta hydrolase fold. *Protein Eng.* **1992**, *5*, 197–211, doi:10.1093/protein/5.3.197.
43. Ollis, D.L.; Carr, P.D. Alpha/Beta Hydrolase Fold: An Update. *Protein Pept. Lett.* **2009**, *16*, 1137–1148, doi:10.2174/092986609789071298.
44. Nardini, M.; Dijkstra, B.W. α/β hydrolase fold enzymes: the family keeps growing. *Curr. Opin. Struct. Biol.* **1999**, *9*, 732–737, doi:10.1016/S0959-440X(99)00037-8.
45. Gil-Ordóñez, A.; Martín-Fontecha, M.; Ortega-Gutiérrez, S.; López-Rodríguez, M.L. Monoacylglycerol lipase (MAGL) as a promising therapeutic target. *Biochem. Pharmacol.* **2018**, *157*, 18–32, doi:10.1016/J.BCP.2018.07.036.
46. Dinh, T.P.; Carpenter, D.; Leslie, F.M.; Freund, T.F.; Katona, I.; Sensi, S.L.; Kathuria, S.; Piomelli, D. Brain monoglyceride lipase participating in endocannabinoid inactivation. *Proc. Natl. Acad. Sci. U. S. A.* **2002**, *99*, 10819–10824, doi:10.1073/pnas.152334899.
47. Blankman, J.L.; Simon, G.M.; Cravatt, B.F. A Comprehensive Profile of Brain Enzymes that Hydrolyze the Endocannabinoid 2-Arachidonoylglycerol. *Chem. Biol.* **2007**, *14*, 1347–1356, doi:10.1016/j.chembiol.2007.11.006.
48. Chon, S.H.; Yin, X.Z.; Dixon, J.L.; Storch, J. Intestinal monoacylglycerol metabolism: Developmental and nutritional regulation of monoacylglycerol lipase and monoacylglycerol acyltransferase. *J. Biol. Chem.* **2007**, *282*, 33346–33357, doi:10.1074/jbc.M706994200.
49. Rakhshandehroo, M.; Sanderson, L.M.; Matilainen, M.; Stienstra, R.; Carlberg, C.; De Groot, P.J.; Müller, M.; Kersten, S. Comprehensive analysis of PPARα-dependent regulation of hepatic lipid metabolism by expression profiling. *PPAR Res.* **2007**, *2007*, doi:10.1155/2007/26839.

50. Patsouris, D.; Mandard, S.; Voshol, P.J.; Escher, P.; Tan, N.S.; Havekes, L.M.; Koenig, W.; März, W.; Tafuri, S.; Wahli, W.; et al. PPARα governs glycerol metabolism. *J. Clin. Invest.* **2004**, *114*, 94–103, doi:10.1172/jci20468.
51. Rosen, E.D.; Walkey, C.J.; Puigserver, P.; Spiegelman, B.M. Transcriptional regulation of adipogenesis. *Genes Dev.* **2000**, *14*, 1293–1307, doi:10.1101/gad.14.11.1293.
52. Han, L.; Shen, W.J.; Bittner, S.; Kraemer, F.B.; Azhar, S. PPARs: Regulators of metabolism and as therapeutic targets in cardiovascular disease. Part II: PPAR-β/δ and PPAR-γ. *Future Cardiol.* **2017**, *13*, 279–296, doi:10.2217/fca-2017-0019.
53. Harmon, G.S.; Dumlao, D.S.; Ng, D.T.; Barrett, K.E.; Dennis, E.A.; Dong, H.; Glass, C.K. Pharmacological correction of a defect in PPAR-γ signaling ameliorates disease severity in Cftr-deficient mice. *Nat. Med.* **2010**, *16*, 313–318, doi:10.1038/nm.2101.
54. Yang, X.; Zhang, D.; Liu, S.; Li, X.; Hu, W.; Han, C. KLF4 suppresses the migration of hepatocellular carcinoma by transcriptionally upregulating monoglyceride lipase. *Am. J. Cancer Res.* **2018**, *8*, 1019–1029.
55. Ghaleb, A.M.; Yang, V.W. Krüppel-like factor 4 (KLF4): What we currently know. *Gene* **2017**, *611*, 27–37, doi:10.1016/j.gene.2017.02.025.
56. Dotsey, E.Y.; Jung, K.M.; Basit, A.; Wei, D.; Daglian, J.; Vacondio, F.; Armirotti, A.; Mor, M.; Piomelli, D. Peroxide-dependent MGL sulfenylation regulates 2-AG-mediated endocannabinoid signaling in brain neurons. *Chem. Biol.* **2015**, *22*, 619–628, doi:10.1016/j.chembiol.2015.04.013.
57. Scalvini, L.; Vacondio, F.; Bassi, M.; Pala, D.; Lodola, A.; Rivara, S.; Jung, K.M.; Piomelli, D.; Mor, M. Free-energy studies reveal a possible mechanism for oxidation-dependent inhibition of MGL. *Sci. Rep.* **2016**, *6*, doi:10.1038/srep31046.
58. Lowe, M.E. Pancreatic Triglyceride Lipase and Colipase: Insights Into Dietary Fat Digestion. *Gastroenterology* **1994**, *107*, 1524–1536, doi:10.1016/0016-5085(94)90559-2.
59. Wang, H.; Eckel, R.H. Lipoprotein lipase: from gene to obesity. *Am. J. Physiol. - Endocrinol. Metab.* **2009**, *297*, E271–E288, doi:10.1152/ajpendo.90920.2008.
60. Yen, C.L.E.; Nelson, D.W.; Yen, M.I. Intestinal triacylglycerol synthesis in fat absorption and systemic energy metabolism. *J. Lipid Res.* **2015**, *56*, 489–501, doi:10.1194/jlr.R052902.
61. Grabner, G.F.; Zimmermann, R.; Schicho, R.; Taschler, U. Monoglyceride lipase as a drug target: At the crossroads of arachidonic acid metabolism and endocannabinoid signaling. *Pharmacol. Ther.* **2017**, *175*, 35–46, doi:10.1016/j.pharmthera.2017.02.033.
62. Herkenham, M.; Lynn, A.B.; Little, M.D.; Johnson, M.R.; Melvin, L.S.; De Costa, B.R.; Rice, K.C. Cannabinoid receptor localization in brain. *Proc. Natl. Acad. Sci. U. S. A.* **1990**, *87*, 1932–1936, doi:10.1073/pnas.87.5.1932.
63. Pagotto, U.; Marsicano, G.; Cota, D.; Lutz, B.; Pasquali, R. The Emerging Role of the Endocannabinoid System in Endocrine Regulation and Energy Balance. *Endocr. Rev.* **2006**, *27*, 73–100, doi:10.1210/er.2005-0009.
64. Munro, S.; Thomas, K.L.; Abu-Shaar, M. Molecular characterization of a peripheral receptor for cannabinoids. *Nature* **1993**, *365*, 61–65, doi:10.1038/365061a0.
65. Di Marzo, V. The endocannabinoid system: Its general strategy of action, tools for its pharmacological manipulation and potential therapeutic exploitation. *Pharmacol. Res.* **2009**, *60*, 77–84, doi:10.1016/j.phrs.2009.02.010.
66. Duncan, M.; Thomas, A.D.; Cluny, N.L.; Patel, A.; Patel, K.D.; Lutz, B.; Piomelli, D.; Alexander, S.P.H.; Sharkey, K.A. Distribution and function of monoacylglycerol lipase in the gastrointestinal tract. *https://doi.org/10.1152/ajpgi.90500.2008* **2008**, *295*, 1255–1265, doi:10.1152/AJPGI.90500.2008.
67. Brinker, A.; Dixon, J.L.; Zhou, Y.X.; Chon, S.-H.; Malik, N.; Quadro, L.; Storch, J.; Douglass, J.D. Over-Expression of Monoacylglycerol Lipase (MGL) in Small Intestine Alters Endocannabinoid Levels and Whole Body Energy Balance, Resulting in Obesity. *PLoS One* **2012**, *7*, e43962, doi:10.1371/journal.pone.0043962.

68. Yoshida, K.; Kita, Y.; Tokuoka, S.M.; Hamano, F.; Yamazaki, M.; Sakimura, K.; Kano, M.; Shimizu, T. Monoacylglycerol lipase deficiency affects diet-induced obesity, fat absorption, and feeding behavior in CB1 cannabinoid receptor-deficient mice. *FASEB J.* **2019**, *33*, 2484–2497, doi:10.1096/fj.201801203R.
69. Rathkolb, B.; Fuchs, H.; Gailus-Durner, V.; Aigner, B.; Wolf, E.; Hrabě de Angelis, M. Blood Collection from Mice and Hematological Analyses on Mouse Blood. *Curr. Protoc. Mouse Biol.* **2013**, *3*, 101–119, doi:https://doi.org/10.1002/9780470942390.mo130054.
70. Rathkolb, B.; Hans, W.; Prehn, C.; Fuchs, H.; Gailus-Durner, V.; Aigner, B.; Adamski, J.; Wolf, E.; Hrabě de Angelis, M. Clinical Chemistry and Other Laboratory Tests on Mouse Plasma or Serum. *Curr. Protoc. Mouse Biol.* **2013**, *3*, 69–100, doi:https://doi.org/10.1002/9780470942390.mo130043.
71. Römisch-Margl, W.; Prehn, C.; Bogumil, R.; Röhring, C.; Suhre, K.; Adamski, J. Procedure for tissue sample preparation and metabolite extraction for high-throughput targeted metabolomics. *Metabolomics* **2012**, *8*, 133–142, doi:10.1007/s11306-011-0293-4.
72. Zukunft, S.; Prehn, C.; Röhring, C.; Möller, G.; Hrabě de Angelis, M.; Adamski, J.; Tokarz, J. High-throughput extraction and quantification method for targeted metabolomics in murine tissues. *Metabolomics* **2018**, *14*, 1–12, doi:10.1007/s11306-017-1312-x.
73. R Core Team R A Language and Environment for Statistical Computing 2020.
74. Dobin, A.; Davis, C.A.; Schlesinger, F.; Drenkow, J.; Zaleski, C.; Jha, S.; Batut, P.; Chaisson, M.; Gingeras, T.R. STAR: Ultrafast universal RNA-seq aligner. *Bioinformatics* **2013**, *29*, 15–21, doi:10.1093/bioinformatics/bts635.
75. Anders, S.; Pyl, P.T.; Huber, W. HTSeq-A Python framework to work with high-throughput sequencing data. *Bioinformatics* **2015**, *31*, 166–169, doi:10.1093/bioinformatics/btu638.
76. Livak, K.J.; Schmittgen, T.D. Analysis of Relative Gene Expression Data Using Real-Time Quantitative PCR and the 2−ΔΔCT Method. *Methods* **2001**, *25*, 402–408, doi:10.1006/METH.2001.1262.
77. Benjamini, Y.; Hochberg, Y. Controlling the False Discovery Rate: A Practical and Powerful Approach to Multiple Testing. *J. R. Stat. Soc. Ser. B* **1995**, *57*, 289–300, doi:10.1111/j.2517-6161.1995.tb02031.x.
78. Holm, S. A Simple Sequentially Rejective Multiple Test Procedure. *Scand. J. Stat.* **1979**, *6*, 65–70.
79. Pang, Z.; Chong, J.; Zhou, G.; De Lima Morais, D.A.; Chang, L.; Barrette, M.; Gauthier, C.; Jacques, P.É.; Li, S.; Xia, J. MetaboAnalyst 5.0: narrowing the gap between raw spectra and functional insights. *Nucleic Acids Res.* **2021**, *49*, W388–W396, doi:10.1093/NAR/GKAB382.
80. Love, M.I.; Huber, W.; Anders, S. Moderated estimation of fold change and dispersion for RNA-seq data with DESeq2. *Genome Biol.* **2014**, *15*, doi:10.1186/s13059-014-0550-8.
81. Garelli, S.; Salituro, N.; Pontesilli, G.M.; Ricciardiello, L.; Vicennati, V.; Pagotto, U. Treatment: New Drugs. *Encycl. Endocr. Dis.* **2019**, 464–472, doi:10.1016/B978-0-12-801238-3.65344-8.
82. Apovian, C.M.; Aronne, L.J.; Bessesen, D.H.; McDonnell, M.E.; Murad, M.H.; Pagotto, U.; Ryan, D.H.; Still, C.D. Pharmacological Management of Obesity: An Endocrine Society Clinical Practice Guideline. *J. Clin. Endocrinol. Metab.* **2015**, *100*, 342–362, doi:10.1210/JC.2014-3415.
83. Imperatore, R.; Morello, G.; Luongo, L.; Taschler, U.; Romano, R.; De Gregorio, D.; Belardo, C.; Maione, S.; Di Marzo, V.; Cristino, L. Genetic deletion of monoacylglycerol lipase leads to impaired cannabinoid receptor CB1R signaling and anxiety-like behavior. *J. Neurochem.* **2015**, *135*, 799–813, doi:10.1111/jnc.13267.
84. Taschler, U.; Eichmann, T.O.; Radner, F.P.W.; Grabner, G.F.; Wolinski, H.; Storr, M.; Lass, A.; Schicho, R.; Zimmermann, R. Monoglyceride lipase deficiency causes desensitization of intestinal cannabinoid receptor type 1 and increased colonic μ-opioid receptor sensitivity. *Br. J. Pharmacol.* **2015**, *172*, 4419–4429, doi:10.1111/bph.13224.

85. Chanda, P.K.; Gao, Y.; Mark, L.; Btesh, J.; Strassle, B.W.; Lu, P.; Piesla, M.J.; Zhang, M.Y.; Bingham, B.; Uveges, A.; et al. Monoacylglycerol lipase activity is a critical modulator of the tone and integrity of the endocannabinoid system. *Mol. Pharmacol.* **2010**, *78*, 996–1003, doi:10.1124/mol.110.068304.
86. Casellas, J. Inbred mouse strains and genetic stability: a review. *Animal* **2011**, *5*, 1–7, doi:10.1017/S1751731110001667.
87. Haemmerle, G.; Lass, A.; Zimmermann, R.; Gorkiewicz, G.; Meyer, C.; Rozman, J.; Heldmaier, G.; Maier, R.; Theussl, C.; Eder, S.; et al. Defective lipolysis and altered energy metabolism in mice lacking adipose triglyceride lipase. *Science (80-.).* **2006**, *312*, 734–737, doi:10.1126/science.1123965.
88. Di Marzo, V. The endocannabinoid system in obesity and type 2 diabetes. *Diabetologia* **2008**, *51*, 1356–1367, doi:10.1007/s00125-008-1048-2.
89. Schlosburg, J.E.; Blankman, J.L.; Long, J.Z.; Nomura, D.K.; Pan, B.; Kinsey, S.G.; Nguyen, P.T.; Ramesh, D.; Booker, L.; Burston, J.J.; et al. Chronic monoacylglycerol lipase blockade causes functional antagonism of the endocannabinoid system. *Nat. Neurosci.* **2010**, *13*, 1113–1119, doi:10.1038/nn.2616.
90. Grabner, G.F.; Eichmann, T.O.; Wagner, B.; Gao, Y.; Farzi, A.; Taschler, U.; Radner, F.P.W.; Schweiger, M.; Lass, A.; Holzer, P.; et al. Deletion of monoglyceride lipase in astrocytes attenuates lipopolysaccharide-induced neuroinflammation. *J. Biol. Chem.* **2016**, *291*, 913–923, doi:10.1074/jbc.M115.683615.
91. Botham, K.M.; Wheeler-Jones, C.P.D. Postprandial lipoproteins and the molecular regulation of vascular homeostasis. *Prog. Lipid Res.* **2013**, *52*, 446–464, doi:10.1016/j.plipres.2013.06.001.
92. Suganami, T.; Nishida, J.; Ogawa, Y. A paracrine loop between adipocytes and macrophages aggravates inflammatory changes: Role of free fatty acids and tumor necrosis factor α. *Arterioscler. Thromb. Vasc. Biol.* **2005**, *25*, 2062–2068, doi:10.1161/01.ATV.0000183883.72263.13.
93. Kondo, H.; Abe, I.; Gotoh, K.; Fukui, A.; Takanari, H.; Ishii, Y.; Ikebe, Y.; Kira, S.; Oniki, T.; Saito, S.; et al. Interleukin 10 Treatment Ameliorates High-Fat Diet-Induced Inflammatory Atrial Remodeling and Fibrillation. *Circ. Arrhythm. Electrophysiol.* **2018**, *11*, e006040, doi:10.1161/CIRCEP.117.006040.
94. Chang, B.; Xu, M.J.; Zhou, Z.; Cai, Y.; Li, M.; Wang, W.; Feng, D.; Bertola, A.; Wang, H.; Kunos, G.; et al. Short- or long-term high-fat diet feeding plus acute ethanol binge synergistically induce acute liver injury in mice: An important role for CXCL1. *Hepatology* **2015**, *62*, 1070–1085, doi:10.1002/hep.27921.
95. Gotoh, K.; Inoue, M.; Masaki, T.; Chiba, S.; Shiraishi, K.; Shimasaki, T.; Matsuoka, K.; Ando, H.; Fujiwara, K.; Fukunaga, N.; et al. Obesity-related chronic kidney disease is associated with spleen-derived IL-10. *Nephrol. Dial. Transplant.* **2013**, *28*, 1120–1130, doi:10.1093/ndt/gfs440.
96. Blüher, M.; Fasshauer, M.; Tönjes, A.; Kratzsch, J.; Schön, M.R.; Paschke, R. Association of interleukin-6, C-reactive protein, interleukin-10 and adiponectin plasma concentrations with measures of obesity, insulin sensitivity and glucose metabolism. *Exp. Clin. Endocrinol. Diabetes* **2005**, *113*, 534–537, doi:10.1055/s-2005-872851.
97. Wensveen, F.M.; Jelenčić, V.; Valentić, S.; Šestan, M.; Wensveen, T.T.; Theurich, S.; Glasner, A.; Mendrila, D.; Štimac, D.; Wunderlich, F.T.; et al. NK cells link obesity-induced adipose stress to inflammation and insulin resistance. *Nat. Immunol.* **2015**, *16*, 376–385, doi:10.1038/ni.3120.
98. Kratofil, R.M.; Kubes, P.; Deniset, J.F. Monocyte Conversion During Inflammation and Injury. *Arterioscler. Thromb. Vasc. Biol.* **2017**, *37*, 35–42, doi:10.1161/ATVBAHA.116.308198.
99. Liu, Y.; Lu, X.; Li, X.; Du, P.; Qin, G. High-fat diet triggers obesity-related early infiltration of macrophages into adipose tissue and transient reduction of blood monocyte count. *Mol. Immunol.* **2020**, *117*, 139–146, doi:10.1016/j.molimm.2019.11.002.

100. Zimmermann, R.; Laitinen, J.T.; Aaltonen, N.; Taschler, U.; Lehtonen, M.; Navia-Paldanius, D.; Savinainen, J.R.; Radner, F.P.W. Increased tonic cannabinoid CB1R activity and brain region-specific desensitization of CB1R Gi/o signaling axis in mice with global genetic knockout of monoacylglycerol lipase. *Eur. J. Pharm. Sci.* **2015**, *77*, 180–188, doi:10.1016/j.ejps.2015.06.005.
101. Hubatsch, I.; Ridderström, M.; Mannervik, B. Human glutathione transferase A4-4: An Alpha class enzyme with high catalytic efficiency in the conjugation of 4-hydroxynonenal and other genotoxic products of lipid peroxidation. *Biochem. J.* **1998**, *330*, 175–179, doi:10.1042/bj3300175.
102. Fernández-Sánchez, A.; Madrigal-Santillán, E.; Bautista, M.; Esquivel-Soto, J.; Morales-González, Á.; Esquivel-Chirino, C.; Durante-Montiel, I.; Sánchez-Rivera, G.; Valadez-Vega, C.; Morales-González, J.A. Inflammation, Oxidative Stress, and Obesity. *Int. J. Mol. Sci.* **2011**, *12*, 3117–3132, doi:10.3390/ijms12053117.
103. Grimsrud, P.A.; Picklo, M.J.; Griffin, T.J.; Bernlohr, D.A. Carbonylation of adipose proteins in obesity and insulin resistance: Identification of adipocyte fatty acid-binding protein as a cellular target of 4-hydroxynonenal. *Mol. Cell. Proteomics* **2007**, *6*, 624–637, doi:10.1074/mcp.M600120-MCP200.
104. Mattson, M.P. Roles of the Lipid Peroxidation Product 4-Hydroxynonenal in Obesity, the Metabolic Syndrome, and Associated Vascular and Neurodegenerative Disorders. *Exp. Gerontol.* **2009**, *44*, 625–633, doi:10.1016/j.exger.2009.07.003.
105. Arisawa, K.; Ichi, I.; Yasukawa, Y.; Sone, Y.; Fujiwara, Y. Changes in the phospholipid fatty acid composition of the lipid droplet during the differentiation of 3T3-L1 adipocytes. *J. Biochem.* **2013**, *154*, 281–289, doi:10.1093/jb/mvt051.
106. Hamada, Y.; Nagasaki, H.; Fujiya, A.; Seino, Y.; Shang, Q.L.; Suzuki, T.; Hashimoto, H.; Oiso, Y. Involvement of de novo ceramide synthesis in pro-inflammatory adipokine secretion and adipocyte–macrophage interaction. *J. Nutr. Biochem.* **2014**, *25*, 1309–1316, doi:10.1016/J.JNUTBIO.2014.07.008.
107. Moore, E.M.; Linsenbardt, D.N.; Melón, L.C.; Boehm, S.L. 2nd Ontogenetic differences in adolescent and adult C57BL/6J and DBA/2J mice: anxiety-like, locomotor, and consummatory behaviors. *Dev. Psychobiol.* **2011**, *53*, 141–156, doi:10.1002/dev.20501.
108. Pann, P.; Angelis, M.H. de; Prehn, C.; Adamski, J. Mouse Age Matters: How Age Affects the Murine Plasma Metabolome. *Metab. 2020, Vol. 10, Page 472* **2020**, *10*, 472, doi:10.3390/METABO10110472.
109. Pinchuk, L.M.; Filipov, N.M. Differential effects of age on circulating and splenic leukocyte populations in C57BL/6 and BALB/c male mice. *Immun. Ageing* **2008**, *5*, 1, doi:10.1186/1742-4933-5-1.

6 Appendix

Table A1. Composition of the experimental diets.

	Control	HFD		Control	HFD
Energy			**Fatty acids [%]**		
Metabolizable Energy	15 MJ/kg	21.4 MJ/kg	C 8:0	-	-
Carbohydrates	66 kJ%	21 kJ%	C10:0	-	-
Fat	11 kJ%	60 kJ%	C12:0	-	0.03
Protein	23 kJ%	19 kJ%	C14:0	0.02	1.03
Crude Nutrients [%]			C16:0	0.45	8.06
Dry matter	95.2	94.0	C16:1	0.02	0.78
Crude protein	20.8	24.1	C17:0	ns	0.38
Crude fat	4.2	34.6	C18:0	0.19	5.61
Crude fiber	5.0	6.0	C18:1	1.07	12.13
Crude ash	5.6	6.1	C18:2	2.12	2.37
N free extracts	59.4	23.3	C18:3	0.26	0.33
Starch	46.8	0.5	C20:0	0.02	0.04
Sugar	10.8	9.5	C20:1	-	0.01
Dextrin	ns	15.3	C20:4	ns	0.07
Minerals [%]			C20:5	-	-
Calcium	0.90	0.98	C22:6	-	-
Phosphorus	0.63	0.65	**Vitamins [per kg]**		
Sodium	0.19	0.20	Vitamin A	15,000 IU	15,000 IU
Magnesium	0.21	0.17	Vitamin D3	1,500 IU	1,500 IU
Potassium	0.97	0.98	Vitamin E	150 mg	150 mg
Amino acids [%]			Menadione (K)	20 mg	20 mg
Lys	1.71	1.98	Vitamin C	30 mg	30 mg
Met	0.69	0.83	Thiamin (B1)	16 mg	16 mg
Cys	ns	0.46	Riboflavin (B2)	16 mg	16 mg
Met + Cys	0.98	1.28	Pyridoxine (B6)	18 mg	18 mg
Thr	0.93	1.07	Cobalamin (B12)	30 µg	30 µg
Trp	0.27	0.31	Nicotinic acid	49 mg	45 mg
Arg	0.76	0.88	Pantothenic acid	56 mg	55 mg
His	0.66	0.76	Folic acid	19 mg	19 mg
Val	1.42	1.64	Biotin	310 µg	310 µg
Ile	1.09	1.25	Chlorine-Chloride	1,040 mg	2,300 mg
Leu	2.05	2.36	Inositol	80 mg	80 mg
Phe	1.11	1.29	**Trace elements [per kg]**		
Phe + Tyr	2.22	2.57	Iron	166 mg	139 mg
Gly	0.43	0.50	Manganese	98 mg	82 mg
Glu	4.69	5.41	Zinc	65 mg	56 mg
Asp	1.55	1.79	Copper	14 mg	12 mg
Pro	2.39	2.76	Iodine	1.20 mg	0.97 mg
Ala	0.68	0.79	Selenium	0.14 mg	0.13 mg
Ser	1.24	1.43	Cobalt	0.15 mg	0.13 mg

Metabolizable Energy calculated with Atwater factors. Crude protein calculated from nitrogen content (N × 6.25). ns: not specified.

Table A2. Comparison of model fit for the prediction of body weight.

Group	Model	Added effects	DF	LL	LLR	*p*-value
1	1	Intercept-only	2	-1651		
	2	Random intercept	3	-1623	56	<0.001
	3	Diet week	4	-1138	970	<0.001
	4	Random slope	6	-1015	246	<0.001
	5	Diet	8	-997	37	<0.001
	6	Genotype	12	-994	5	0.279
2	1	Intercept-only	2	-1444		
	2	Random intercept	3	-1384	120	<0.001
	3	Diet week	4	-953	862	<0.001
	4	Random slope	6	-773	360	<0.001
	5	Diet	8	-753	40	<0.001
	6	Genotype	12	-751	5	0.313
3	1	Intercept-only	2	-5045		
	2	Random intercept	3	-4783	524	<0.001
	3	Diet week	4	-3869	1828	<0.001
	4	Random slope	6	-3191	1356	<0.001
	5	Diet	8	-3139	104	<0.001
	6	Genotype	12	-3131	15	0.004
4	1	Intercept-only	2	-4115		
	2	Random intercept	3	-3733	764	<0.001
	3	Diet week	4	-3032	1402	<0.001
	4	Random slope	6	-2281	1501	<0.001
	5	Diet	8	-2233	97	<0.001
	6	Genotype	12	-2232	2	0.716

Models were fitted separately for each group. As baseline an intercept-only model was fitted (1). A random intercept for individual mice (2), the predictor diet week (3), a random slope for diet week (4) as well as the predictors diet (5) and genotype (6) were added consecutively. The improvement of fit over the respective previous model was calculated using the chi-square test. DF: Degrees of freedom; LL: Log Likelihood; LLR: Log likelihood ratio.

Table A3. Model coefficient statistics for the prediction of body weight with WT, CD mice as reference.

Group	Coefficient	Value	SE	DF	*t*-value	*p*-value
1	Diet week	0.94	0.07	476	12.98	<0.001
	Diet (HFD)	1.80	0.57	36	3.13	0.003
	Genotype (KO)	0.37	0.57	36	0.65	0.522
	Diet week : Diet (HFD)	0.64	0.10	476	6.22	<0.001
	Diet week : Genotype (KO)	0.10	0.10	476	1.02	0.309
	Diet (HFD) : Genotype (KO)	-0.47	0.81	36	-0.58	0.566
	Diet week : Diet (HFD) : Genotype (KO)	-0.29	0.15	476	-2.02	0.044
2	Diet week	0.55	0.07	470	8.08	<0.001
	Diet (HFD)	1.33	0.46	36	2.88	0.007
	Genotype (KO)	-0.68	0.46	36	-1.48	0.147
	Diet week : Diet (HFD)	0.37	0.10	470	3.88	<0.001
	Diet week : Genotype (KO)	0.13	0.10	470	1.37	0.172
	Diet (HFD) : Genotype (KO)	0.89	0.65	36	1.37	0.179
	Diet week : Diet (HFD) : Genotype (KO)	-0.06	0.14	470	-0.44	0.658
3	Diet week	0.45	0.04	1354	11.05	<0.001
	Diet (HFD)	1.37	0.89	56	1.53	0.132
	Genotype (KO)	-0.37	0.89	56	-0.42	0.677
	Diet week : Diet (HFD)	0.62	0.06	1354	10.73	<0.001
	Diet week : Genotype (KO)	0.00	0.06	1354	0.08	0.932
	Diet (HFD) : Genotype (KO)	-0.25	1.26	56	-0.19	0.846
	Diet week : Diet (HFD) : Genotype (KO)	0.22	0.08	1354	2.74	0.006
4	Diet week	0.28	0.03	1217	8.60	<0.001
	Diet (HFD)	0.27	0.75	56	0.36	0.717
	Genotype (KO)	-0.91	0.75	56	-1.22	0.228
	Diet week : Diet (HFD)	0.52	0.05	1217	10.47	<0.001
	Diet week : Genotype (KO)	0.00	0.05	1217	-0.06	0.955
	Diet (HFD) : Genotype (KO)	1.44	1.06	56	1.36	0.179
	Diet week : Diet (HFD) : Genotype (KO)	0.00	0.07	1217	0.06	0.950

SE: Standard Error; DF: Degrees of freedom.

Table A4. Comparison of model fit for the prediction of fat mass, lean mass, or free fluid.

		Fat mass				Lean mass				Free fluid			
Group	Model	DF	LL	LLR	*p*	DF	LL	LLR	*p*	DF	LL	LLR	*p*
1	1	2	-209			2	-213			2	-14		
	2	3	-209	<0.01	1.000	3	-213	<0.01	1.000	3	-14	<0.01	1.000
	3	4	-183	52.19	<0.001	4	-135	157.31	<0.001	4	17	63.62	<0.001
	4	6	-167	32.11	<0.001	6	-129	12.03	0.002	6	24	13.87	0.001
	5	10	-163	7.75	0.101	10	-128	1.78	0.777	10	26	3.04	0.551
2	1	2	-163			2	-180			2	-26		
	2	3	-163	<0.01	1.000	3	-180	<0.01	1.000	3	-26	<0.01	0.742
	3	4	-147	33.64	<0.001	4	-81	198.04	<0.001	4	-5	40.62	<0.001
	4	6	-125	43.12	<0.001	6	-76	10.14	0.006	6	0	11.41	0.003
	5	10	-123	3.63	0.459	10	-74	3.76	0.440	10	2	3.13	0.537
3	1	2	-826			2	-548			2	-173		
	2	3	-820	12.33	<0.001	3	-546	3.06	0.080	3	-169	7.79	0.005
	3	4	-712	215.29	<0.001	4	-483	126.67	<0.001	4	-66	205.29	<0.001
	4	6	-553	319.22	<0.001	6	-480	4.92	0.085	6	29	190.07	<0.001
	5	10	-546	12.75	0.013	10	-479	2.44	0.656	10	30	2.28	0.685
4	1	2	-671			2	-415			2	-67		
	2	3	-654	32.35	<0.001	3	-415	<0.01	0.908	3	-55	24.65	<0.001
	3	4	-586	136.07	<0.001	4	-346	137.81	<0.001	4	-2	105.29	<0.001
	4	6	-458	256.30	<0.001	6	-343	5.37	0.068	6	78	159.56	<0.001
	5	10	-458	0.84	0.933	10	-339	8.91	0.063	10	79	2.92	0.571

Separate models were calculated for each group and outcome. As baseline an intercept-only model was fitted (1). A random intercept for individual mice (2) as well as the predictors diet week (3), diet (4), and genotype (5) were added consecutively. The improvement of fit over the respective previous model was calculated using the chi-square test. DF: Degrees of freedom; LL: Log Likelihood; LLR: Log likelihood ratio; *p*: *p*-value.

Table A5. Model coefficient statistics for the prediction of fat mass, lean mass, or free fluid with WT, CD mice as reference.

		Fat mass					Lean mass					Free Fluid				
Group	**Coefficient**	**Value**	**SE**	**DF**	***t***	***p***	**Value**	**SE**	**DF**	***t***	***p***	**Value**	**SE**	**DF**	***t***	***p***
1	Diet week	0.29	0.10	36	2.88	0.007	0.70	0.07	36	10.23	<0.001	0.04	0.01	36	4.21	<0.001
	Diet (HFD)	-0.21	0.88	36	-0.24	0.813	-0.15	0.56	36	-0.27	0.792	0.03	0.08	36	0.36	0.719
	Genotype (KO)	0.06	0.88	36	0.07	0.946	0.45	0.56	36	0.80	0.430	0.04	0.08	36	0.48	0.631
	Diet week : Diet (HFD)	0.68	0.14	36	4.76	<0.001	0.19	0.10	36	1.95	0.059	0.03	0.01	36	2.44	0.020
	Diet week : Genotype (KO)	0.05	0.14	36	0.33	0.746	0.00	0.10	36	0.00	1.000	0.00	0.01	36	0.00	1.000
	Diet (HFD) : Genotype (KO)	-0.21	1.24	36	-0.17	0.867	-0.38	0.80	36	-0.48	0.637	-0.01	0.12	36	-0.09	0.932
	Diet week : Diet (HFD) : Genotype (KO)	-0.32	0.20	36	-1.59	0.121	0.04	0.14	36	0.26	0.794	-0.02	0.02	36	-0.96	0.345
2	Diet week	0.10	0.06	36	1.58	0.123	0.51	0.03	36	18.82	<0.001	0.03	0.01	36	3.09	0.004
	Diet (HFD)	0.12	0.53	36	0.23	0.823	0.33	0.31	36	1.07	0.294	0.06	0.12	36	0.50	0.621
	Genotype (KO)	0.17	0.53	36	0.32	0.751	-0.44	0.31	36	-1.42	0.164	-0.05	0.12	36	-0.42	0.680
	Diet week : Diet (HFD)	0.30	0.09	36	3.29	0.002	0.03	0.04	36	0.72	0.474	0.04	0.01	36	2.44	0.020
	Diet week : Genotype (KO)	0.02	0.09	36	0.23	0.816	0.05	0.04	36	1.35	0.186	0.00	0.01	36	0.17	0.867
	Diet (HFD) : Genotype (KO)	0.20	0.75	36	0.27	0.792	0.40	0.44	36	0.91	0.367	0.05	0.17	36	0.29	0.771
	Diet week : Diet (HFD) : Genotype (KO)	0.04	0.13	36	0.30	0.764	-0.02	0.05	36	-0.33	0.747	-0.02	0.02	36	-1.13	0.266
3	Diet week	0.28	0.03	172	9.34	<0.001	0.20	0.02	172	8.01	<0.001	0.02	0.00	172	7.59	<0.001
	Diet (HFD)	1.26	0.99	56	1.27	0.210	0.09	0.65	56	0.14	0.893	0.06	0.08	56	0.77	0.442
	Genotype (KO)	0.01	0.99	56	0.01	0.990	-0.13	0.65	56	-0.20	0.844	-0.01	0.08	56	-0.11	0.912
	Diet week : Diet (HFD)	0.61	0.04	172	14.23	<0.001	-0.07	0.03	172	-1.92	0.057	0.03	0.00	172	9.10	<0.001
	Diet week : Genotype (KO)	0.01	0.04	172	0.13	0.897	-0.02	0.03	172	-0.62	0.535	0.00	0.00	172	0.02	0.987
	Diet (HFD) : Genotype (KO)	0.43	1.40	56	0.31	0.759	-0.52	0.93	56	-0.56	0.577	0.01	0.12	56	0.05	0.957
	Diet week : Diet (HFD) : Genotype (KO)	0.12	0.06	172	1.93	0.055	0.06	0.05	172	1.24	0.216	0.00	0.01	172	0.89	0.373
4	Diet week	0.14	0.02	150	5.68	<0.001	0.15	0.02	150	9.15	<0.001	0.01	0.00	150	4.83	<0.001
	Diet (HFD)	0.39	0.88	56	0.45	0.656	0.36	0.41	56	0.88	0.382	0.03	0.06	56	0.57	0.572
	Genotype (KO)	-0.08	0.87	56	-0.09	0.931	-0.68	0.40	56	-1.68	0.098	0.01	0.06	56	0.14	0.889
	Diet week : Diet (HFD)	0.52	0.04	150	12.44	<0.001	-0.04	0.03	150	-1.39	0.167	0.03	0.00	150	7.54	<0.001
	Diet week : Genotype (KO)	0.01	0.04	150	0.28	0.778	0.00	0.02	150	-0.16	0.871	0.00	0.00	150	-1.37	0.172
	Diet (HFD) : Genotype (KO)	0.67	1.23	56	0.54	0.591	0.18	0.57	56	0.31	0.755	0.02	0.09	56	0.21	0.833
	Diet week : Diet (HFD) : Genotype (KO)	0.00	0.06	150	-0.05	0.964	0.00	0.04	150	-0.09	0.931	0.00	0.00	150	0.62	0.533

SE: Standard Error; DF: Degrees of freedom; *t*: *t*-value; *p*: *p*-value.

Abbreviations

2-AG	2-Arachidonoylglycerol
4-HNE	4 Hydroxynonenal
ABHD5	1-acylglycerol-3-phosphate O-acyltransferase
AOC	Area over the curve
aP2	Adipocyte fatty acid binding protein 4
AR	Adrenergic receptor (e.g. α_2-AR, $\beta_{1,2}$-AR)
ATGL	Adipose triglyceride lipase
AUC	Area under the curve
BAT	Brown adipose tissue
cAMP	Cyclic adenosine monophosphate
CB	Cannabinoid receptors (e.g. CB_1, CB_2)
CD	Control diet
cGMP	Cyclic guanosine monophosphate
CV	Coefficient of variation
CXCL1	C-X-C motif chemokine ligand 1
DAG	Diacylglycerol
DF	Degrees of freedom
EC	Endocannabinoid
ESI	Electrospray ionization
FFA	Free fatty acid
FIA	Flow injection analysis
GSTA4	Glutathione S-transferase A4
GTT	Glucose tolerance test
HFD	High-fat diet
HSL	Hormone-sensitive lipase
IFN-γ	Interferon γ
IL	Interleukin (e.g. IL-1β, IL-2, IL-4, IL-5, IL-6, IL-10, IL-12p70)
ITT	Insulin tolerance test
KO	Knockout
LC	Liquid chromatography
MAG	Monoacylglycerol
MGLL	Monoacylglycerol lipase
MS/MS	Tandem mass spectrometry
NCBI	National Center for Biotechnology Information
NEFA	Non-esterified fatty acids
NP	Natriuretic peptides
NPR-A	Type A natriuretic peptide receptors
NPR-C	Type C natriuretic peptide receptors
OECD	Organisation for Economic Co-operation and Development
p	*p*-value
PC	Phosphatidylcholines

PCA	Principle component analysis
PDE3B	Phosphodiesterase 3B
PI3K	Phosphoinositol 3 kinase
PKA	Protein kinase A
PKG	Protein kinase G
PLIN1	Perilipin 1
PLS-DA	Partial least squares discriminant analysis
PPAR	Peroxisome-proliferator-activated receptor (e.g. PPARα, PPARγ, and PPARβ/δ)
PPRE	PPAR-specific response element
qNMR	Quantitative nuclear magnetic resonance analysis
qPCR	Quantitative real-time PCR
SAT	Subcutaneous adipose tissue
SE	Standard error
SM	Sphingomyelins
sMRM	Scheduled multiple reaction monitoring measurement
t	*t*-value
T2D	Type 2 diabetes
TAG	Triacylglycerol
TNF-α	Tumor necrosis factor α
VAT	Visceral adipose tissue
WAT	White adipose tissue
WT	Wildtype

Danksagung

Der Weg zur fertigen Dissertation gestaltete sich länger als geplant und war mit einigen Umwegen und Sackgassen gespickt. Zahlreiche Menschen haben es mir möglich gemacht diesen Weg zu Ende zu gehen. Dafür möchte ich mich an dieser Stelle bedanken. Beginnen möchte ich mit meinem Doktorvater Prof. Jerzy Adamski, der mir dir die Möglichkeit gab an diesem Thema zu forschen. Ich danke ihm ganz besonders für seine stehts offenstehende Bürotür und sein unumstößliches Vertrauen in mich und meine Arbeit. Besonderer Dank gilt auch meiner Mentorin Dr. Gabriele Möller für ihre unerschöpflichen Projektideen und detailversessenen Textkorrekturen. Dr. Janina Tokarz danke ich herzlich für viele fruchtbare Diskussionen insbesondere zum Thema Grafikdesign und Ästhetik wissenschaftlicher Abbildungen.

Herrn Prof. Robert Zimmermann danke ich für die Bereitstellung des MGLL KO Mausmodels. Frau Dr. Sybille Sabrautzki danke ich für Ihre Unterstützung bei den Anpassungen des Tierversuchsantrages. Besonders bedanken möchte ich mich bei Prof. Dr. Martin Hrabě de Angelis für die Möglichkeit den Tierversuch in der *German Mouse Clinic* (GMC) umzusetzen. In diesem Zusammenhang gilt mein Dank auch den Screeningleitern der GMC für ihre Unterstützung, Dr. Jan Rozman, Dr. Julia Calzada-Wack, Dr. Birgit Rathkolb und Dr. Juan Antonio Aguilar-Pimentel. Herzlich bedanken möchte ich mich auch bei Marion Schieweg. Ohne ihre helfenden Hände wäre die praktische Durchführung des Tierversuches undenkbar gewesen. Mein Dank geht diesbezüglich auch an Gabriele Zieglmeier und Maria Kugler für ihre tatkräftige Unterstützung. Meiner Bachelorstudentin Anne Scheuvens danke ich für die Validierung des MGLL KO im Mausmodell. Bei Mark Haid und Alexander Cecil bedanke ich mich für ihre Hilfe in Sachen R und Statistik. Aus ihren Büros kam ich oft mit genauso vielen neuen Fragen wie Antworten. Cornelia Prehn und Silke Becker danke ich für ihre Unterstützung rund um Massenspektrometrie und Metabolomics. Conni möchte ich auf diesem Wege auch für die zahlreichen Gespräche abseits des Wissenschaftsalltags danken.

Diese Arbeit wäre nicht möglich gewesen ohne den Rückhalt meiner Familie. Ich danke ganz besonders meiner Frau Steffi für ihre eiserne Geduld und dafür, dass sie mir immer den Rücken freigehalten hat. Meiner Tochter Flora danke ich für die willkommene Zerstreuung und Freude, für die sie während meiner Arbeit an dieser Dissertation gesorgt hat und sicherlich noch weiter sorgen wird. Meinen Eltern Berit und Hartmut danke ich dafür, dass sie den Grundstein für den Menschen gelegt haben, der ich heute bin und für ihre bedingungslose Unterstützung.

Abschließend möchte ich allen danken, die hier nicht namentlich genannt wurden und mich auf diesem Weg begleitet haben, allen Mitarbeitern der Research Unit Molecular Endocrinology and Metabolism und der GMC, den Post-Docs, Studenten und Praktikanten.